N 70 41026

NASA CR 72750

PSU AERSP 70-1

THREE DIMENSIONAL ANALYSIS AND MEASUREMENT OF THE FLOW IN A THREE BLADED ROCKET PUMP INDUCER

by

A. PONCET, B. LAKSHMINARAYANA

Prepared from work done under

NASA Grant NGL 39-009-007

CASE FILE COPY

Technical Management

NASA Lewis Research Center

Cleveland, Ohio

Liquid, Rocket Technology

Werner R. Britsch

Department of Aerospace Engineering

The Pennsylvania State University

University Park, Pa.

July, 1970

NASA CR 72750

PSU AERSP 70-1

THREE DIMENSIONAL ANALYSIS AND MEASUREMENT OF THE FLOW IN A THREE BLADED ROCKET PUMP INDUCER

by

A. PONCET, B. LAKSHMINARAYANA

Prepared from work done under

NASA Grant NGL 39-009-007

Technical Management

NASA Lewis Research Center

Cleveland, Ohio

Liquid, Rocket Technology

Werner R. Britsch

Department of Aerospace Engineering

The Pennsylvania State University

University Park, Pa.

July, 1970

ACKNOWLEDGMENTS

Credit for initiating this fundamental research on inducer flow goes to George F. Wislicenus and W. R. Britsch.

Grateful acknowledgment is made to Robert Nagel who took all the rotating probe measurements, and to Edward Jordan for his assistance in electronic instrumentation.

The authors also wish to thank H. Bosch and P. Cooper for making available the computer program they wrote for the solution of the inducer flow field.

The research contained in this report was performed under the sponsorship of the National Aeronautics and Space Administration, and was conducted at the Department of Aerospace Engineering of The Pennsylvania State University and is currently operating under contract No. NGL 39-009-007.

TABLE OF CONTENTS

	Page
ACKNOWLEDGMENTS	ii
LIST OF FIGURES	v
NOMENCLATURE	viii
1. INTRODUCTION	
1.1. Statement of the Problem	1
1.2. Previous Related Work	3
1.3. Background of the Present Investigation	7
1.4. Methods and Means of Investigation	11
2. THEORETICAL ANALYSIS	
2.1. Influence of Blade Blockage on Exit Velocity	14
2.2. Numerical Solution of the Flow Field	19
2.2.1. Quasi Three Dimensional Method	20
2.2.2. Exact Method of Solution	21
2.3. Approximate Viscid Solution	28
3. EXPERIMENTAL PROGRAM AND RESULTS	
3.1. Apparatus Used in the Experiment	33
3.1.1. Three Bladed Inducer	33
3.1.2. Conventional Probes	34
3.1.3. Apparatus for Instantaneous Velocity Measurements	35
3.1.4. Pressure Transfer Device (PTD)	36
3.2. Flow Survey at the Exit Using Stationary Probes	36
3.3. Instantaneous Velocity Measurements at Inducer Exit	40
3.3.1. Abstract of the Method	40
3.3.2. Averaging Procedure	44
3.3.3. Accuracy Criteria and Limitations	45
3.3.4. Blade to Blade Distribution of Time Averaged Velocities at the Exit	48
3.3.5. Passage Averaged Values of Velocities at the Exit	51
3.3.6. Blade to Blade Distribution of Turbulence Intensity	52
3.4. Flow Survey Inside the Blade Passage Using Rotating Probes	55
3.5. Flow Visualization Method	57
1. Limiting Streamline Angle on the Blades	58
2. Tuft Grid at Exit	58

TABLE OF CONTENTS CONTINUED

Page

4. DISCUSSION 59

5. CONCLUSIONS 65

APPENDIX 1: Derivation of Accuracy Criteria for Instantaneous Velocity Measurements 70

APPENDIX 2: Fortran Listing of the Program Used for Deriving Instantaneous Velocities from Hot Wire Measurements 72

REFERENCES 77

LIST OF FIGURES

Figure	Title	Page
1	Photographs of Three and Four Bladed Inducer	79
2	Axial Velocity Perturbation Due to Blockage	80
3	Inducer Geometry for Numerical Analysis	81
4	Outlet Results of Exact Numerical Analysis	82
5a	Blade Pressure Distribution at Hub	83
5b	Blade Pressure Distribution at Mid Radius	84
5c	Blade Pressure Distribution at Tip	85
6	Inducer Inlet and Outlet Angles	86
7	Radial Variation of the Loss Coefficient and Function F(r) (Equation 17) for the Three Bladed Inducer	87
8	Radial Variation of Absolute Tangential Velocity from Approximate Viscid Analysis	88
9	Hot Wire Probe and Associated Equipment	89
10	Location of the Flow Measuring Stations	90
11a	Block Diagram for Instantaneous Velocity Measurements	91
11b	Multi sensor Anemometer	92
12a	Axial and Radial Velocity at Station 2a	93
12b	Absolute Tangential and Relative Velocity at Station 2a	94
	Blade to Blade Distribution at Station 2a of:	
13a	Radial Velocity, R = 0.582	95
13b	Relative, Absolute Tangential and Axial Velocities, R = 0.582	96
13c	Turbulence Intensities T_z, T_θ, R = 0.582	97

LIST OF FIGURES CONTINUED

Figure	Title	Page
13d	Turbulence Intensities T_r, T_w, R = 0.582	98
14a	Radial Velocity, R = 0.752	99
14b	Relative, Absolute Tangential and Axial Velocities, R = 0.752	100
14c	Turbulence Intensities T_z, T_θ, R = 0.752	101
14d	Turbulence Intensities T_r, T_w, R = 0.752	102
15a	Radial Velocity, R = 0.86	103
15b	Relative, Absolute Tangential and Axial Velocities, R = 0.860	104
15c	Turbulence Intensities T_z, T_θ, R = 0.860	105
15d	Turbulence Intensities T_r, T_w, R = 0.860	106
16a	Radial Velocity, R = 0.920	107
16b	Relative, Absolute Tangential and Axial Velocities, R = 0.920	108
16c	Turbulence Intensities T_z, T_θ, R = 0.920	109
16d	Turbulence Intensities T_r, T_w, R = 0.920	110
	Blade to Blade Variation of Stagnation and Static Heads, Resultant Velocity of the Relative Flow at Station 2 and:	
17a	R = 0.974	111
17b	R = 0.920	112
17c	R = 0.863	113
17d	R = 0.808	114
17e	R = 0.754	115
17f	R = 0.720	116

LIST OF FIGURES CONTINUED

Figure	Title	Page
17g	R = 0.672	117
17h	R = 0.617	118
17i	R = 0.562	119
17j	R = 0.506	120
18	Radial Variation of ε_o and ε_w at various chordwise location	121
19a	Radial Variation of Stagnation and Static Coefficients at Various Axial Locations	122
19b	Radial Variation of Axial Velocity at Various Axial Location	123
19c	Radial Variation of Absolute Tangential Velocity at Various Axial Location	124
20	Hub Static Pressure Distribution	125
21	Annulus Wall Static Pressure Distribution	126

NOMENCLATURE

A_1, A_2, A_3 B_1, B_2, B_3	calibration parameters for hot wire measurements
d_h	hydraulic passage
E	accuracy of turbulence intensity measurements
f	digitizing speed of the ADC unit
F_r	friction force in r direction
F_θ	friction force in θ direction
F_z	friction force in z direction
g_o	gravity acceleration
h	static head
k	correction factor for the deviation from the cosine law
J_1	Bessel function of first kind
L	loss term in streamline momentum equation
L_o	distance along the streamline
m	direction tangent to the streamline in the meridional plane
$\vec{n}$	normal to the blade surface
n	number of blades
n'	direction normal to the streamline in the meridional plane
n_o	number of measuring points within the blade passage
N	number of averaging passages
P	static pressure
r,θ,z	rotating cylindrical system
r	local radius

NOMENCLATURE CONTINUED

R_n	Reynolds number $\overline{W}\, d_h/\nu$
$R = r/r_t$	non dimensionalized radius
R_{ht}	ratio of hub to tip radii
S	source distribution
2s	normal distance from blade to blade
t	blade thickness
$T, \sigma/x$	Turbulence intensity (Root Mean Square value of the fluctuating velocity divided by the local averaged velocity)
U	local blade speed = Ωr
v'_z	perturbation in axial velocity ($= \frac{\partial \phi}{\partial x}$)
V_z	upstream axial velocity
$\overline{v}_z$	local axial velocity
V	resultant absolute velocity
W	resultant relative velocity
x	meridional coordinate lying on a cylindrical surface
Y_1	Bessel function of second kind
y	coordinate perpendicular to the meridional plane on a cylindrical surface
z	axial location
α	angle between limiting streamline and m direction
β	angle of the flow with inducer axis
β'	angle of the blade with inducer axis
$\delta = 1 - \frac{tn}{2\pi r}$	blockage factor
ε	accuracy criterium for blade to blade averaged velocities
ε_p	accuracy criterium for approximate program

NOMENCLATURE CONTINUED

ε_w	limiting streamline angle
ε_o	maximum deviation angle of the streamline outside the blade boundary layer region
Φ	inlet flow coefficient
ϕ	velocity potential (perturbation in the case of blade blockage)
ν	kinematic viscosity
ρ	fluid density
γ'	angle between n and r directions
μ	normal distance to the blade
Ω	inducer's angular velocity
τ	streamline unbalance
ψ_T	Stagnation head rise coefficient $(\frac{2gH}{U_t^2})$
ψ_s	Static head coefficient
λ_R	Loss coefficient
$\zeta(r),\xi(r),F(r)$	defined in equation 18

Subscripts

r,θ,z	components along r,θ,z directions
m	refers to the meridional direction
t,c	refer to the values at the tip
p,s	refer to pressure and suction surfaces
h	refers to the values at the hub
R	refers to the relative flow
1	refers to the leading edge
2	refers to the trailing edge

1. INTRODUCTION

1.1 Statement of the Problem

Multibladed pump inducers are used to increase the suction specific speed of centrifugal impellers for liquid rocket engines. Cavitation in rocket pumps is in general handled by inducers, which are secondary pumps designed to pass the required flow under cavitating conditions and produce enough head rise to permit the primary pump to operate cavitation free. Their main characteristics are very high solidity (ratio of the chord length of the blade to the blade spacing) and very low flow coefficient (ratio of inlet axial velocity to blade tip speed). While their specific geometry is dictated by cavitation requirements, the flow inside the long and narrow passages between the blades is subjected to major effects due to turbulence and viscosity, thus making the prediction of the flow behaviour in these inducers very difficult.

The Department of Aerospace Engineering of The Pennsylvania State University has conducted investigation and analysis of the flow in pump inducers under NASA sponsorship since November, 1963. It has designed and tested in air a four-bladed inducer model of three feet diameter (ref. 4). The investigation carried out on a three-bladed inducer of the same blade profile and flow characteristics is reported in this thesis.

The secondary motions in these inducers are not confined to thin regions at the blades but extend over the entire cross section of the flow. The development of three dimensional turbulent boundary layers on the blade surfaces combined with the interaction between the suction and pressure surface boundary layers makes the flow truly three dimensional.

The principal objective of this thesis is to obtain a quantitative measurement of these secondary motions. It is hoped that a quantitative understanding of these secondary flows can serve the establishment of a theoretical model for the eventual analysis of the turbomachinery flow dominated by secondary fluid motions caused by viscosity and turbulence. In addition, attempts are made to establish the three dimensional inviscid flow through such inducers. Hence the purpose of this thesis has been:

1) to develop a measuring technique using hot-wire probes to obtain the blade to blade variation of the three components of the velocity and turbulence at the three bladed inducer exit.

2) to predict the three dimensional inviscid flow in the inducer solving numerically the exact equations of motion.

3) to approximately predict the flow at inducer exit using radial equilibrium and an empirical expression for the viscous losses.

4) to investigate the axial flow velocity perturbation due to radially varying blade blockage.

5) to carry out a complete flow survey using stationary probe at the exit of the inducer and a rotating probe inside the blade passage of the three-bladed inducer.

6) to visualize the flow using ammonia streak technique and a tuft grid to derive respectively the limiting streamline angles on the blade surfaces and the maximum radial inward flow at mid passage for the three-bladed inducer.

The performance of the three-bladed inducer is discussed thoroughly and compared with the performance of the four-bladed inducer previously studied in this department.

1.2 Previous Related Work

A survey of the existing literature on axial flow inducers reveals very little theoretical analysis for the prediction of the three dimensional flow characteristics. Although this particular case is related to the three dimensional flow problems of turbomachinery in general, the presence of large secondary flows caused by three dimensional boundary layers makes it essential to include the viscous effects in the solution of the flow field. Because of the lack of accurate information concerning the real flow processes and the complexity of the viscid equations of motion governing this flow, very little progress has been made toward a meaningful solution of the flow field. For the above reasons, most of the design and analysis of the inducer fluid flow is based on conventional two dimensional methods.

On the assumption of a fully developed turbulent flow along with assumed velocity profiles in both radial and mainstream directions of the channel and an empirically determined skin friction loss coefficient, an approximate solution using the simplified radial equilibrium equation in an integrated form has been obtained for a four-bladed inducer in reference 4 . This analysis leads to a good prediction of the outlet absolute tangential velocity. However, due to the lack of accurate information concerning the radial velocity profiles inside the blade passages, the axial velocities are predicted only qualitatively. A first step toward the study of the three dimensional boundary layer in such a channel is carried out by A. Jabbari (reference 3), who investigated the growth of the boundary layer on a single helical blade of constant thickness rotating at the same speed as the inducer. A logical extension of this investigation to study the boundary layer growth in a

rotating channel to be undertaken by this department should lead to some valuable information for an exact prediction of the flow.

An attempt to predict the exit head rise and flow coefficient for an 80° helical inducer by taking into account the losses has been made by J. C. Montgomery (reference 11). This author uses the simplified radial equilibrium equation together with an arbitrary expression for the losses to predict the exit flow characteristics. Although his analysis predicts the large axial velocity gradient in the radial direction at exit, the procedure of trying arbitrary loss distributions to obtain the desired solution for the exit flow coefficient lacks the physical support. It does not provide any specific method of relating the loss distribution to a given geometrical and flow characteristic of the machine.

Among the attempts made toward a general solution of the equations governing the flow, the main contribution is due to P. Cooper and H. Bosch (ref. 2). Using a numerical procedure, these authors solved the equations of motion iteratively in three dimensions for an exact solution of the flow field. This analysis, however, has its limitations and it is proposed to treat it in more detail in a following section.

On the experimental aspects of the flow, several authors have studied the overall inducer performance with different configurations and inlet angles and tested in various fluids such as water, liquid hydrogen, or nitrogen under a wide range of flow parameters (see references 9, 10, 11, 12, 14, 15, 16). However, in most cases these studies are very specific and deal with cavitation performance and overall efficiency rather than with a general and basic investigation of the flow phenomena in inducers. The cavitating and non-cavitating performance of a 84°, 81° and 78° inducer under different flow coefficients has been studied by

Acosta (1). Acosta observes a deterioration in the radial distribution of the axial velocity and head rise at exit at a flow coefficient $\Phi = 0.07$ under non-cavitating condition, with a backflow near the hub and a sharp positive gradient in head rise near the tip. These results are similar to those obtained for the three-bladed inducer reported in this thesis. Acosta attributes the large departure from design values based on the Simplified Radial Equilibrium Equation (SRE) to strong three dimensional and viscous effects. Acosta also notices a decrease in efficiency at large solidity, which is confirmed by the results obtained for the 4 and 3 bladed inducers tested in this department. This effect can be attributed to the influence of blade blockage on the flow characteristics and an increase in viscous and turbulent mixing losses due to decrease in channel width.

R. F. Soltis and D. A. Anderson (15) were led to similar conclusions while investigating the non-cavitating performance of a 78° axial inducer under various flow coefficients. Using the simplified radial equilibrium equation which relates the static head rise gradient and the tangential velocity:

$$\frac{\partial h}{\partial r} = \frac{V_\theta^{\,2}}{g_o r}$$

They derived the outlet axial velocity profile using experimental values for the total pressure and outlet flow angles. However, at their station of measurement, located about 1/5 diameter downstream of the rotor, the radial velocities are likely to be very small and the flow nearly axisymetric since the wake diffusion in such inducers is very rapid.

This analysis serves to establish that the flow is axisymmetric at small axial distances downstream of trailing edge (which may correspond

to large distance along the streamline path since the streamlines follow tightly wound helical path), but cannot account for the existence of large head rise near the tip. Similar observations are made by P. J. Mullan (9), P. R. Meng and R. D. Moore (10), J. C. Montgomery (11), W. M. Osborn (12). R. F. Soltis, D. C. Urasek and M. J. Miller (16) carried an investigation in tandem bladed inducer operated in water. Their results show an appreciable increase in efficiency and head rise compared to conventional inducers. Control of the boundary layer growth on the rear part of the blades in a tandem bladed inducer should improve the flow appreciably by reducing the interaction effects between pressure and suction surface boundary layers.

The main conclusions of the various studies described above are:

1) The overall head rise coefficient increases when the operating flow coefficient decreases, especially in the tip region.

2) The total head rise coefficient increases when the solidity of the blades is decreased in the practical range of solidities used in the inducers.

3) The radial distribution of outlet velocity tends to deteriorate when the flow coefficient is decreased. At low flow coefficients and for most inducer configurations, there is a large positive radial gradient in exit axial velocity with a backflow near the hub. This backflow is probably linked to a large redistribution of the flow as it leaves the trailing edge, the radial velocity decaying from presumably large positive values inside the blade passage to zero as the flow becomes axisymmetric downstream. However, the radial velocity at exit of

inducers has never been measured prior to this study. An attempt is made in this thesis to measure the radial velocity using a three dimensional hot-wire probe set-up.

1.3 Background of the Present Investigation

As stated in section 1.2, the Department of Aerospace Engineering at The Pennsylvania State University has conducted the investigation of the flow in a four-bladed pump inducer. The three-bladed inducer reported in this thesis is of the same design and is described in section 3.1.1.

The most important observations and conclusions obtained from four bladed inducer results are, (ref. 4):

1. At or near design flow coefficient, no back flow was observed at the inlet of the inducer. A separated region of flow exists near the hub at the discharge side of the inducer. This can be explained qualitatively on the basis of simplified radial equilibrium equation, when applied to the actual rather than the design head distribution. However the actual region of separation is much smaller than that derived by the condition of radial equilibrium.

The measurements indicate that this back flow region originates on the stationary hub just after it has left the rotating hub. Furthermore, this extent of back flow was observed to grow continuously downstream.

The extent of back flow increases considerably at the inlet of tip region and outlet hub region at flow coefficients lower than the design value.

2. The flow visualization experiments carried out near the exposed leading part of the inducer indicate that the radial motions in the

main flow (not under the influence of blade skin friction) are smaller where as the radial motions near the blade surfaces are considerable.

3. The test inducer, designed approximately for uniform head distribution over its discharge area (assuming ideal flow) actually produces a nonuniform head. Near the tip the actual head of the absolute flow was found to be 2 - 3 times that at hub and mid radius. This non-uniform head distribution can be explained qualitatively by real fluid effects and is in agreement with the observations of other investigators.

The flow survey carried out at the trailing edge and farther downstream indicate that the radial distribution of the axial velocity component changes considerably between the two stations. The stagnation pressure at the tip is found to decrease continuously as the flow travels downstream, whereas it remains essentially constant at mid radius and hub.

4. Measurement of the relative flow inside the blade passages (obtained with use of a rotating probe and pressure transfer device) indicate that a major portion of the total flow losses along the stream path occurs near the leading edge. This is probably due to the presence of laminar flow on the blades near the leading edge and the consequent large radial flow and associated mixing effects near the tip. The flow losses at the tip were found to be very much higher than those at other radial locations.

5. A complete flow survey of the relative flow inside the blade passage at the trailing edge revealed the presence of a loss core located slightly inward from the blade tip. The radial movement inside the blade boundary layer, when encountered by the annulus wall tends to deflect towards the mid passage and then radially inward. The mixing

effects due to these secondary flows are responsible for large losses observed experimentally. The measurements indicate the presence of large loss regions near the mid passage extending all the way from mid radius to the tip region of the blades.

6. The blade boundary layers were found to be quite thin near the hub and mid radius, being thicker on suction surface than the pressure surface.

The expected radial motions within the blade passages have been qualitatively confirmed by flow visualization experiments and appeared to be quite strong all along the blade length.

The wall shear stress estimated from the boundary layer profiles inside the blade passage appeared to be much higher than that of an equivalent stationary channel having the same relative flow.

7. At the trailing edge, the relative velocities averaged circumferentially over the passage had a maximum value near the mid radius. For a third of the blade height from the tip the relative velocities were considerably less than their design values.

The angles of the relative flow downstream of the trailing edge were found to be nearly uniform in the circumferential direction, their deviation from the design values being greatest near the tip.

8. A new frictionloss coefficient applicable to inducers operating in the range of flow coefficients $\Phi = 0.065$ to 0.2 was defined and derived from the inducer data available in the open literature. This empirical friction coefficient is found to increase exponentially towards the blade tip. For the Penn State four bladed inducer, the radial variation of frictional losses estimated from this newly derived empirical loss coefficient agreed closely with the measured values.

9. A circumferentially averaged radial equilibrium equation was used to predict the relative and absolute tangential velocities. The analysis was based on suitable assumptions for the radial and mainflow velocity profiles (based on the existing three dimensional turbulent boundary layer data available). The agreement between the theory and experiment was reasonably good.

10. The axial velocities predicted, using the continuity and axial momentum equations with assumed radial velocity profiles and the derived tangential velocity distribution agreed qualitatively with the values measured from a stationary probe.

11. Measurements carried out at several stations downstream (Ref. 5) indicated that the axial velocity profiles under went marked change as the flow proceeded downstream. The back flow region near the hub developed after the flow had left the rotating hub and grew continuously as the flow proceeded downstream.

12. Measurement of the instantaneous three dimensional velocities carried out using X configuration hot wire indicated that the radial velocities at the exit were of the same order of magnitude as the axial velocities over most of the radial locations.

13. The limiting streamline angle of the flow near the wall measured by ammonia streak technique revealed that these angles are generally higher than those measured on a single blade (reference 3). The maximum deviation of the streamlines from the cylindrical surface (outside the boundary layer region) obtained by means of a tuft grid mounted at the exit of the inducer showed substantial radial inward flow from mid radius to tip.

14. The blade to blade variation of the relative velocity derived from rotating probe measurements indicated that in addition to conventional boundary layer type of profiles near the blades, a wake type of profile existed from mid radius to tip. A qualitative analysis carried out indicated that the radial inward flow at mid passage at these radii was the cause for the wake type of profile.

The flow measurements for the four bladed inducer have indicated that the channel had a fully developed flow at most of the axial locations. In reference 4, it was anticipated that a decrease in the solidity of the blades might improve the performance of the inducer by reducing the interaction of the pressure and suction surface blade boundary layers near the tip. This was accomplished by removing one of the blades of the four bladed inducer and equally spacing the others, thus decreasing the solidity by twenty-five percent.

This thesis presents the performance of the three bladed inducer.

1.4 Methods and Means of Investigation

The complexity of the flow in inducers makes meaningful predictions extremely difficult. A flow model such as proposed in reference 4 based on the assumption of fully developed turbulent flow and radial equilibrium leads to a good approximation of the tangential velocity at exit, but does not predict the axial velocity measured. This is due to lack of accurate information regarding the radial velocity distribution at exit. This approximate viscid analysis is applied to the case of the three bladed inducer in section 2.3.

In order to understand the extent of three dimensional effects, it is essential to have a knowledge of the inviscid flow field of the three

dimensional flow caused by radially varying blade blockage, flow turning, finite hub to tip ratio and other effects. This is accomplished by using an existing numerical solution of the flow field proposed by Cooper and Bosch. This three dimensional method employs a numerical procedure to solve the equations of motion expressed in finite difference form and requires the use of computers with large storage capacity and fast computation time. This approach is discussed in section 2.2.

In order to study the flow perturbations due to radial gradient of blade blockage, which is large in the case of the Penn State inducer, an analysis carried out by Lewis and Horlock is used. The predicted perturbations in axial velocity are found to be of appreciable magnitude.

The final solution of the entire flow field, including viscous effects, can be carried out only by introducing some approximations in the three dimensional turbulent equations of motion governing this flow. Experiment is the only source which helps to make these approximations. Hence the following experimental program is undertaken. It has been stressed that a good knowledge of the entire flow field is necessary for the design and prediction of inducer performance. Because of the three dimensional character of the flow within the blade passages, accurate measuring techniques are scarce. In this thesis, a method using a configuration of three hot wire sensors is developed to get the blade to blade distribution of the three components of the velocity at exit of the three bladed inducer. This technique is extended to the measurement of the local turbulence intensity and the method thus provides a good means of measuring the extent of secondary flow or the deviation from the design flow (section 3.3).

Finally, conventional experimental techniques such as flow visualization and the use of both stationary and rotating pitot tubes are used for measurement of the flow inside the blade passage and at several stations downstream of the inducer (see sections 3.2, 3.4, 3.5).

2. THEORETICAL ANALYSIS

An accurate assessment of all significant perturbations in inviscid flow is essential for the final prediction of the flow including viscous effects. An important contribution towards the three dimensional inviscid solution is made by Cooper and Bosch (reference 2). This solution is extended for the Penn State inducer in section 2.2 to determine the three dimensional inviscid perturbations. Although blockage is included in the above numerical method of analysis, the solution reveals little about the perturbations in meridional flow caused by various sources. The finite blade thickness and its variation in radial direction causes significant flow perturbations. This effect is considered in section 2.1.

In section 2.3, an earlier analysis based on empirically determined skin friction coefficient is used to predict tangential velocities at the exit of the three bladed inducer.

2.1 Influence of Blade Blockage on Exit Velocity

The axial velocities measured at the exit of inducers are generally found to be substantially different from the design values. These departures are caused by (a) radially varying blade thickness - the blade blockage effect, (b) the radial flows inside the blade boundary layers.

In order to find out the contribution of the blade blockage effect on axial velocity deviations the following analysis is carried out.

The blockage factor is defined as

$$\delta = 1 - \frac{tn}{2\pi r} \qquad (1)$$

t being the thickness of the blade in the tangential direction,

n being the number of blades,

r being the local radius.

which gives for the three bladed inducer (Fig. (2)):

$$\delta \simeq .800 \text{ at the hub}$$

$$.980 \text{ at the tip}$$

and for the four bladed inducer:

$$.730 \text{ at the hub}$$

$$.970 \text{ near the tip}$$

Such a variation of blade thickness from hub to casing imposes a non-uniform blockage upon the meridional flow; this should give rise to significant perturbations in axial velocity.

R. I. Lewis and J. H. Horlock (reference 6) have developed an analogous source actuator disk theory accounting for the effects of varying blade thickness, and have pointed out the significant effects on the meridional flow perturbations due to blade blockage. Following Lewis and Horlock's theory, perturbations due to blade thickness are governed by

$$\text{div grad } \phi = S \tag{2}$$

ϕ being the scalar perturbation potential due to source distribution and S the source distribution representing the finite blade thickness in a uniform stream. In the case of known geometry, where an approximate expression for the blockage factor $\delta(z,r)$ can be found, the source distribution $S(z,r)$ per unit volume can be derived from the equation given by Lewis and Horlock:

$$\frac{1}{V_z} S(z,r) = \frac{\partial}{\partial z} \left(\frac{1}{\delta}\right) \tag{3}$$

where V_z is the local undisturbed axial velocity without blockage, herein taken as unity. This expression is derived from continuity considerations between the blades for the incremental change in axial velocity $\overline{v_z}$. Knowing the blockage factor δ from the blade geometry, the source function $S(z,r)$ can be determined. Using this, equation (2) can then be solved. Lewis and Horlock's expression for axial velocity perturbation outside the blade passage is given by;

$$\overline{v_z} = V_z + v_z'$$

$$v_z' = \pm \left\{ \frac{1}{2} \int_{z_1}^{z_2} S(z_s, r)\, e^{-(\pm)\lambda_1 (z - z_s)}\, dz_s \right.$$

$$\left. - \frac{1}{r_t^2 - r_h^2} \int_{z_1}^{z_2} \int_{r_h}^{r_t} r \quad S(z_s, r) e^{-(\pm)\lambda_1 (z - z_s)}\, dr dz_s \right\} \tag{4}$$

where

$\overline{v_z}$ is the local resultant velocity

v_z' is the velocity perturbation due to blockage

r_h and r_t are the hub and casing radius

z_s is the axial location at point of integration

z_1 and z_2 are respectively the leading and trailing edge axial coordinates.

The sign convention is + for $z>z_2$ and - for $z<z_1$.

Within the blade row the velocity perturbation is given by,

$$v_z' = \frac{1}{2} \{ \int_{z_1}^{z} S(z_s, r)\, e^{-\lambda_1 (z - z_s)}\, d z_s$$

$$- \int_{z}^{z_2} S(z_s, r)\, e^{\lambda_1 (z - z_s)}\, d z_s \}$$

$$+ \frac{1}{r_t^2 - r_h^2} \{ \int_{z_1}^{z_2} \int_{r_h}^{r_t} r\, S(z_s, r)\, (1 - e^{-\lambda_1 (z - z_s)})\, dr\, dz_s \tag{5}$$

$$- \int_{z_1}^{z_2} \int_{r_h}^{r_t} r\, S(z_s, r)\, (1 - e^{\lambda_1 (z - z_s)})\, dr\, d z_s \}$$

λ_1 is determined by the condition of vanishing radial velocity at hub and casing:

$$J_1 (\lambda_1 r_h)\, Y_1 (\lambda_1 r_t) - J_1 (\lambda_1 r_t)\, Y_1 (\lambda_1 r_h) = 0 \tag{6}$$

J_1 and Y_1 being Bessel functions of first and second kind. With values of $r_h = 1$ and $r_t = 2$, this leads to

$$\lambda_1 = 3.1976$$

It should be noted however that this analysis takes into account the perturbations due to blade blockage only, without allowing for perturbation due to annulus area changes. The latter effect is taken

into account in the definition of the undisturbed velocity V_z which is based on the local velocity without blades.

Equations 4 and 5 are integrated numerically for the geometry given in Fig. (2) for both four and three bladed inducers, for which the blockage factors can be approximated by:

$$\delta = \frac{7.1\ r^3\ (5 - z)^2 - z\ (4.5 - z)}{7.1\ r^3\ (5 - z)^2}$$

for four bladed inducer.

and for three bladed inducer:

$$\delta = \frac{9.4\ r^3\ (5 - z^2) - z\ (4.5 - z)}{9.4\ r^3\ (r - z)^2} \qquad (7)$$

(The axial coordinate is undimensionalized with respect to tip radius, $z = z/r_t$)

The results plotted in Fig. (2) show that the perturbation in axial velocity due to blade blockage reaches 13% of the local unperturbed axial velocity for the four bladed inducer and 10% for the three bladed, at hub near the trailing edge. It is apparent that immediately beyond the trailing edge, the minimum in axial velocity occurs near the hub; in fact the varying blade blockage from hub to tip imposes a strong upward radial velocity especially near the hub which is responsible for a redistribution of the flow directed toward the tip. Figure (2) also shows that the gradient in axial velocity across the trailing edge is very large in both cases. It is to be noted that the qualitative nature of the axial velocity i.e. decrease near the hub and increase towards the tip is predicted here by taking into account only the blockage effect

on the meridional flow (Fig. 19b). However there is no quantitative agreement between measured and predicted distributions of axial velocity.

It is apparent from this result that an accurate prediction should include a complete three dimensional solution with viscous effects incorporated in the analysis. One of the useful conclusions of this analysis is that the blade blockage effect does contribute towards the decrease in axial velocity near the hub and its effect should be taken into account in the analysis for predicting the three dimensional flow.

2.2 Numerical Solution of the Flow Field

The availability of modern computers with large storage capacity and fast computation time greatly enlarge the possibility of solving the complete equations of motion. One of early attempts in this direction was carried out by Cooper and Bosch (reference 2) for the case of three dimensional inviscid flow through inducers. The author used these computer programmes, with some modifications to account for trailing edge boundary conditions, to predict the three dimensional inviscid flow through three bladed inducer.

The quasi-three dimensional solution described in the following paragraph is used as a first approximation for the input data of the three dimensional program in section 2.2.2. Because of the low convergence rate for a satisfactory solution of the flow field from the exact program, the initial conditions have to be as accurate as possible. The quasi-three dimensional solution, which predicts the flow quantities from what amounts to combining the axisymmetric solution with a blade to blade solution, is a better initial approximation than the values based

on one dimensional analysis. This approach results in considerable saving in the computer time required for the exact program.

2.2.1 Quasi Three Dimensional Method

One of the computer programs developed by Cooper and Bosch derives the blade to blade average quantities using axisymmetric equations. These quantities are then used in a blade to blade solution using an integrated form of the scalar momentum equation in the tangential direction. A two dimensional meridional solution resulting from the streamline momentum equation together with the simple normal equilibrium equation is employed to determine the average quantities for the velocity and pressure within the blade passage,

$$g_o \frac{dp}{\rho} = d\left(\frac{\Omega^2 r^2}{2}\right) - d\left(\frac{w^2}{2}\right) - dL \tag{8}$$

$$g_o \frac{dp}{dn'} = \frac{V_\theta^2 \cos \gamma'}{r} \tag{9}$$

L is the friction loss term along the streamline

m is the direction tangent to the streamline

n' is the direction normal to the streamline

γ' is the angle between the streamline and r coordinate.

These quantities are then used in a blade to blade superimposed solution using an integrated form of the scalar momentum equation in the θ direction,

$$\frac{\partial p}{\partial \theta} = \frac{\rho}{g_o} V_m \frac{d}{dm} (rV_\theta) \tag{10}$$

together with the continuity equation.

These equations are solved numerically using a residual technique. The computer program was somewhat modified to take into account the variation in blade thickness at each location within the grid of points representing the blade. The geometry and leading parameters are shown in Fig. (3). The grid is made of 26 points in the axial direction and 7 points between hub and casing. The solution of this program is used as input data for the exact three dimensional approach described in section 2.2.2. The accuracy criterium as defined in reference 2,

$$\tau \leq \varepsilon_p \, (\Omega^2 r_t) \, \frac{\rho}{g_o} \tag{11}$$

τ being the streamline unbalance (or residual), is satisfied in about 200 seconds on IBM 360-67 computer using a Fortran IV G compiler, with a value of 0.001 for ε_p.

2.2.2. Exact Method of Solution

This method developed by Cooper and Bosch solves the momentum and continuity equations iteratively in three dimensions for a finite grid of points representing the channel between the blades. The non linear partial differential equations governing the flow in a rotating polar coordinate system r, θ, z are:

r momentum

$$\frac{g_o}{\rho}\frac{\partial p}{\partial r} + W_r \frac{\partial W_r}{\partial r} + \frac{W_\theta}{r}\frac{\partial W_r}{\partial \theta} + W_z \frac{\partial W_r}{\partial z} - \frac{1}{r}(W_\theta + r\Omega)^2 + F_r = 0$$

θ momentum

$$\frac{g_o}{\rho}\frac{\partial p}{\partial \theta} + W_r \frac{\partial W_\theta}{\partial r} + \frac{W_\theta}{r}\frac{\partial W_\theta}{\partial \theta} + W_z \frac{\partial W_\theta}{\partial z} + \frac{W_r W_\theta}{r} + 2\, W_r \Omega + F_\theta = 0$$

z momentum

$$\frac{g_o}{\rho}\frac{\partial p}{\partial z} + W_r\frac{\partial W_z}{\partial r} + \frac{W_\theta}{r}\frac{\partial W_z}{\partial \theta} + W_z\frac{\partial W_z}{\partial z} + F_z = 0 \qquad (12)$$

continuity

$$\frac{W_r}{r} + \frac{\partial W_r}{\partial \theta} + \frac{1}{r}\frac{\partial W_\theta}{\partial \theta} + \frac{\partial W_z}{\partial z} + \frac{1}{\rho}\left(W_r\frac{\partial \rho}{\partial r} + \frac{W_\theta}{r}\frac{\partial \rho}{\partial \theta} + W_z\frac{\partial \rho}{\partial z}\right) = 0$$

These equations, where Ω is the angular velocity of the inducer, W_r, W_θ, W_z the relative velocities in radial, tangential, and axial directions respectively, are expressed in a finite difference form and rearranged to give four residuals which are reduced to zero by a relaxation procedure. A complete description of the numerical technique and the computer program can be found in reference 2.

This method of solution has been applied by the author with some modifications. The flow is assumed to be incompressible throughout thus eliminating the last three terms inside the bracket in the continuity equation above. A grid of 7 x 7 x 26 is chosen to represent the blade passage, and the initial values at each of those grid points are derived from the approximate solution results, described in section 2.2.1. As shown in Fig. (3), 7 stations are chosen in both the radial and tangential directions. The boundary condition to be satisfied on the hub, annulus walls, and the blade surfaces is

$$\vec{W} \cdot \vec{n} = 0 \qquad (13)$$

where $\vec{n}$ is the direction normal to the channel boundaries.

Among the 26 equally spaced axial stations, the first station corresponds to the upstream through flow boundary where the initial conditions are applied. For the boundary value problem to be consistent, these initial upstream conditions must specify the three components of

the velocity and the pressure, and the tangential velocity on the second axial station which thus defines the whirl at inlet of the inducer, herein taken as zero. The four last stations correspond to the downstream through flow boundary, and extends about one fifth of the chord length downstream of the trailing edge. With the condition (13) to be satisfied on these stagnation stream surfaces, the set of boundary conditions for this problem is complete. The program has been suitably modified for use in IBM 360-67 system at The Pennsylvania State University. The solution obtained from this program was checked against a known solution for the case of a paddle wheel channel similar to that carried out by Cooper and Bosch (reference 2).

a) First Run

The program was first run for twenty-four cycles for the Penn State inducer, with the geometry shown in Fig. (2). The design air inlet angles at the leading edge are shown on Fig. (6). Normally, as suggested by P. Cooper and H. Bosch (2), the upstream through flow boundary should be applied about one channel width upstream of the leading edge to take into account the upstream effects of the channel. Since the Penn State inducer is designed for light loading on the inlet portion of the blades, the upstream perturbation due to leading edge loading can be considered negligible.

Furthermore, four axial stations have been chosen to represent the downstream extension of the blades, accounting for 1/5 of the blade chord length.

The extension of the stagnation stream surfaces downstream with the condition that no flow crosses them satisfies the requirement that the

flow be uniformly periodic at exit with spacing of $2\pi/n$, n being the number of blades. The extension of these surfaces, together with the manual method of adjusting them to unload them, has been discussed by P. Cooper and H. Bosch.

The blade static pressures obtained by this program are shown on Fig. (5a, 5b, 5c) at hub, mid radius, and tip respectively. The negative pressures and gradient of pressure observed near the leading edge are consistent with hub and wall static pressure probe measurement. In view of the results shown in Fig. (5a, 5b, 5c), it can be said that the condition of closure of the blade pressure diagram at the trailing edge is far from being satisfied. As indicated by Cooper and Bosch, probably more stations would be required downstream for the stagnation stream surfaces to satisfy the closure condition. This method requires considerable amount of computer time, and hence is not the most efficient method. Cooper and Bosch also tried to satisfy this condition by forcing the pressures according to the equation,

$$p = \frac{\rho}{g_o} (r^2\Omega^2 + W_1^{\,2} - W_r^{\,2} - W_\theta^{\,2} - W_z^{\,2}) \qquad (14)$$

W_1 being the relative velocity at inlet at radius r. This method is subject to criticism since equation (14) is valid only along a streamline and not at any radius.

The main effort of the work reported here has been to try more efficient methods to satisfy the Kutta-Joukowski condition at the trailing edge. On Dr. Wislicenus' suggestion, a first try with forced stagnation pressure at the trailing edge (relative velocity equal to zero) has been attempted without success. The coarseness of the grid along with input problems did not allow for a detailed specification of

the trailing edge. According to the sketch below, by locating and fixing the stagnation point on the trailing edge, it is possible to simulate real fluid effects. However, the grid of points has to represent in detail the trailing edge, and consequently has to be very dense in order for the large velocity gradients induced by this method to be confined around the stagnation point.

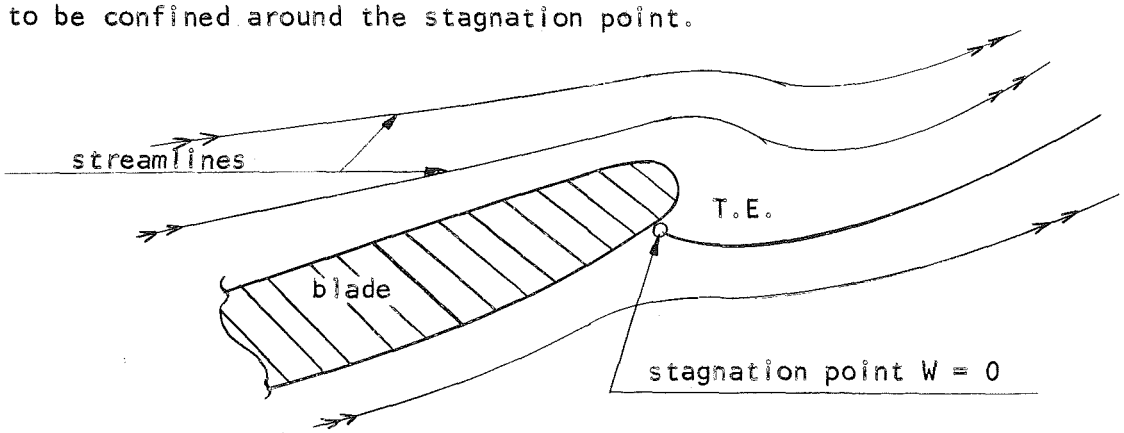

b) Second Run

A second attempt was made by setting the exit direction of the flow free, that is the boundary condition

$$\vec{W} \cdot \vec{n} = 0 \tag{15}$$

is no longer required on the downstream stagnation stream surfaces. For the mathematical problem to be consistent, this condition is replaced by setting the pressure on these downstream extensions of the blades equal to the average between pressure and suction surfaces at that particular radius:

$$p = \frac{p_s + p_p}{2} \tag{16}$$

Mathematically, this condition is equivalent to the boundary condition (15). Hence, according to the discussion given by P. Cooper and H. Bosch (2), the number of independent discrete variables is the same as in the previous case, and the solution to this problem exists and is unique. With this modification the condition of closing the blade

pressure diagram is perfectly fulfilled, Fig . (5a, 5b, 5c). The exit flow direction is then determined by both axial and tangential velocities, which satisfy the equations of motion and continuity.

Although the frequent manual manipulation of the downstream extensions of the blades is eliminated by this method, it should be stressed that the new condition specified by equation (16) is valid only on the downstream stagnation surfaces. Because the static pressure coefficient is not necessarily constant in the tangential direction at any fixed radius, this condition would not prevent a tangential pressure gradient to exist across the stagnation stream surfaces. Consequently, these surfaces have to be set up at the beginning of the numerical process from the exit deviation angles predicted by the design or any approximate method. As the computation proceeds, they can be readjusted after a few cycles from the exit deviation angles derived from the program. With such a procedure, a method for automatically adjusting the stagnation stream surfaces could be relatively easily incorporated in the program.

Although more cycles would have been required for the solution to stabilize, the results of Fig. (5a, 5b, 5c) show that the Kutta-Joukowski condition for the blade pressure distribution is satisfied. Also plotted on Fig. (5a, 5b, 5c) is the experimental rise in static pressure through the inducer. This experimental data is obtained through static taps on the casing and holes drilled on the hub midway between the blades and from static pressure taps on the blade surface. The agreement between predicted static pressure and experiment is good at all radii. The average flow properties obtained by this method at the inducer exit are shown plotted in Fig. (4). The radial distribution

of axial velocity shows a trend similar to that of the experiment (stationary probe measurements). The discrepancy in magnitude between the predicted and experimental results is due to radial velocities induced by viscous effects near the blade surfaces.

The absolute tangential velocity, although substantially higher than the design value, is approximately constant from hub to mid radius and then decreases near the tip. Wislicenus meanstreamline method (reference 17), on which the design of the Penn State inducer is based, predicts deviation angles of the order of 18° at the root and 5° at the tip. These large deviations are probably due to the empirical equation used by Wislicenus for deriving the deviation of the camber line from the mean streamline. These empirically determined deviations are based on NASA cascade tests carried out at moderate solidities. This method is yet to be perfected to make it valid for all types of turbomachinery. Hence the discrepancy between the results of the three dimensional program and the design values may be due to:

1) The three dimensional effects such as blade blockage and the large circumferential extent of the blades,

2) The inaccuracy of the meanstreamline method,

3) The crudeness of the method adopted in this thesis to satisfy the Kutta-Joukowski condition.

The outlet deviation angles are slightly lower than those of the design as shown in Fig.(6). Since the stagger angles of the blades are large, a slight change in deviation angles results in considerable change in absolute tangential velocities. This accounts for the large discrepancy between the predicted and design values of the absolute tangential velocity shown in Fig.(4).

The trend observed for the radial velocity distribution is probably due to blade blockage effect. The experimental values of the radial velocity derived from hot wire measurements, Fig.(12a), are very much higher than the predicted ones. Here also, the importance of the viscous effects which are neglected in the present analysis probably accounts for much of the discrepancy observed. The radial distribution of the static pressure coefficient shown in Fig.(4) is consistent with the absolute tangential velocities and is higher than the design which assumes larger flow deviation angles at the trailing edge.

In summary, it can be concluded that the program with the above modifications for pressure distribution provides a good means for predicting the flow in axial inducers. The accuracy depends on the number of grid points which can reasonably be chosen. An ultimate step would be to include real effects to the solution through the loss terms in equation (12). A loss subroutine was constructed for this analysis but has not been included in any additional run because of cost problems.

The program was used with a Fortran IV H compiler using an optimization procedure which shortens the time required for repetitive calculations. It was executed on an IBM 360-67 approximately ten times faster than the Univac 1107 system used by P. Cooper and H. Bosch.

2.3 Approximate Viscid Solution

The two inviscid analyses carried out so far do not predict accurately the flow in axial inducers. It is apparent that the viscosity of the fluid in the long and narrow passages between the blades accounts for major departure of the flow characteristics from the design values, especially near the tip. In addition, the secondary flows induced by

the interaction between the pressure and suction surface boundary layers near the tip produce complex flows and increase the flow losses. Although the prediction of these radial velocities and the flow losses is extremely difficult, a first attempt to include viscous effects has been made by B. Lakshminarayana (reference 4). In view of the great difficulties involved in solving the complete equations of motion of the turbulent flow inside the passage, B. Lakshminarayana sought to account for the viscous effects in an approximate way by using an empirical pressure loss coefficient derived from various tests carried out at the NASA Lewis Research Center, M.I.T. Gas Turbine Lab., and TRW Cleveland (references 18, 19, 20, 9). This analysis takes into account the three dimensional nature of the flow and energy losses due to friction in solving continuity, axial momentum and circumferentially averaged radial equilibrium equations. The inducer passages are assumed to have fully developed turbulent flow. The assumption for the velocity profiles in both tangential and radial directions are based on the present state of the knowledge of the three dimensional boundary layer, Fig. (7).

An empirical friction loss coefficient applicable to inducers operating at low flow coefficients is derived from tests reported in references (18, 19, 20, 9). The friction loss coefficient λ_R in the following equation is plotted in Fig. (7).

$$\frac{2g_o H_{Loss}}{U_t^2} = \lambda_R \frac{R_{ht}}{\Phi} \frac{1}{R_n^{1/4}} \frac{L_o}{d_h} \left(\frac{\overline{W}}{U_t}\right)^2$$

where, Fig.(7):

H_{Loss} is the head loss due to friction

R_{ht} is the ratio of hub and tip radii

R_n is the Reynolds number Wd_h/ν

d_h is the hydraulic mean diameter $= \frac{4\pi r}{n} \cos \beta$

L_o is the length of the channel

α is the limiting streamline angle with m coordinate

β is the angle of the meridional component of the flow with the inducer axis

The radial equilibrium equation, which incorporates all these assumptions and is valid for any noncavitating inducer, is derived from equation (12). The resulting radial equilibrium equation is,

$$- \frac{0.275}{\cos^2\beta} \overline{W}_\theta \left(\tan \alpha \frac{\partial \overline{W}_\theta}{\partial x} + \overline{W}_\theta \sec^2\alpha \frac{\partial \alpha}{\partial x}\right) + 1.015\, \overline{W}_\theta \cdot \frac{\partial \overline{W}_\theta}{\partial r}$$

$$+ 1.015 \frac{\overline{W}_\theta^{\,2}}{r} - 2\,\Omega\, \overline{W}_\theta + \frac{\partial}{\partial r} \left(\frac{\lambda_R}{R_n^{1/4}} \frac{R_{ht}}{\Phi} \frac{L_o}{d_h} \frac{\overline{W^2}}{2}\right) = 0 \qquad (17)$$

where x is the coordinate parallel to the blade camber line and lying on a cylindrical surface. $\overline{W}_\theta$ and $\overline{W}_m$ are defined on Fig. (7).

The basic assumptions made in deriving this equation are:

1. The loss term F_r in the radial momentum equation is small.
2. The radial gradient in axial velocity is very small at any particular radius.
3. The flow properties are symmetrical about the mid passage (see Fig. (7)).
4. The relative velocity W at any radius is parallel to the mean blade camber line at that radius.

5. $\overline{W}_\theta$ varies linearly with x, the distance along the blade, from leading edge to trailing edge.

6. The angle α between the limiting streamline and $\overline{W}_m$ varies linearly from zero at the leading edge to the maximum measured value at the trailing edge.

In the case of the Penn State inducer, equation (17) reduces to:

$$\overline{W}_\theta \cdot \frac{\partial \overline{W}_\theta}{\partial r} \left(1.015 + 2\,F\,(r)\right) + \frac{\overline{W}_\theta^{\,2}}{r} \left(1.015 + rF'(r) - \zeta\,(r)\right)$$

$$= 2\Omega\,\overline{W}_\theta\,\left(1 - \xi\,(r)\right) \qquad (18)$$

with

$$\zeta(r) = \frac{0.061}{\sin^2\beta}\left(\tan\alpha + \alpha\sec^2\alpha\right)$$

$$\xi(r) = \frac{0.03\,\tan\alpha}{\sin^2\beta}$$

$$F(r) = \frac{1}{2}\,\frac{\lambda_R}{R_n^{\,1/4}}\,\frac{R_{ht}}{\Phi}\,\frac{L_o}{d_h}\,\frac{1}{\sin^2\beta}$$

λ_R is the friction loss factor, derived in reference 4 and shown in Fig. (7). Its validity has been proved for the range of flow coefficients $\Phi = 0.065$ to 0.2. $F(r)$ is shown plotted on Fig. (7) for the three bladed inducer.

Equation (18) is solved for the three bladed inducer with the loss coefficient λ_R given by B. Lakshminarayana. The values of the functions $\zeta(r)$, $\xi(r)$ are the same as for the four bladed inducer, reference 4. The boundary condition assumed for the solution of the differential equation (18) is that the tangential velocity $\overline{W}_\theta$ at hub is the same as

that of design. The predicted value of the absolute tangential velocity V_θ is shown plotted versus radius in Fig. (8). It can be seen that the agreement between predicted values and values measured from a stationary pitot tube at station 4, Fig. (10), is good. The steep rise in tangential velocity near the tip is confirmed by this analysis.

It is quite clear from this analysis that if the precise nature of velocity profiles and shear stresses is known, it is possible to predict the flow accurately. Theoretical and experimental investigation of the boundary layer in a rotating helical channel, currently under investigation in this department, should provide valuable information for the accurate prediction of the flow properties in such low flow coefficient, high solidity inducers.

3. EXPERIMENTAL PROGRAM AND RESULTS

In carrying out the following experiments, the main goal is to investigate as completely as possible the flow characteristics such as time averaged and instantaneous velocities, static and total heads of the relative and absolute flow. The importance of this experimental data for a better understanding and prediction of the flow has been pointed out in section 1.1. It is to be stressed here that this study deals only with the noncavitating performance of the inducer, aimed at understanding the basic flow phenomena.

3.1. Apparatus Used in the Experiment

3.1.1 Three Bladed Inducer

The experimental investigation is carried out in a three foot diameter model designed and built in the laboratory. The inducer test facility is shown in Fig.(1). This model was originally studied with 4 blades, and later with three equally spaced blades. The blades were designed by G. F. Wislicenus and B. Lakshminarayana following the mean streamline method (reference 17). The design blade and flow angles are specified on Fig. (6). The inducer model has a rotational speed of 450 RPM, giving a Reynolds number of 7×10^5 based on tip radius. The RPM is determined to an accuracy of one tenth of RPM by means of a photocell, disk and electronic counter. Important parameters of the inducer are as follows:

Number of blades	= 3
Hub/Tip ratio (outlet)	= 0.5
Tip diameter	= 36.0 inches
Design value of flow coefficient (inlet)	= 0.065
Blade tip velocity	= 71.4 feet/second
Blade chord at	
Tip section	= 82.96 inches
Mid-span	= 63.18 inches
Hub	= 49.94 inches

Holes on the blade suction and pressure surfaces are connected to the metallic tubes embedded in the blade and are used for the limiting streamline angle measurements as well as the blade static pressure measurements. Figure (10) shows the location of the stations of measurement along the inducer axis. Stations 1 and 2 are located inside the blade passage and are used for rotating probe measurements. Station 2a is located slightly outside the blade passage, distant of .25 inches from the blade trailing edge. Hot wire measurements are taken at station 2a.

3.1.2. Conventional Probes

The total pressure probe used for stationary and rotating probe measurements is described in reference 8. The outside and inside diameters of the probe are respectively 0.125 and 0.055 inches. This combination gives a good sensitivity for a Mach number up to 0.045 which is within the range of velocities encountered in the present investigation. The static pressure probe used in the stationary probe

measurements is standard, with four static holes each having a diameter of 0.010 inches and located 0.20 inches from the probe tip.

For the measurement of the flow angles at exit a tuft probe made of teflon material is used. The same type of tuft is used for the qualitative measurement of the radial inward flow at the exit.

3.1.3. Apparatus for Instantaneous Velocity Measurements, Fig. (11a)

Hot Wire Anemometer and Probes:

Two dual channel hot wire constant-temperature anemometers designed and developed by the turbulence group at The Pennsylvania State University are used for this experimentation. Their original circuitry is shown on Fig. (11b), which is slightly modified for higher output voltage level. The Thermo Systems sensors used are made of tungsten hot wires of 3μ diameter and a length to diameter ratio of 700. The probe configuration and mounting mechanism are shown on Fig. (9).

An x configuration probe whose wires are aligned in the tangential and axial directions and a single wire probe aligned in the radial direction are used for these measurements. They are mounted on a traverse gear such that position error is negligibly small (Fig. (9)).

Peripheric Instrumentation

A very low turbulence calibration tunnel built in this laboratory is used for calibration of the hot wires. This wind tunnel has a cross section of 2 x 2 inches and operates within the range of air velocities of 0 to 300 feet per second.

A precision micromanometer manufactured by Flow Corporation is used to obtain the pressure measurements in the investigation. This manometer

has a minimum reading scale of 0.0001 inches. Its accuracy is ±0.09 per cent of the minimum static pressure measured in this particular experimental program.

Digital and RMS voltmeters manufactured by Hewlett Packard and Ballantine Laboratory Inc. respectively are used for instantaneous velocity measurements. The data is recorded on a CEC data tape analog tape recorder at a speed of 3.75 ips and displayed at 30 ips in an analog to digital converter (ADC) unit (Pastoriza Electronics, Inc.). The signals are visualized on a 4 channel storage Tektronix 600 oscilloscope. Finally, the digital tapes are processed by the University IBM 360-67 and IBM 1401 (calcomplotter) computers.

A block diagram of the instrumentation used for the instantaneous velocity measurements is shown in Fig. (11a).

3.1.4. Pressure Transfer Device (PTD)

A one channel pressure transfer device is used for the rotating probe measurements and is described in details in reference 3. This device is mounted inside the hub nose cone of the model inducer and connected to a micromanometer. A similar ammonia transfer device is used to transfer ammonia from a static container to the location at which limiting streamline angles are to be measured.

3.2 Flow Survey at the Exit Using Stationary Probes

A complete flow survey at the exit of the inducer is carried out at stations 3, 4, 5 and 6 shown in Fig. (10). Total pressure and angles of the absolute flow are measured using total and tuft probes. The static pressures are measured at the hub and annulus walls at these

stations. The radial distribution of the static head coefficient is derived by using the simplified radial equilibrium equation near the walls,

$$\frac{1}{\rho}\frac{\partial p}{\partial r} = \frac{V_\theta^2}{r}$$

This distribution has been compared with the one derived from a static probe and both were found to be consistent. These results are discussed and compared with similar measurements made for the four bladed inducer previously studied in this department and reported in references 4 and 5.

Stagnation and Static Pressure Coefficients

The radial distribution of stagnation pressure coefficient (ψ_t) and static pressure coefficient (ψ_s) at various stations are shown plotted and compared with the higher solidity four bladed inducer results in Fig. (19a).

The static pressure coefficients are found to be consistently higher than those of the four bladed inducer (about 35 percent) at all radii. Surprisingly the radial gradient of static pressures remains the same in both cases. A slight decrease in the gradient is observed as the flow proceeds downstream, Fig. (19a).

The stagnation pressure coefficients are found to be about 15 to 20 percent higher than those of the four bladed inducer except near the tip. Furthermore, it can be observed by comparing ψ_t distribution at station (3) and (4) that the mixing losses downstream of the present inducer still exist but in fact are appreciably lower than those of the four bladed inducer. Even though the steep increase in the values of ψ_t towards the tip is there even in the present case, this steep rise is confined to a smaller portion of the blade height near the tip than

the one measured in the four bladed inducer. There is appreciable improvement in the stagnation head distribution from hub to mid radius. No appreciable improvement in the head distribution is observed near the tip, and hence additional modifications in the form of boundary layer control or redesign are necessary to obtain an acceptable energy distribution.

Radial Distribution of Axial Velocity

The radial distribution of axial velocities at station 3, 4, 5, 6 is shown plotted in Figure (19b).

The back flow is present at all downstream stations except at station 3. At station 3 the radial distribution of axial velocity is more uniform than that observed in the four bladed inducer and has appreciably higher value at mid radius. This indicates that the blade blockage effect which is higher in the case of a four bladed inducer has appreciable effect on the axial velocity distribution at the trailing edge of the blades. The axial velocity profiles show a marked deterioration from that observed in the four bladed inducer at all other stations. The extent of back flow region near the hub is appreciably higher than that of the four bladed inducer.

The predicted axial velocities from the exact analysis described in section 2.2.2 are shown plotted and compared with experimental values for the three bladed inducer in Fig.(4). This plot shows the influence of the blade blockage. It is clear, from the observed discrepancy between the predicted (inviscid) and measured values, that it is essential to include the radial velocity induced by viscous effects for accurate prediction of axial velocity.

Radial Distribution of Absolute Tangential Velocities

The radial variation of absolute tangential velocities is plotted in Figure (19c).

At stations 4 and 5 the tangential velocities from hub to mid radius are higher than those observed in the four bladed inducer whereas from mid radius to tip a slight decrease is observed. To some extent there is an improvement in the V_θ distribution. These measurements are consistent with stagnation head rise coefficients described earlier. Even though the average increase in tangential velocities is small, there is considerable (about 15% to 30%) increase in stagnation head coefficients at these locations. The ratio of the actual head to the Euler head is a measure of the hydrodynamic efficiency. It is clear that there is appreciable decrease in the frictional effects when the solidity is decreased. The hydrodynamic efficiencies are generally higher in the case of three bladed inducer. Further improvement in the performance is possible only by boundary layer control.

The measured V_θ is shown compared with values predicted from inviscid theory and approximate viscid theory on figures (4) and (8) respectively.

Hub and Annulus Wall Static Pressures

Wall static pressure coefficients measured on the hub wall with the aid of a pressure transfer device and on the annulus wall are plotted in Fig. (20) and (21) respectively.

The values of pressure coefficient measured at all axial stations are considerably higher than those of a four bladed inducer. Furthermore, the negative radial pressure gradient observed at some of the axial

stations of a four bladed inducer has almost disappeared. The magnitude of the negative pressures observed near the leading edge is considerably reduced in the present case. These results again confirm substantial improvement in the flow behavior when the solidity is decreased.

3.3. Instantaneous Velocity Measurements at Inducer Exit

3.3.1. Abstract of the Method

In order to obtain a better understanding of the flow phenomena in axial flow inducers, an attempt is made to measure all three components of the three dimensional instantaneous velocity at the inducer exit using a three hot-wire probe and the associate equipment described in section 3.1.3, Fig. (11a). As pointed out earlier in Chapter 2, the radial velocity components are the most difficult to predict and measure. However, from a good knowledge of their magnitude and distribution, considerable improvement can be made in the prediction of the flow.

The block diagram describing the method of measurement and the equipment required is shown on Fig. (11a). Those measurements are taken at station 2a, Fig. (10), which is located a quarter of an inch from the trailing edge of the blades. Since the radial velocity decays rapidly downstream of the trailing edge, it is essential to carry out these measurements as close to the trailing edge as practicable. Since the three components of the velocity constitute three unknowns, it is necessary to use three sensing wires to derive the magnitudes of the three velocity components (V_θ or W_θ, V_r, V_z). The probe traverse

mechanism set up on the annulus wall is fixed tangentially, but is movable in the axial and radial directions (Fig. (9)).

The three signals picked up from the hot wire anemometers are memorized in a magnetic tape, then digitized on an analog to digital converter unit, (ADC), to be finally processed on an IBM 360-67 computer, Fig. (11a).

Considering the fixed frame of reference r, θ, z, each one of the three wires is aligned with one of the coordinate axes. The three non-linearized voltage signals picked up by the probe are called E_1, E_2, E_3. Since the angle between the wire in θ direction and the resultant velocity is very small, a correction to the deviation of the cosine law is used. According to King's law, the signals picked up by the three sensors are,

$$E_1^2 = A_1 + B_1 \, (V_{z\theta})^{1/2}$$
$$E_2^2 = A_2 + B_2 \, (V_{zr})^{1/2} \qquad (19)$$
$$E_3^2 = A_3 + B_3 \, (V_{r\theta})^{1/2}$$

The sensitivity of the hot wire to the flow direction is generally assumed to be given by the normal component or cosine law, whereby the effective cooling velocity is obtained from the magnitude of the vector component of the free stream normal to the axis of the wire. However, it has been proved that the finite values of the length to diameter ratio, l/d, of the hot wires produce deviations from the cosine law. According to the sketch below, the effective cooling velocity V_e in a free stream V_o is

$$V_e = V_o \, (\cos^2 \sigma + k^2 \sin^2\sigma)^{1/2}$$

σ being the angle of incidence between the free stream direction and the normal to the axis of the wire, and k is an experimentally determined parameter reflecting deviations from the cosine law. This deviation is important in the case of the wire sensing the resultant of the radial and axial velocity as shown in the following sketch:

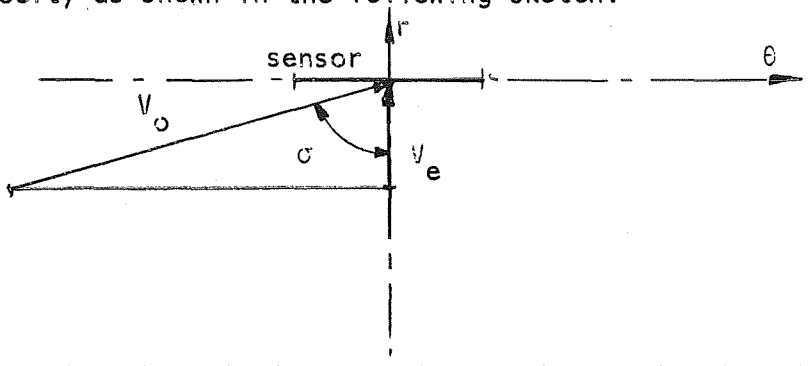

With this correction the velocity sensed by each wire is given by:

$$V_{z\theta} = (V_\theta^2 + V_z^2)^{1/2}$$

$$V_{zr} = (V_z^2 + V_r^2 + k^2 V_\theta^2)^{1/2}$$

$$V_{r\theta} = (V_r^2 + V_\theta^2)^{1/2}$$

leading to the following equations:

$$V_\theta^2 = \left(\frac{V_{z\theta}^2}{2} - \frac{V_{zr}^2}{2} + \frac{V_{r\theta}^2}{2}\right) / \left(1 - \frac{k^2}{2}\right)$$

$$V_r^2 = \frac{1-k^2}{1-k^2/2} \quad \frac{V_{r\theta}^2}{2} - \frac{V_{z\theta}^2}{2-k^2} + \frac{V_{zr}^2}{2-k^2} \qquad (20)$$

$$V_z^2 = \frac{1-k^2}{2-k^2} \quad V_{z\theta}^2 - \frac{V_{r\theta}^2}{2-k^2} + \frac{V_{zr}^2}{2-k^2}$$

W. H. Schwarz and C. A. Friehe (13) have carried measurements for the deviation from the cosine law which give for this case a correction factor of k = 0.26 for l/d = 700. With this correction, the coefficients in the above equations are:

$$1 - \frac{k^2}{2} = .966$$

$$1 - k^2 = .932$$

Since the radial and axial velocities are an order of magnitude lower than the tangential velocity these corrections are not small. The relative velocities are then given by,

$$W_r = V_r$$

$$W_\theta = V_\theta - \Omega r \qquad (21)$$

$$W_z = V_z$$

The signal processing is carried out in five steps:

1) The signals from the tape recorder are digitized in the ADC unit as input data for the computer program reproduced in Appendix 2.

2) The digitized values of the signals are arranged in two dimensional arrays, this being dictated by the averaging method discussed in the following section.

3) All digitized values are then linearized individually according to equation (19), with the parameters A_1 and B_1 accurately determined by probe calibration.

4) Then the values of the resultant velocities are obtained from equations (20) and (21) to give the three components of the instantaneous velocity, and averaged over consecutive blade passages (see section 3.3.2).

5) Finally the turbulent intensity is computed for each component (see section 3.3.3).

A computer program written for processing the digitized data is given in Appendix 2.

3.3.2. Averaging Procedure

The three signals are functions of time with a periodicity equal to three times the rotative speed of the machine. The only requirement for the condition that each sample of the signal corresponds to the same θ location within the blade passage is that the sampling frequency be a multiple of the periodicity of the signal. In other words, the following relationship has to be satisfied between the signal frequency (3Ω), the number of samples n_o within the blade passage and the sampling frequency f of the ADC unit:

$$n_o \times 3\Omega = f \tag{22}$$

The ADC unit used in the Department of Aerospace Engineering of The Pennsylvania State University has a fixed digitizing speed of 9000 words per second/per channel. Hence, the number of sampling points within the blade passage would be 400 for Ω = 450 RPM. Because of data blocksize limitations, this number n_o is reduced to 50 by artificially multiplying the frequency of the signals 3Ω by 8 with the ability of the analog tape recorder to record at 3.75 IPS and display at 30 IPS.

A nine track digital tape is used to transfer the data to the computer which has a blocksize reading capacity of 12384 words at a time. This consideration limits the number of sets of 50 points equally spaced along one blade passage to 80. Thus the number of data available for determining the time average velocity or turbulence intensity at any of the 50 passage positions is eighty.

Hence the blade to blade distribution of time averaged velocity is obtained through the averaging of the 80 consecutive sequences:

$$80 \left\{ \begin{array}{l} e_1^1,\ e_2^1,\ e_3^1 \ldots\ldots e_{50}^1 \\ e_1^2,\ e_2^2,\ e_3^2 \ldots\ldots e_{50}^2 \\ \vdots \qquad\qquad\qquad\qquad \vdots \\ e_1^{80},\ e_2^{80},\ e_3^{80} \ldots\ldots e_{50}^{80} \end{array} \right.$$

The fourth channel of the ADC unit is used as a control for the read out of the data by the computer.

3.3.3. Accuracy Criteria and Limitations

A rough estimate of the accuracy of the blade to blade distribution of time averaged velocity is derived from reference 7. It is assumed that each instantaneous value within the blade passage is statistically independent. This assumption is supported by the fact that each value belongs to a physically different blade passage and that the integral scale T of the process could not be more than one period. The accuracy obtained is then given by (see Appendix 1):

$$\varepsilon^2 = \frac{(T)^2}{N} \tag{23}$$

ε is the difference between the actual average and the expected value, divided by the expected value. T is the turbulence level, that is the Root Mean Square (RMS) value of the fluctuating velocity divided by the expected value E{V} of the velocity. N is the number of samples averaged upon.

The turbulence measurements described in the following section have pointed out a turbulence intensity of 10 to 15% for the relative velocity W, 75 to 80% in the radial direction (based on mean radial

velocity), and 15 to 20% in the tangential direction. The corresponding estimate for the precision ε is, according to equation 23 and with $N = 80$,

$$\begin{cases} 1.12 \text{ to } 1.7\% \text{ for } W \\ 8.35 \text{ to } 9\% \text{ for } V_r \\ 4.5\% \text{ for } V_z \\ 1.67 \text{ to } 2.24\% \text{ for } V_\theta \end{cases}$$

Theoretically, these values may seem small and quite acceptable. However, during the course of the experiment some qualitative limitations were noticed. These limitations are:

1) It was pointed out in section 3.2.2 that the relationship (22) has to hold in order for the samples taken to be at a fixed location between the blades. Digitizing rate and analog tape recorder speeds are known to be accurate. However the inducer rpm can only be held fixed at ± 1/10 of a rpm of the nominal rotative speed (450 rpm). This could have led to a corresponding maximum shift of 2.3° in the θ location of the samples over the entire averaging period. This represents 2 per cent of the blade spacing. Since the velocity gradients are not very large, a change in 1/10 of a RPM during the sampling time is unlikely to introduce any appreciable error.

2) One of the very important limitations of this method lies in the fact that a three wire sensor can only detect the magnitudes of the flow along each coordinate direction without providing any indication as to the directions of the velocity. This is particularly true for the radial component of the velocity which is expected to reverse inside the passage near the blade tip.

3) Finally, the limitations of the ADC unit contribute to the accuracy of the method through its minimum increment while digitizing a fluctuating voltage. The maximum positive voltage accepted is 4 volts, divided in 128 windows, thus fractioning it in 0.031 volts increments which correspond to jump in velocity of 1.5 ft/sec for a fluid velocity fluctuating around 20 ft/sec or 2.3 ft/sec for a fluid velocity fluctuating around 40 ft/sec. As can be seen from Figures (13), (14), (15), (16), the velocity profiles are not smooth even through the combined effect of turbulence and averaging.

Turbulence Intensity Measurements

The method of signal processing explained earlier is extended to turbulence intensity calculation. Since the instantaneous values of the three components of the velocity together with the averaged values are known for each sampling point within the blade passage, the root mean square of the fluctuating components of the velocity divided by the averaged value at each point are computed by the program.

As in most turbulent cases, the probability density of the velocity is approximately Gaussian so that an expression for the accuracy of those results can be derived (see Appendix 1);

$$E = \sqrt{\frac{2}{N}} \qquad (24)$$

E is an estimate of the accuracy of the measurements, giving 16% accuracy for N = 80.

3.3.4. Blade to Blade Distribution of Time Averaged Velocities at The Exit.

The blade to blade variations of the three components of the absolute velocity at station 2a(Fig. (10)) are obtained at seven radii. The values at four typical radii near hub (R = .582), mid radius (R = .752), tip (R = .920) and halfway between mid radius and tip (R = .860) are shown plotted in Figures (13, 14, 15, 16) respectively. In these figures the blade locations are identified on the basis of the measurement of turbulence intensities which are likely to be maximum at the center of the wake.

1) Radial Velocity

The blade to blade distribution of radial velocities derived from hot wire measurements are plotted in Figures (13a, 14a, 15a, 16a) for R = .582, .752, .860, .960 respectively. The radial velocity distribution near the hub (R = .582), plotted in Fig. (13a), is almost linearly decreasing from pressure to suction surface except in a small region near the blade surface. The radial velocity outside the blade surface region can be attributed to blade blockage. At R = 0.752, the radial velocity distribution normally encountered inside the boundary layer of a rotating blade can be observed (Fig. (14a)). The radial velocity is maximum very near the blade surfaces and is of appreciable magnitude at all other regions. The trend in radial velocity observed gives no indication as to the presence of a radial inward flow.

At R = 0.860, the maximum radial velocity occurs near the suction surface. It should be emphasized here that the hot wire sensors can detect only the magnitude and not the direction of the radial velocity. Hence it is quite probable that a small region within the passage beyond

the point A (Fig. (15a)) has radial inflow as compared to radial outflow at all other regions. The tuft probe mounted at the exit does reveal the presence of radial inward flow at this radius. Thus the peak observed at point B in Fig. (15a) might represent the magnitude of the maximum radial inward velocity.

The radial velocity distribution plotted in Fig. (16a) for R = 0.920 shows the presence of large radial inward flow. The maximum radial velocity region corresponds to the mid passage. In an earlier report (reference 5), a possible explanation for the existence of minimum relative velocity inside the blade passage is given. This region corresponds to the location where the radial inward flow is maximum.

The blade boundary layer region in which the radial outflow occurs is small. This is confirmed by rotating probe measurements to be described later (see Fig. (17b)).

Also apparent from Fig. (13a, 14a, 15a, 16a) is the fact that the magnitude of the radial velocity increases from hub to tip. It can be seen from Fig. (14a) that the suction surface boundary layer is larger than that of the pressure surface. Also the radial outward flows inside the pressure and suction surface boundary layers decrease towards the tip (compare Figures (15a) and (16a).

The radial velocities very near the suction and pressure surfaces derived from the measurement of the limiting streamline angle ε_w (see section 3.5.1) are shown plotted in Fig. (14a, 15a, 16a) and compared with hot wire measurements. The discrepancy observed is within experimental error.

It is to be noticed here that the gradient in radial velocity $\frac{\partial V_r}{r\partial\theta}$ is not as large as measured by Jabbari (3) on a rotating helical blade.

Since the turbulence level is high, the boundary layer wakes are likely to diffuse very fast as the flow proceeds downstream, thus considerably decreasing the velocity gradients in the tangential direction.

Furthermore, the radial velocities plotted in Fig. (13a), (14a), (15a), (16a) are of the same order of magnitude as the axial velocities.

2) Absolute Tangential and Axial Velocity Distribution

The absolute tangential velocity near the hub (R = .582), mid radius (R = .752), halfway between mid radius and tip (R = .860), and at the tip (R = .920) are shown plotted in Figures (13b), (14b), (15b), (16b) respectively. The distribution observed is generally uniform with maximum tangential velocity at the blade locations from hub to mid radius. At R = 0.86 and 0.92 (Fig. 15b, 16b) where there is a likelihood of radial inward flow outside the blade boundary layers, the tangential velocity is maximum within the blade passage. Also shown plotted in Figures (13b), (14b), (15b), (16b) are the axial velocity distributions. The blade to blade profiles are also surprisingly very uniform, with minimum axial velocities at the blade locations, as apparent in Fig. (14b).

3) Relative Velocity

The relative velocity distributions from blade to blade at the four radial positions reported here are shown plotted in Fig. (13b), (14b), (15b), (16b). From hub to mid radius the maximum relative velocity is located approximately at mid blade passage, whereas from mid radius to tip the maximum occurs near the blade locations. Also plotted on these Figures is the relative velocity distribution obtained from rotating probe measurements (see section 3.4). Although there is a discrepancy in magnitude between the two measurements especially near the tip, the

trend observed is similar. The reason for this discrepancy between the two measurements is given in section 3.3.5.

3.3.5. Passage Averaged Values of Velocities at the Exit

The blade to blade velocities discussed in section 3.3.4 are averaged over the blade passage. These are plotted in Fig. (12a),(12b) and compared with stationary and rotating probe measurements reported later. The good agreement between the axial velocity profile at station 2a derived from instantaneous velocity measurements and stationary probe (section 3.2) is evident from Fig. (12a). Also evident from this figure is the fact that the radial velocity measured is of the same order of magnitude as the axial velocity and increases from hub to tip. It is to be noted here that the average refers to $\overline{|v_r|}$ and not $\overline{v}_r$.

The magnitude of averaged radial velocities ($\overline{|v_r|}$) plotted in Fig. (12a) confirms the earlier conclusion that the viscid and real fluid effects account for much of the flow characteristics at exit. Shown plotted in Fig. (12b) is the radial distribution of absolute tangential velocity at station 2a compared with stationary probe measurements. Although the trend of the two measurements is the same, with a large positive gradient near the tip, there is appreciable discrepancy between the two measurements. Part of this discrepancy is due to the fact that the stationary probe reads the resultant of the tangential and radial velocity (when the radial velocities are small compared to tangential velocities) without providing any means of deriving them separately. This accounts for about half of the discrepancy between the two measurements. The remaining discrepancy must be attributed to the experimental error. One possible source of error is due to the sensitivity of the

hot wire sensing V_{zr} to the deviation from the cosine law (section 3.3.1). The corrected data derived from reference (13) lacks in accuracy for the particular extreme case of $l/d = 700$.

Also shown plotted in Fig. (12b) is the relative velocity at station 2a derived from instantaneous velocity measurements, compared to rotating probe measurements at station 2. The design value is also shown together with the corresponding rotating probe measurements at station 2 for the four bladed inducer. The discrepancy between instantaneous and rotating probe measurements can be partially explained by the flow redistribution that takes place between station 2 and 2a.

Nevertheless, an appreciable decrease in relative velocity can be noted between 3 and 4 bladed inducers at exit. This is consistent with a corresponding increase in static head. A large loss region is still present near the tip although it is somewhat reduced from that of a four bladed inducer.

3.3.6. Blade to Blade Distribution of Turbulence Intensity

The instantaneous and time averaged values of the three velocity components reported earlier are used to derive the turbulence components in all the three directions at various locations of the blade passage. The definitions for turbulence intensities used in this thesis are as follows:

$$T_r = \frac{\overline{(v_r'^2)}^{1/2}}{\overline{|V_r|}} \qquad T_z = \frac{\overline{(v_z'^2)}^{1/2}}{\overline{V_z}}$$

$$T_\theta = \frac{\overline{(v_\theta'^2)}^{1/2}}{\overline{V_\theta}} \qquad T_w = \frac{\overline{(w'^2)}^{1/2}}{\overline{W}}$$

The accuracy of these turbulent intensities which are based on only eighty samples is given in section 3.3.3.

The turbulent intensity components are shown plotted from blade to blade at R = .752, .860, .920 in Figures (13c and d, 14c and d, 15c and d, 16c and d) respectively.

The Radial Component T_R

The radial component of the turbulence intensity shown plotted in Fig. (13d), (14d), (15d), (16d) for R = .582, .752, .860, .920 respectively is nearly uniform from blade to blade. However, near the hub (Fig. (13d)) the maximum is well marked at the blade locations and the turbulent intensity increases from suction to pressure surface, whereas near the tip the distribution is more uniform (Fig. (16d)). The passage averaged turbulent intensity in the radial direction increases from about 70% near the hub to 75% at mid radius and tip. A slight maximum of 78% is found between mid radius and tip, Fig. (15d). This is consistent with the observation that there is large flow mixing due to the interaction between the pressure and suction surface boundary layers somewhere between mid radius and tip.

The Axial Component T_z

The axial component of the turbulence intensity is shown plotted in Fig. (13c), (14c), (15c), (16c) at the same radial stations as above. Near the hub peaks in turbulent intensity are apparent at the blade locations, whereas near the tip it appears to be randomly distributed. Turbulence intensity in the axial direction appears to be approximately

constant from hub to tip around 40%, with a slight maximum of 43% in the boundary layer interaction region located between mid radius and tip.

The Tangential Component T_θ

Shown plotted in Fig. (13c), (14c), (15c), (16c) is the tangential component of the turbulent intensity. Much more uniformly distributed than the components in the radial and axial directions, the tangential component is approximately constant from hub to tip around 20%, with a slight maximum at the blade locations.

Turbulent Intensity T_w

The turbulence intensity of the relative flow is shown plotted in Fig. (13d), (14d), (15d), (16d) at the same four radial stations from hub to tip. The distribution seems to be very uniform from blade to blade across the wake. The intensity is approximately constant from hub to tip around 14%.

One of the major conclusions from these results is that the flow is generally very turbulent. The radial and axial components of the turbulence are maximum somewhere between the mid radius and tip. It was anticipated that the mixing and large radial motions due to boundary layer interactions at these locations of the blade passage would show a substantial change in flow properties from the rest of the blade passage. This is confirmed by this experiment.

3.4. Flow Survey Inside the Blade Passage Using Rotating Probes

To find the flow properties inside the blade passage the flow is surveyed at station 2 (Fig. (10)) using a rotating pitot tube and a pressure transfer device described in sections 3.1.2, 3.1.4. The stagnation head $(\psi_T)_R$ of the relative flow from blade to blade is determined at ten radial locations at station 2. The static pressures ψ_s at corresponding radii are taken from holes drilled on the pressure and suction surfaces. These static pressures are assumed to vary linearly from pressure to suction surface. The relative velocities are then derived from $(\psi_T)_R$ and ψ_s.

The blade to blade distributions of the stagnation head of the relative flow and the static pressure coefficient at 10 radial stations from hub to tip, at station 2 (Fig. (10)), are shown in Fig. (17a-j). Also shown plotted on these figures is the corresponding relative velocity.

The usual flow turning effect in addition to the boundary layer growth on the blade can be seen from the relative velocity plots for R = 0.506 through R = 0.720 (Figures 17f - j). The boundary layer growth on the suction surface is generally higher than that of the pressure surface. However it seems that the extent of the pressure and suction surface boundary layers have diminished considerably compared to the four bladed inducer (Ref. 5), Figures (17a),(17d),(17j). From hub to about mid radius Fig. (17f - j), the blade to blade distribution of relative stagnation head is uniformly distributed and rather constant, whereas from mid radius to tip it decreases from pressure to suction surface Fig. (17a - e).

The relative velocity increases from pressure surface to suction surface from hub to mid radius due to the usual flow turning effect (Fig. 17f - j), where as from mid radius to tip a minimum is noticeable within the passage located nearer to the suction surface (Fig. 17a - e). Also, it can be seen from Fig. (17d) that the trend of the relative velocity is unusual in that it decreases from pressure to suction surface. This distribution of relative velocity is unconventional, and is probably caused by the interaction effect between the blade boundary layers which generates a large radial inward flow within the blade passage. The variations in radial velocities from blade to blade are thus large, causing the type of profile observed in Fig. (17a - d). This effect is most noticeable at radius R = .808, Fig. (17d), where the radial inward flow is likely to be maximum within the blade passage. Similar conclusions are reached from instantaneous velocity measurements and the relative velocities obtained by both methods are shown compared in Figures (17b, 17e, and 17h). It is to be observed that radial velocities and turbulent intensities (T_R, T_z) are maximum here (See Figures 15a, 15c). Although the trend observed is the same, the discrepancy between the two measurements has been explained in section 3.3.5, and is partly due to experimental error.

The three bladed and four bladed inducer results are compared in Figures (17a, d, j). It can be observed from these figures that while the static pressure coefficients have increased from three to four bladed inducer, the stagnation head of the relative flow has nearly remained the same. Consequently, a decrease in relative velocity is observed in the case of three bladed inducer (See Figures (17a, d, j).

Also, the head and relative velocity profiles are more uniform than in the case of the four bladed inducer from hub to mid radius.

3.5. Flow Visualization Method

As explained in reference (4), a knowledge of the limiting streamline angles on the blade surface provides very useful information on the nature and magnitude of the radial flows and the direction of the wall shear stress. With a view to obtain this information for a future theoretical solution of the flow, an attempt is made to derive these angles by ammonia streak technique and smoke produced by titanium tetrachloride.

1) Limiting Streamline Angle on the Blades.

The method of deriving the limiting streamline angle on the blades at the leading edge has been described in reference 3. A solution of titanium tetrachloride and carbon tetrachloride is prepared. When exposed to the airflow, this solution generates a white, dense smoke capable of being photographed. The mixture is brushed on the surface of the blade and photographs are taken while the blade is rotating. The deflection of the smoke filament from the tangential direction gives an indication of ε_w. The results of this measurement at the leading edge are shown plotted in Fig. (18) and compared with four bladed inducer results. ε_w is seen to be decreasing linearly from hub to tip, where its value reaches nearly zero. Surprisingly ε_w at the leading edge is lower than in the case of the four bladed inducer.

The second method to derive the limiting streamline angle at exit is the ammonia streak filament method. The static pressure holes drilled on the surface of the blade (see section 3.1.1) are used in

combination with the ammonia transfer device. A small amount of ammonia gas at low velocities is fed into the tubes at various tangential and radial locations of the blade surface. A sheet of ozalid paper sensitive to ammonia is pasted along the edges of the static holes and traces of ammonia are recorded on the ozalid paper while the inducer is in rotation. The results of the measurement of ε_w at trailing edge on suction and pressure surface are shown in Fig. (18) and compared with the four bladed inducer results. ε_w on the suction surface is seen to decrease from 50° at mid radius to zero at tip near the trailing edge. Its value is generally higher than the corresponding ε_w for the four bladed inducer, where as ε_w is lower on the pressure surface. Furthermore, the magnitudes of ε_w are generally higher than those observed on a single helical blade, (reference 3). These results suggest that radial velocities encountered in inducer passages, where considerable velocity and pressure gradients exist in all directions, are generally higher than those observed on a single helical blade.

2) Tuft Grid at Exit

The maximum deviation of the streamlines from the cylindrical surface (ε_o), outside the blade boundary layer regions, and obtained from a tuft grid mounted at exit of the inducer is shown plotted in Fig. (18). Although there are appreciable radial inward flows from mid radius to tip, their magnitudes are generally lower than those of the four bladed inducer. This confirms the earlier observation that the blade boundary layer's interaction effects can be reduced by decreasing the solidity of the inducer.

4. DISCUSSION

Three Bladed Inducer Performance

Axial Velocity

The outlet radial distribution of axial velocity derived from stationary probe measurements shown plotted in Fig. (19b) at several axial stations indicate that the backflow region near the hub originates at the trailing edge and extends downstream. The flow separation zone reaches 50% of the annulus region far down stream of the inducer. A large flow redistribution is seen to occur between stations 3 and 4, probably due to large axial gradients in radial velocity. The axial velocity perturbation at exit obtained from the blade blockage analysis of section 2.1,plotted in Fig. 19b,seems to indicate that blade blockage effects are not negligible in the case of the Penn State inducer. Furthermore, the qualitative trend of the distribution is predicted at stations 3 and 4, thus accounting for the part of the change in axial velocity downstream. The agreement between instantaneous velocity and stationary probe measurements for the axial velocity is good (Figure 12a).

The comparison between measured axial velocity at station 4 and the predicted values derived from the exact inviscid analysis described in section 2.2.2 shows that the three dimensional inviscid effects on axial velocity are not small. However, the three dimensional inviscid solution does not predict the back flow near the hub and the very steep gradient near the tip. This shows that an accurate prediction of the flow at the exit of inducers has to include viscid effects. In an earlier report (references 4, 5) it is argued that all the deviations in axial velocity are due to viscid effects. The present analyses tend to indicate that

this is not quite true and that three dimensional inviscid effects account for some of the deviations. The blade to blade variation of axial velocity is very uniform at all radii from hub to tip, with a slight minimum at the blade location, Fig. (13b). The axial component of the turbulence intensity from blade to blade at exit and at several radii is also surprisingly uniform throughout the blade passage with value around 40%.

Radial Velocity

The averaged radial velocity ($|\overline{V_r}|$) at station 2a increases from hub to tip, Fig. (12a). The radial velocities, derived from three dimensional hot wire measurements, are found to be of the same order of magnitude as the axial velocity in the entire passage. The departure between the predicted (Fig. (4)) and the measured radial velocities at outlet is very large. A major reason for the existence of the radial velocity in the passage is due to viscid and real fluid effects. The blade to blade distribution of radial velocity between mid radius and tip, Fig. (15a), (16a), is found to be characteristic of three dimensional boundary layer interaction effects. The flow visualization indicates the presence of large radial outward flow within the blade boundary layers and radial inward flow within the blade passage from mid radius to tip. These measurements confirm the reliability of the radial velocity profiles derived from hot wire measurements (see Fig. (15a), (16a)). These results show that the radial velocities encountered in inducers are of the same order of magnitude as the axial velocity, at least near the exit of the blade passage.

Absolute Tangential Velocity

The radial distribution of absolute tangential velocity indicates a steep rise in the values near the tip (Fig. (19c)). Furthermore, there is considerable change in the tangential velocity as the flow proceeds downstream. Fig. (4) shows the comparison between the predicted tangential velocity at exit using the three dimensional analysis of section 2.2.2, and the experimental value at station 3. The predictions are good from hub to mid radius while the discrepancy is large near the tip. Hence it is obvious that accurate prediction of the tangential velocity predicted by the approximate viscid analysis of section 2.3 agrees well with the experiment (Fig. (8)), thus showing the validity of the pressure loss coefficient derived in reference (4) and plotted in Fig. (7). There is some discrepancy between the tangential velocities derived from hot wire measurements and the stationary probe, Fig. (12b). Part of it is due to the fact that stationary probes sense both the radial and tangential velocity and the remaining could be attributed to the experimental error, since the correction factor for the deviation of the cosine law used in hot wire measurements is not known very accurately for this particular case. The blade to blade distribution of absolute tangential velocity is found to be uniform throughout the blade passage at exit, Fig. (13b), (14b), (15b), (16b), with maximum values at the blade location from hub to mid radius. The maximum tangential velocity occurs outside the blade boundary layer near the tip region. The tangential component of the turbulent intensity has a maximum value of 22% in the boundary layer interaction zone which is located between mid radius and tip.

Relative Velocity

The relative velocity increases from hub to about mid radius and is very close to the design values (Fig. (12b)). From mid radius to tip, the departure between the design and measured values is very large thus indicating a major flow departure and large mixing losses in this region. The discrepancy between the rotating probe and hot wire measurements for the relative velocity is due to the differences in the methods explained earlier. It should also be noted that the rotating probe measurements are taken within the passage at station 2, while the hot wire measurements at station 2a are taken outside the blade passage. Thus, part of the discrepancy is more apparent than real due to the flow redistribution. The blade to blade variation of relative velocity, shown plotted in Fig. (13b), (14b), (15b), (16b) for four radial stations at exit, is nearly uniform indicating the fast decay of the blade wakes. From hub to mid radius, the maximum value for the relative velocity seems to occur near the blade locations.

The turbulence intensity of the relative flow shows a uniform trend near the tip, whereas maximum values at the blade location are noticeable near the hub, (Fig. 13d)). The average value of the turbulence intensity T_W is found to be about 13%.

The reliability of the blade to blade distribution of the relative velocity is confirmed by the comparison between hot wire and rotating probe measurements at three radial stations, Fig. (17b), (17e), (17h). Although the discrepancy in magnitude noted earlier is there, the trend observed is the same. These measurements have provided some valuable information for the theoretical prediction of the flow field including viscous effects.

Comparison of Three and Four Bladed Inducer Performance

From the results reported in this thesis and reference 5, it is found that the three bladed inducer has appreciably better performance than the similar four bladed inducer tested at the same flow coefficient. In particular, the following conclusions can be drawn from the investigation of the flow in three bladed inducer.

1) The stagnation and static head rises are appreciably higher than those of a four bladed inducer at all radii. Even though the steep rise for the head coefficients towards the tip is still present, their gradients are somewhat reduced. Further improvements may be possibly by boundary layer control on the blades. The increase in the values of ψ_t in the case of a three bladed inducer from those of the four bladed inducer is of the order of 15 to 30 per cent.

2) The axial velocity profiles show a marked deterioration from that of a four bladed inducer. There is an increase in the extent of backflow near the hub compared to that of a four bladed inducer. The axial velocities near the blade tip are found to be generally higher than those of a four bladed inducer.

3) There is no appreciable difference in absolute tangential velocities measured at the exit of the two inducers. This indicates an improvement in hydrodynamic efficiency which is defined as the ratio of the actual head to the Euler or ideal head rise.

4) There is considerable improvement in hub wall and annulus wall static pressure distribution. The negative pressures observed near the leading edge of a four bladed inducer are appreciably reduced in the case of a three bladed inducer, Fig. (20). Furthermore, the negative radial

pressure gradient measured in the case of a four bladed inducer at some axial stations has completely vanished in the present case.

5) The relative velocities at the exit are generally lower than the four bladed inducer, especially near the tip. This is consistent with the increase in static pressure observed in the case of three bladed inducer. The flow mixing losses near the tip appear to have decreased.

6) There is substantial improvement in the uniformity of the blade to blade distribution of relative velocities inside the blade passage. The extent of the blade boundary layers seem to have appreciably diminished.

7) The amplitude of the radial inward flow within the blade boundary layer interaction region seems to have been reduced considerably in the case of the three bladed inducer.

Further improvement of the flow characteristics could probably be achieved by boundary layer control on the blade and by a reduction in blade thickness. An improved analysis for the prediction of the flow field at exit should be based on a better knowledge of the radial velocities inside the blade passage. Reliable information on these radial velocities could come from the study of the three dimensional boundary layers in a rotating helical channel, currently under investigation at the Department of Aerospace Engineering of The Pennsylvania State University.

5. CONCLUSIONS

The following conclusions may be drawn from the theoretical and experimental investigations reported in this thesis.

1) The perturbation of the meridional flow caused by the radially varying blade blockage is not negligible for the Penn State inducers. The analysis carried out in section 2.1 predicts perturbation of up to 10% in axial velocity at the exit. The axial velocity profile derived from this analysis agrees qualitatively with the experiment.

2) The program developed by P. Cooper and H. Bosch for the exact solution of the inviscid flow field has been somewhat improved to satisfy the Kutta Joukowski condition at the trailing edge and to include the blade blockage effect. The axial velocity profile at the exit derived from this analysis agrees qualitatively with the experiment. The tangential velocities also agree qualitatively with experiment, except near the tip where viscous and turbulent effects are dominant.

This method of solution could be extended to include real fluid effects by including the dominant shear stress terms in the equations of motion. An initial attempt was made in this direction by the use of the boundary layer data and the skin friction coefficient derived by Jabbari in reference 3. In view of the large number of grid points required and the considerable increase in computer time, no attempt was made to run this program.

3) The approximate viscid analysis of the flow carried out in this thesis is based on the assumption of fully developed turbulent flow inside the passages and takes into account the frictional losses. The friction loss coefficient applicable to inducers operating in the range

of flow coefficients $\Phi = 0.065$ to 0.2 derived empirically by Lakshminarayana in reference 5 is used. This friction factor is found to increase exponentially towards the tip. The values of the relative and absolute tangential velocities predicted from this analysis agree closely with the experimental values. However, further refinements in the radial velocity estimate are necessary for the accurate prediction of the axial velocities at the exit of the inducer.

4) A method measuring the three velocity components and the corresponding turbulent intensities is developed. This procedure which utilizes three hot wires located in the coordinate directions has led to valuable information on the blade to blade variation of all the velocity and turbulence intensity components. More precise information on the deviation from the cosine law for the hot wire probes should be obtained since this is one of the many sources of error involved in this method.

5) The radial velocities obtained from the hot wire measurements are found to be of the same order of magnitude as the axial velocities throughout the flow passage. Near the hub, the radial velocities are found to be nearly uniform across the passage and this is presumably caused by the blade blockage. At other radial locations, the radial velocity distribution across the passage is of the type normally encountered in rotating boundary layers.

6) Almost identical axial velocity profiles at the exit are derived by both hot wire and stationary probe measurements. There is considerable decay in axial velocity profiles in the case of the three bladed inducer.

The blade to blade variation of axial velocities measured at the exit by means of hot wire probes is found to be nearly uniform.

7) Appreciable discrepancy is observed in the absolute tangential velocities at the exit measured by stationary and hot wire probes. Steep rises in tangential velocity are present in the case of the three bladed inducer even though the gradients are somewhat lower than those observed for the four bladed inducer.

The blade to blade variation of tangential velocities measured by hot wire probes indicate peaks near the blade locations from hub to mid radius where as at other radii the peaks occur inside the passage. The blade to blade variation of tangential velocity is found to be generally uniform across the passage.

8) There is slight discrepancy in the blade to blade variation of relative velocities measured by the hot wire probe and the rotating pitot tube. However, the trend in their distribution is the same.

The passage averaged relative velocities measured by both methods show a considerable departure from the design values from mid radius to tip. These averaged relative velocities are somewhat lower than those of the four bladed inducer at these radii.

The blade to blade distribution of the relative velocities measured by the hot wires is found to be nearly uniform. This is probably due to considerable wake diffusion that takes place between the trailing edge and the hot wire measuring station.

9) The stagnation and static head rise of the absolute flow are found to be appreciably higher than those of the four bladed inducer at all radii. The steep rise in stagnation head coefficient is still present in the case of three bladed inducer, even though the gradients observed are somewhat reduced.

10) There is appreciable improvement in the hub and wall static pressure distributions. The negative pressures observed near the leading edge of a four bladed inducer are appreciably reduced in the case of a three bladed inducer.

11) The turbulence intensity components in the radial, axial, tangential and relative directions (based on local mean velocities) are found to be about 75%, 45%, 20% and 15% respectively. Although a maximum in radial and axial turbulence intensity is observed in the boundary layer interaction region at R = 0.860, the turbulence intensities are found to be rather uniform in the entire flow passage. These measurements reveal the highly turbulent nature of the flow in inducers and should be extended to the determination of Reynolds stresses.

12) The measurement of the relative flow inside the blade passage obtained by means of a rotating pitot tube also shows the two different flow patterns across the blade passage; from hub to about mid radius the blade to blade distribution of relative velocity and stagnation head of the relative flow show the usual trend characteristic of flow turning. From mid radius to tip the interaction effect between blade boundary layers becomes apparent and a wake type of profile is seen. This measurement has revealed an appreciable decrease in blade boundary layers as compared to the four blade inducer.

13) The radial inward flows observed by means of tufts mounted at the inducer exit indicate that their magnitudes are generally lower than those observed at the exit of the four bladed inducer.

14) The limiting streamline angles measured on the blade surfaces of the three bladed inducer follow the same trend as four bladed inducer even though their magnitudes are generally higher.

15) Some improvement in exit flow characteristics of axial flow inducers has been achieved by reducing the solidity. The three bladed inducer studied in this thesis presents higher and more uniform head characteristics at exit than the four bladed inducer. The influence of viscosity and the interaction effect between the blade boundary layers have considerably decreased. However a deterioration in exit axial velocity is observed, together with a larger flow separation zone extending downstream of the trailing edge. Further improvement of the inducer should include blade boundary layer control and possibly a blade thickness reduction.

APPENDIX I

Derivation of Accuracy Criteria for Instantaneous Velocity Measurements (Equations 23 and 24)

1) Accuracy of the blade to blade averaged velocities (equation 23)

If N successive samples are taken at any particular location of the blade passage (θ), the value of the velocities at these samples are: $v_1, v_2, v_3 \ldots\ldots v_n$.

Taking the average:

$$\overline{v_n} = \frac{1}{N} \sum_{n=1}^{N} v_n$$

with the assumption that those n values are statistically independent, it can be written:

$$\overline{v_n} - v = \frac{1}{N} \sum_{n=1}^{N} (v_n) - v = \frac{1}{N} \sum_{n=1}^{N} (v_n - v)$$

v being the expected value of the sequence $v_1, v_2 \ldots\ldots v_n$.
(or the value to which the sequence converges for $n = \infty$)

The standard deviation is given by:

$$E\{v_n - v)^2\} = \frac{1}{N^2} \sum_{n,l=1}^{N} E\{v_n - v)(v_l - v)\}$$

the independence of the measurements gives,

$$E\{(v_n - v)\} \quad E\{(v_l - v)\} = 0$$

and $E\{(\overline{v_n} - v)^2\} = \frac{1}{N^2} \sum_{n=1}^{N} E\{(v_n - v)^2\}$

Dividing by v^2

$$\varepsilon^2 = \frac{E\{(\overline{v_n} - v)^2\}}{v^2} = \frac{1}{N^2} \sum_{n=1}^{N} E\{(\frac{v_n - v}{v})^2\}$$

hence

$$\varepsilon^2 = \frac{1}{N} (\sigma/x)^2 \quad \text{or } \varepsilon^2 = \frac{1}{N} (T)^2$$

Note: the notation E{x} accounts for: expectation of the value of x.

2) Accuracy of the turbulent intensities measurements

Since the average is taken over N samples, the square of the relative error for the fluctuations is

$$\frac{E\{(v_n - \overline{v_n})^2\}}{v^2}$$

or $$\frac{1}{N^2} \sum_{n=1}^{N} \frac{E\{(v_n - v)^2\}}{v^2}$$

that is, if $\frac{E\{(v_n - \overline{v_n})^2\}}{v^2} = 2$ for a Gaussian process,

$$\frac{E\{(v_n - v_n)^2\}}{v^2} = \frac{2}{N}$$

And the accuracy with which the turbulent intensities are obtained is:

$$E = \sqrt{\frac{2}{N}}$$

APPENDIX 2

Fortran Listing of the Program Used for Deriving Instantaneous Velocities From Hot Wire Measurements

```
//                TAPE=ALAIN,OUT
//                END OF TAPE CARDS
// EXEC FGCLG,PARM.OBJECT=MAP
//SOURCE.INPUT DD *
C
C     DERIVATION OF THE THREE COMPONENTS OF THE VELOCITY IN THE WAKE
C     OF THE PENN STATE THREE BLADE INDUCER AT STATION 4
C
      REAL*8 O(2,101)
      REAL ZU(6,2000)
      DIMENSION A1(51,80),C1(51,80),B1(51,80),D1(51,80),UT(102),UZ(102),
     1UR(102),W(102),TUT(102),TUR(102),TUW(102),TUZ(102),WT(51),CV(102)
     1,CZ(102),CR(102),CW(102)
      INTEGER*2 IAL(2000),IBL(2000),ICL(2000)
      EQUIVALENCE (L(1),INT),(CC(1),O(1,1))
      LOGICAL*1 CC(16384),L(4)
      READ 1002,K,Y1,Y2,Y3,H1,H2,H3,T1,T2,T3
      PRINT 1007,K,Y1,Y2,Y3,H1,H2,H3,T1,T2,T3
      M=1
      N=1
C     **THE DATA CORRESPONDING TO EACH RADIUS IS READ**
 98   CALL GET (91,CC,16384,KEY)
      IF (KEY) 300,101,301
 301  PRINT 1004
      GO TO 98
 300  PRINT 1003
      N=N+1
      IF (N-4) 98,98,99
 101  IF (N-11)100,100,99
 100  INT=0
      READ 1008,R
      IR=1
      IC=1
C     **THE DATA IS PUT IN TWO DIMENSIONAL ARRAYS**
      DO 200 I=1,16320,4
      L(4)=CC(I)
      A1(IC,IR)=128-INT
      L(4)=CC(I+1)
      B1(IC,IR)=INT-128
      L(4)=CC(I+2)
      C1(IC,IR)=INT-128
      L(4)=CC(I+3)
      D1(IC,IR)=INT-128
      IF(IC.LT.51) GO TO 200
      IC=0
      IR=IR+1
 200  IC=IC+1
      PRINT 1021
      M=M+1
      PRINT 1002,M
      RUP=0.0
      RUM=0.0
      RUO=0.0
C     ** BEGINNING OF THE AVERAGING PROCEDURE**
      DO 3 I=1,51
      PRINT 1001,(I,A1(I,1),B1(I,1),C1(I,1),D1(I,1))
      SUP=0.0
      SUM=0.0
      SUO=0.0
      SUR=0.0
```

```
      DO 4 J=1,80
      SUM=SUM+A1(I,J)
      SUP=SUP+B1(I,J)
      SUR=SUR+D1(I,J)
      RUP=RUP+A1(I,J)
      RUM=RUM+B1(I,J)
      RUQ=RUQ+C1(I,J)
    4 SUQ=SUQ+C1(I,J)
      AV1=SUM/80.0
      AV2=SUP/80.0
      AV3=SUQ/80.0
      AV4=64.0
      TAV1=(AV1/AV4)*Y1
      TAV2=(AV2/AV4)*Y2
      TAV3=(AV3/AV4)*Y3
      R1=(((TAV1*TAV1-H1)*(TAV1*TAV1-H1))/(T1*T1))
      R2=(((TAV2*TAV2-H2)*(TAV2*TAV2-H2))/(T2*T2))
      R3=(((TAV3*TAV3-H3)*(TAV3*TAV3-H3))/(T3*T3))
      X1=R1*R1/(2.0*0.98)
      X2=R2*R2/(2.0*0.98)
      X3=R3*R3/(2.0*0.98)
      UT(I)=(SQRT(ABS(X1-X2+X3)))/71.6
      UZ(I)=(SQRT(ABS(0.96*X1+X2-X3)))/71.6
      UR(I)=(SQRT(ABS(X2+X3*0.96-X1)))/71.6
      WT(I)=R-UT(I)
    3 W(I)=SQRT(UZ(I)*UZ(I)+UR(I)*UR(I)+WT(I)*WT(I))
      RUP=RUP/4080.0
      RUM=RUM/4080.0
      RUQ=RUQ/4080.0
      PRINT 1001,I,RUP,RUM,RUQ
      PRINT 1006
      PRINT 1009,R
      PRINT 1000
C     **TIME AVERAGED VELOCITIES**
      DO 5 I=1,51
    5 PRINT 1001,(I,UZ(I),UR(I),UT(I),WT(I),W(I))
      SUM=0.0
      SUP=0.0
      SUQ=0.0
      SUR=0.0
      SUS=0.0
      DO 30 I=1,51
      SUM=SUM+UT(I)
      SUP=SUP+UZ(I)
      SUQ=SUQ+UR(I)
      SUR=SUR+WT(I)
   30 SUS=SUS+W(I)
      SUM=SUM/51.0
      SUP=SUP/51.0
      SUQ=SUQ/51.0
      SUR=SUR/51.0
      SUS=SUS/51.0
      PRINT 1020
      PRINT 1000
      PRINT 1001,K,SUP,SUQ,SUM,SUR,SUS
C     **TURBULENCE INTENSITY CALCULATION**
      DO 21 I=1,51
      SUP = 0.0
      SUM = 0.0
      SUQ = 0.0
```

```
      SUR = 0.0
      DO 22 J=1,80
      AV1 = A1(I,J)
      AV2 = B1(I,J)
      AV3 = C1(I,J)
      AV4=64.0
      TAV1=(AV1/AV4)*Y1
      TAV2=(AV2/AV4)*Y2
      TAV3=(AV3/AV4)*Y3
      R1=(((TAV1*TAV1-H1)*(TAV1*TAV1-H1))/(T1*T1))
      R2=(((TAV2*TAV2-H2)*(TAV2*TAV2-H2))/(T2*T2))
      R3=(((TAV3*TAV3-H3)*(TAV3*TAV3-H3))/(T3*T3))
      X1=R1*R1/(2.0*0.96)
      X2=R2*R2/(2.0*0.96)
      X3=R3*R3/(2.0*0.96)
      A = (SQRT(ABS(X1-X2+X3)))/71.6
      B = (SQRT(ABS(X1*0.96+X2-X3)))/71.6
      C = (SQRT(ABS(X3*0.96+X2-X1)))/71.6
      D=R-A
      E=SQRT(B*B+C*C+D*D)
      SUP = SUP + (A-UT(I))*(A-UT(I))
      SUQ = SUQ + (B-UZ(I))*(B-UZ(I))
      SUR=SUR+(C-UR(I))*(C-UR(I))
   22 SUM = SUM + (E-W(I))*(E-W(I))
      TUR(I)=((SQRT(SUR/80.0))/UR(I))*100.0
      TUZ(I)=((SQRT(SUQ/80.0))/UZ(I))*100.0
      TUT(I)=((SQRT(SUP/80.0))/UT(I))*100.0
  21  TUW(I)=((SQRT(SUM/80.0))/W(I))*100.0
      PRINT 1012
      PRINT 1013
      DO 16 I=1,51
 16   PRINT 1001,(I,TUT(I),TUZ(I),TUR(I),TUW(I))
      DO 17 I=52,101
      J=I-51
      UZ(I)=UZ(J)
      UR(I)=UR(J)
      UT(I)=UT(J)
      W(I)=W(J)
      TUZ(I)=TUZ(J)
      TUT(I)=TUT(J)
      TUR(I)=TUR(J)
      TUW(I)=TUW(J)
 17   CONTINUE
      UT(101)=0.0
      TUZ(101)=0.0
      W(101)=0.02
      TUR(101)=0.0
C     **GRAPHIC ROUTINES**
      IF (M-2) 98,305,309
 309  IF ((M-5)*(M-6)*(M-7)*(M-8)) 98,306,98
 305  CALL INITQ (IAL,IBL,ICL,ZU,2000)
 306  DO 6 I=1,101
      Q(1,I)=I
  6   Q(2,I)=UR(I)
      CALL GRAPHQ(' $',' $',0,101,0)
      DO 11 I=1,101
   11 Q(2,I)=W(I)
      CALL GRAPHQ(' $',' $',0,101,0)
      DO 9 I=1,101
    9 Q(2,I)=UT(I)
```

```
      CALL SAMEQ
      CALL GRAPHQ(' $',' $',0,101,0)
      DO 8 I=1,101
    8 O(2,I)=UZ(I)
      CALL SAMEQ
      CALL GRAPHQ(' $',' $',0,101,0)
      DO 13 I=1,101
   13 O(2,I)=TUZ(I)
      CALL GRAPHQ(' $',' $',0,101,0)
      DO 12 I=1,101
   12 O(2,I)=TUT(I)
      CALL SAMEQ
      CALL GRAPHQ(' $',' $',0,101,0)
      DO 14 I=1,101
   14 O(2,I)=TUR(I)
      CALL GRAPHQ(' $',' $',0,101,0)
      DO 15 I=1,101
   15 O(2,I)=TUW(I)
      CALL SAMEQ
      CALL GRAPHQ(' $',' $',0,101,0)
 1000 FORMAT (//2X,1HI,10X,2HUZ,10X,2HUR,10X,2HUT,10X,2HWT,10X,1HW/)
 1001 FORMAT (' ',I5,1P6E13.6)
 1002 FORMAT (I2,3F6.3,6E10.3)
 1003 FORMAT (' ',26HTAPE ERROR-PROGRAM STOPPED)
 1004 FORMAT (' ',11HEND OF FILE)
 1006 FORMAT (80H EXIT VELOCITIES NON DIMENSIONALIZED WITH RESPECT TO TI
     1PSPEED AT RADIUS LOCATION)
 1007 FORMAT (' ',I2,3F6.2,6E10.3)
 1008 FORMAT (F10.4)
 1009 FORMAT (' ',F10.4)
 1010 FORMAT(' ',I5,1P4E13.6)
 1011 FORMAT (//2X,1HI,10X,2HA1,10X,2HB1,10X,2HC1,10X,2HD1/)
 1012 FORMAT(' ',38HTURBULENT INTENSITIES AT EACH LOCATION)
 1013 FORMAT(//2X,1HI,10X,2HUT,10X,2HUZ,10X,2HUR,10X,1HW/)
 1020 FORMAT (' ',26HRMS VALUES AT THAT STATION)
 1021 FORMAT (' ',129H*****************************************************
     1*****************************************************************
     1*************)
      GO TO 98
 99   STOP
      END
/*
//DATA.FT91F001 DD UNIT=(2400,,DEFER),VOL=SER=ALAIN,                    X
//              LABEL=(1,NL),DCB=(RECFM=F,BLKSIZE=16384,BUFNO=1)
//DATA.INPUT DD *
 7 0.999 1.350 0.999  .820E+00  .730E+00  .760E+00  .177E 00  .165E 00  .179E 00
     .582
     .638
     .692
     .754
     .809
     .864
     .920
```

REFERENCES

1. Acosta, A. J., "An Experimental Study of Cavitating Inducers", Second Symposium on Naval Hydrodynamics, August 1958, Washington, D. C.

2. Cooper, P., and Bosch, H., "Three Dimensional Analysis of Inducer Fluid Flow", NASA report, CR-54836, TRW ER-6673A, February 1966.

3. Jabbari, A., "Turbulent Boundary Layer Characteristics on a Rotating Helical Blade," M. S. Thesis, Dept. of Aerospace Engineering, The Pennsylvania State University, September 1969. (NASA CR 105649, 1969)

4. Lakshminarayana, B., "Investigation and Analysis of Flow Phenomena of Secondary Motions in Axial Flow Inducers", Semi Annual Progress Report to NASA, The Pennsylvania State University, May 1968.

5. Lakshminarayana, B., "Investigation and Analysis of Flow Phenomena of Secondary Motions in Axial Flow Inducers", Semi Annual Progress Report to NASA, The Pennsylvania State University, June 1969.

6. Lewis, R. I., and Horlock, J. H., "Flow Disturbances Due to Blade Thickness in Turbomachines", Journal of Mechanical Engineering Science, Vol. 11, No. 1, 1969.

7. Lumley, J. L., "Stochastic Vector Fields", Academic Press, 1970.

8. McCafferty, H. G., "Errors in Measuring the Fluctuating Flow at the Discharge of an Inducer", M. S. Thesis, Department of Aerospace Engineering, The Pennsylvania State University, June 1967.

9. Mullan, P. J., "An Investigation of Cavitating Inducers for Turbopumps", Gas Turbine Laboratory, Massachusetts Institute of Technology, Report No. 53, May 1959.

10. Meng, P. R., and Moore, R. D., "Hydrogen Cavitation Performance of 80.6° Helical Inducer Mounted in Line with Stationary Centerbody", NASA TM X-1935.

11. Montgomery, J. C., "Analytical Performance Characteristics and Outlet Flow Conditions of Constant and Variable Lead Helical Inducers for Cryogenic Pumps", NASA TN D-583, March 1961.

12. Osborn, W. M., "Investigation of a Liquid-Fluorine Inducer and Main-Stage Pump Combination Designed for a Suction Specific Speed of 20.000", NASA TM X-1070, March 1965.

REFERENCES CONTINUED

13. Schwarz, W. H., and Friehe, C. A., "Deviations from the Cosine Law for Yawed Cylindrical Anemometer Sensors", Journal of Applied Mechanics, Paper No. 68-WA/APM-16.

14. Sandercock, D. M., and Anderson, D. A., "Cavitation and Non Cavitation Performance of an 80.6° Flat Plate Helical Inducer at Three Rotational Speeds", NASA Technical Note D-1439, November 1962.

15. Soltis, R. F., Anderson, D. A., and Sandercock, D. M., "Investigation of the Performance of a 78° Flat Plate Helical Inducer", NASA Technical Note D. 1170, March 1962.

16. Soltis, R. F., Urasek, D. C., Miller, M. J., "Blade Element Performance of a Tandem-Bladed Inducer Tested in Water", NASA Technical Note D-5562, November 1969.

17. Wislicenus, G. F., "Fluid Mechanics of Turbomachinery", Dover, Vol. II, pp. 646-683.

18. Bosch, H. B., et. al., "Advanced Inducer Study," ER-5288 (NASA Document No. N63-21124); TRW, Inc, Cleveland, May 1963.

19. Sandercock, D. M., et. al., "Cavitation and Noncavitation Performance of an 80.6° Flat Plate Inducer," NACA TN D1439, November 1962.

20. Soltis, R. F., et. al., "Investigation of the Performance of a 78° Flat Plate Helical Inducer," NACA TN 1170, March 1962.

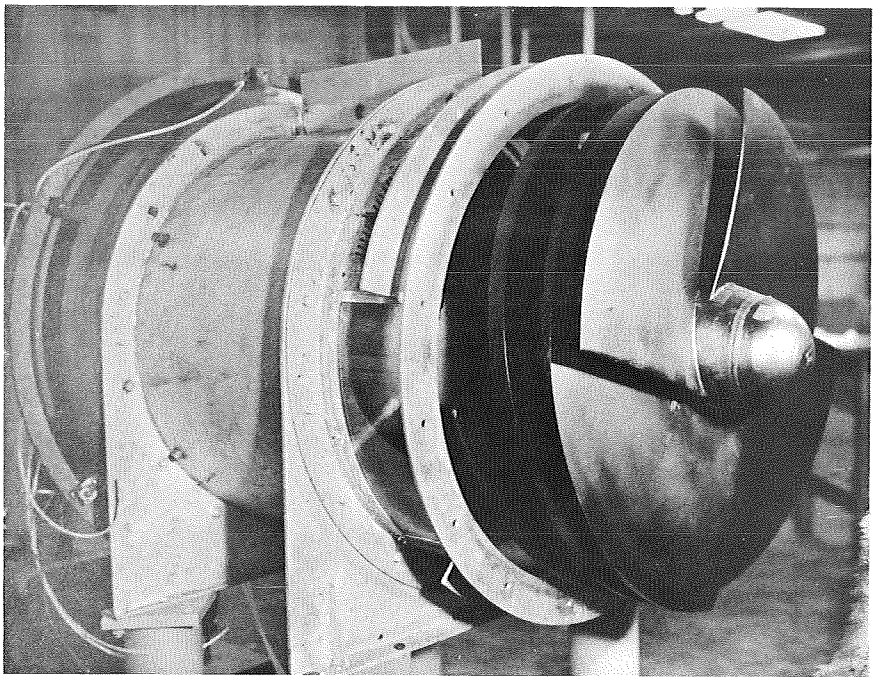

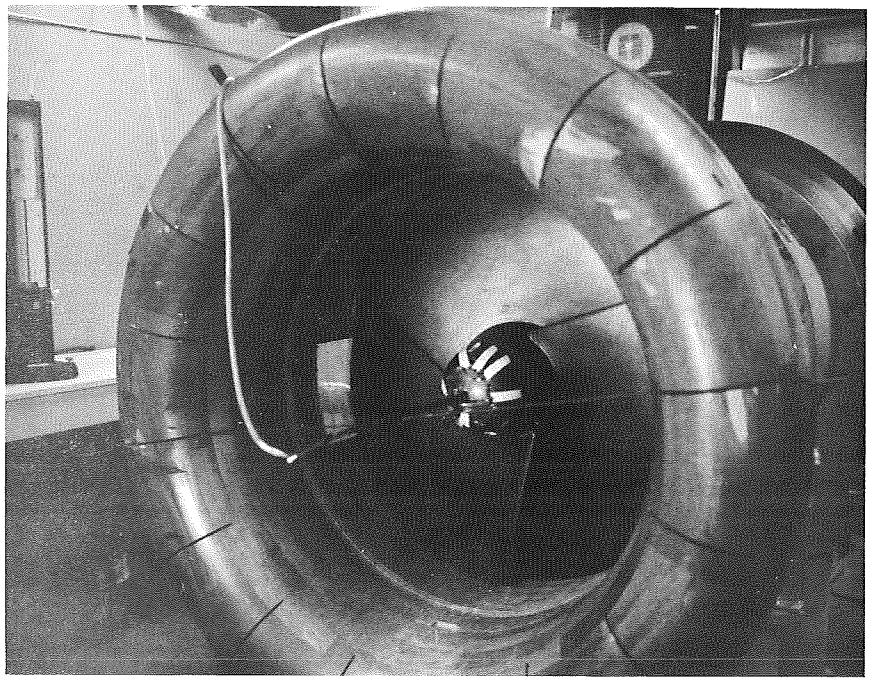

Figure 1: Photographs of Four and Three Bladed Inducers

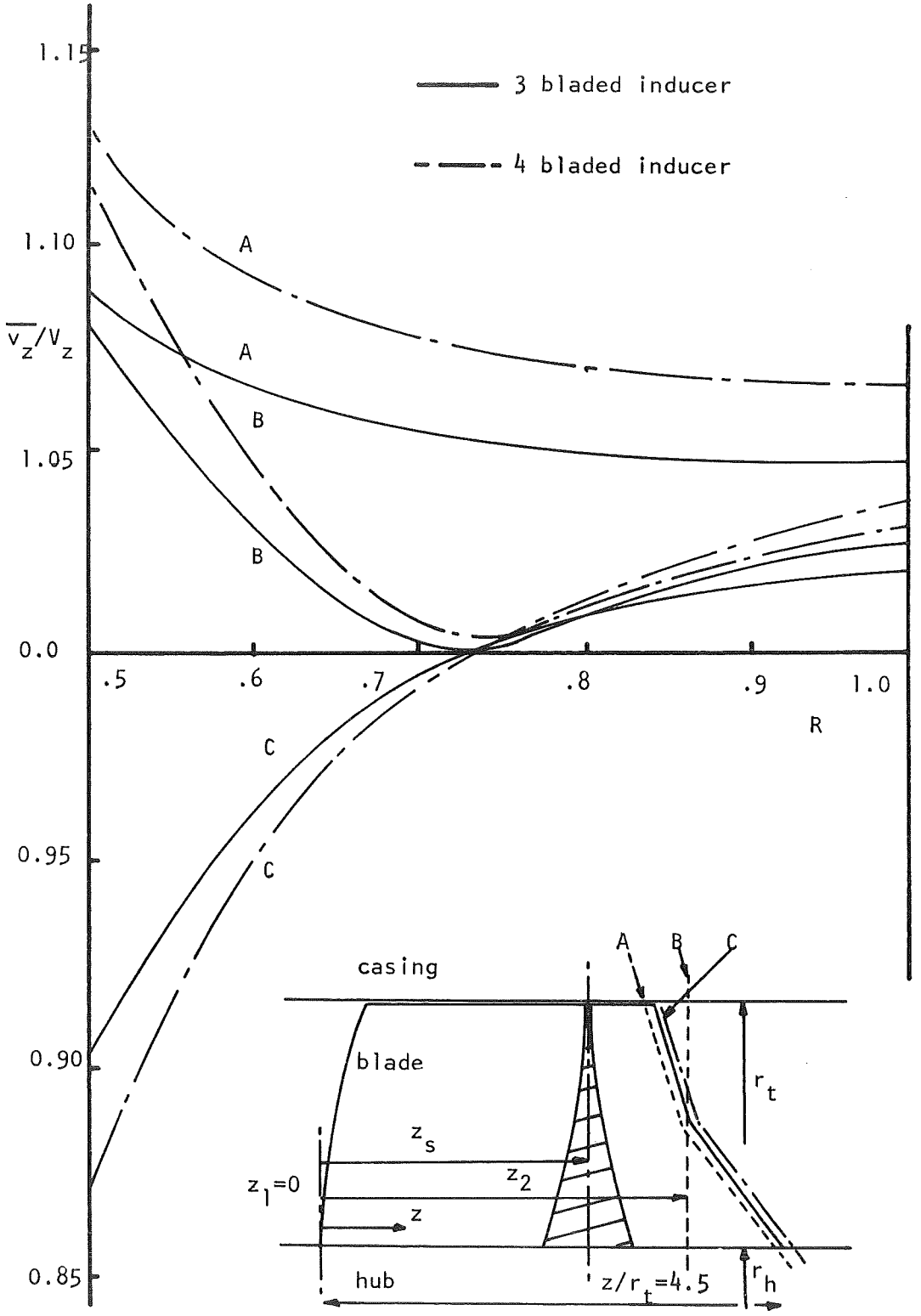

Figure 2: Axial Velocity Perturbation Due to Blockage

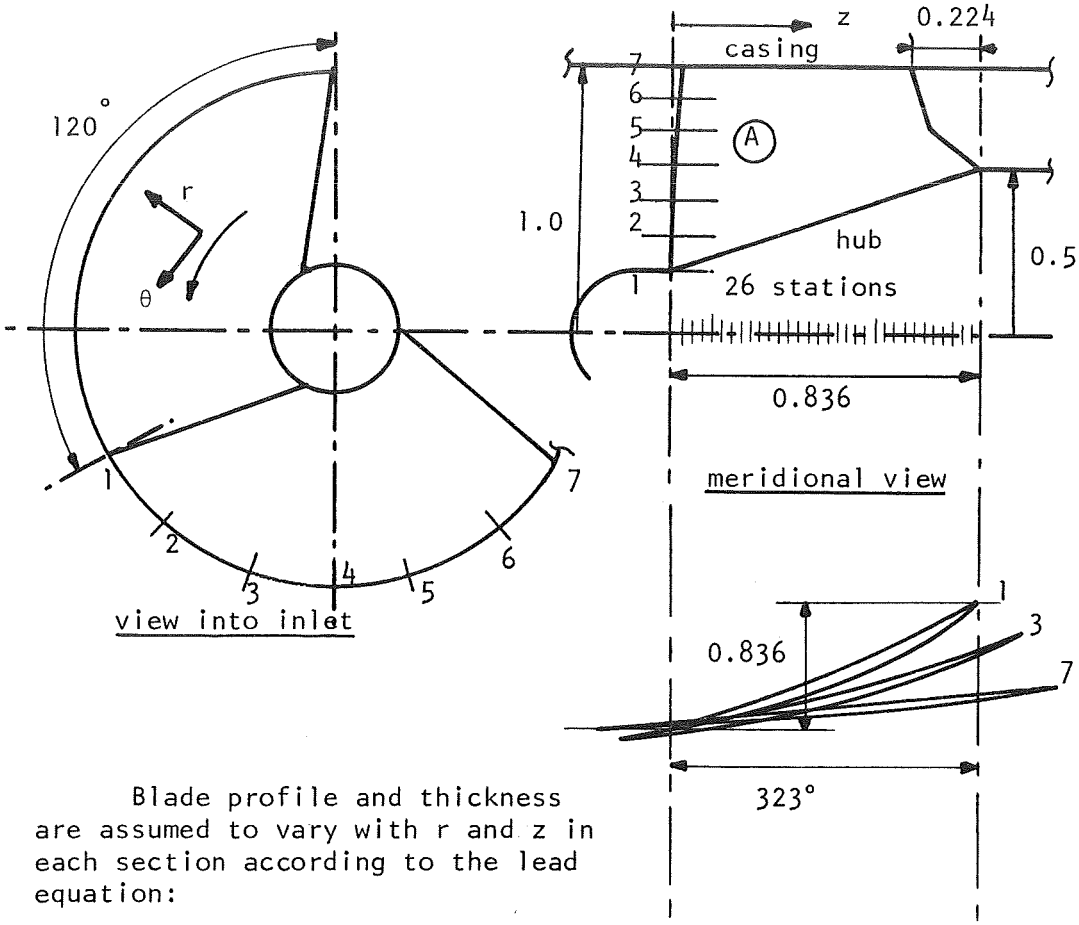

Blade profile and thickness are assumed to vary with r and z in each section according to the lead equation:

(tp is the angular location)

$$tp = az^2 + bz + c$$

a,b,c being function of the radius

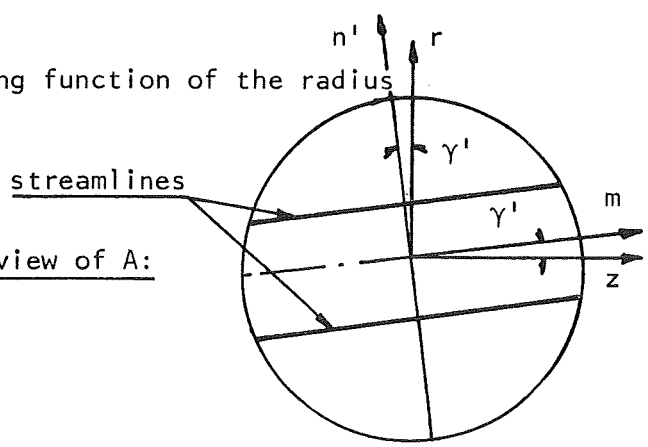

Figure 3: Inducer Geometry for Numerical Analysis

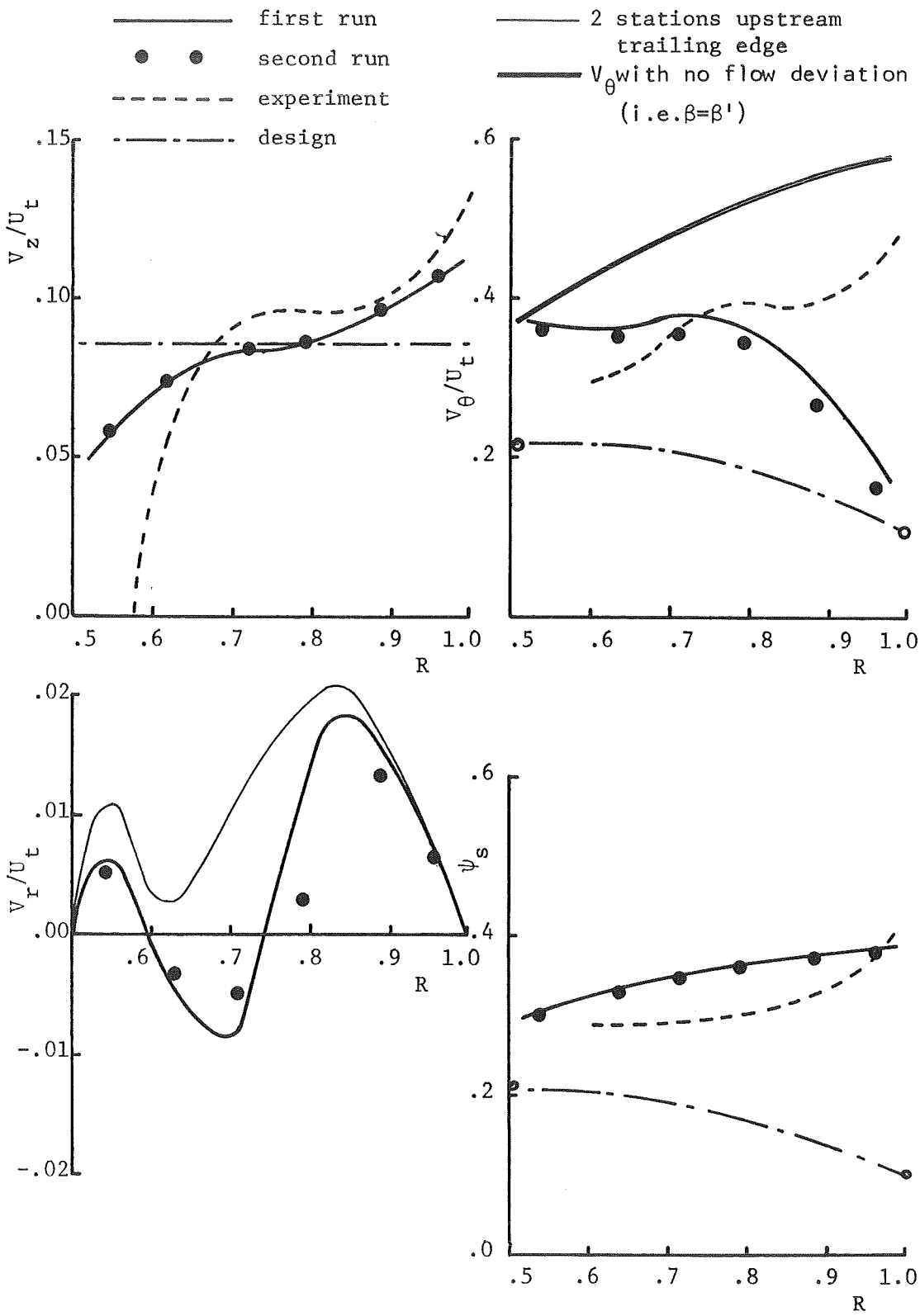

Figure 4:Outlet Results of Exact Numerical Analysis

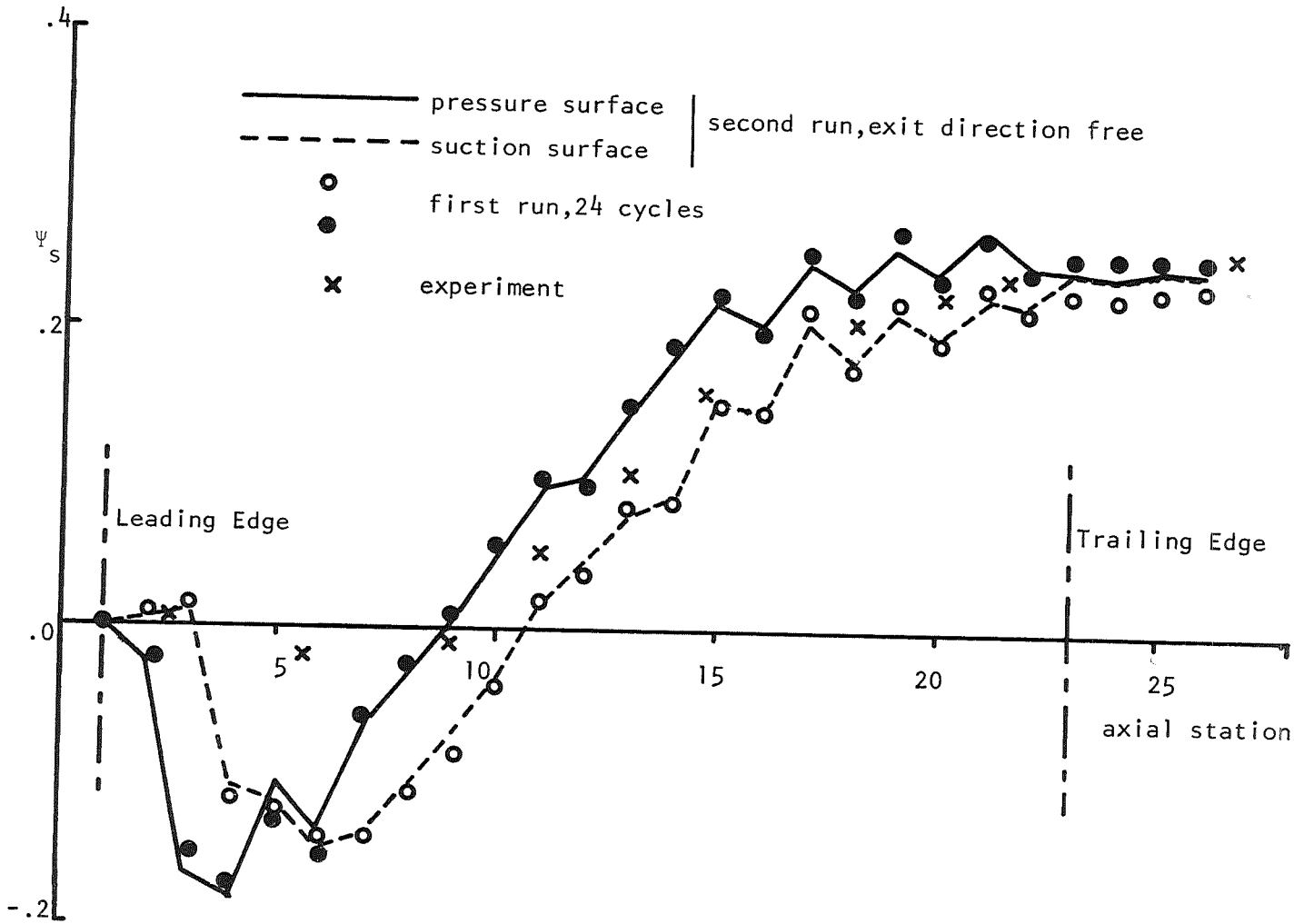

Figure5a: Blade Pressure Distribution at HUB

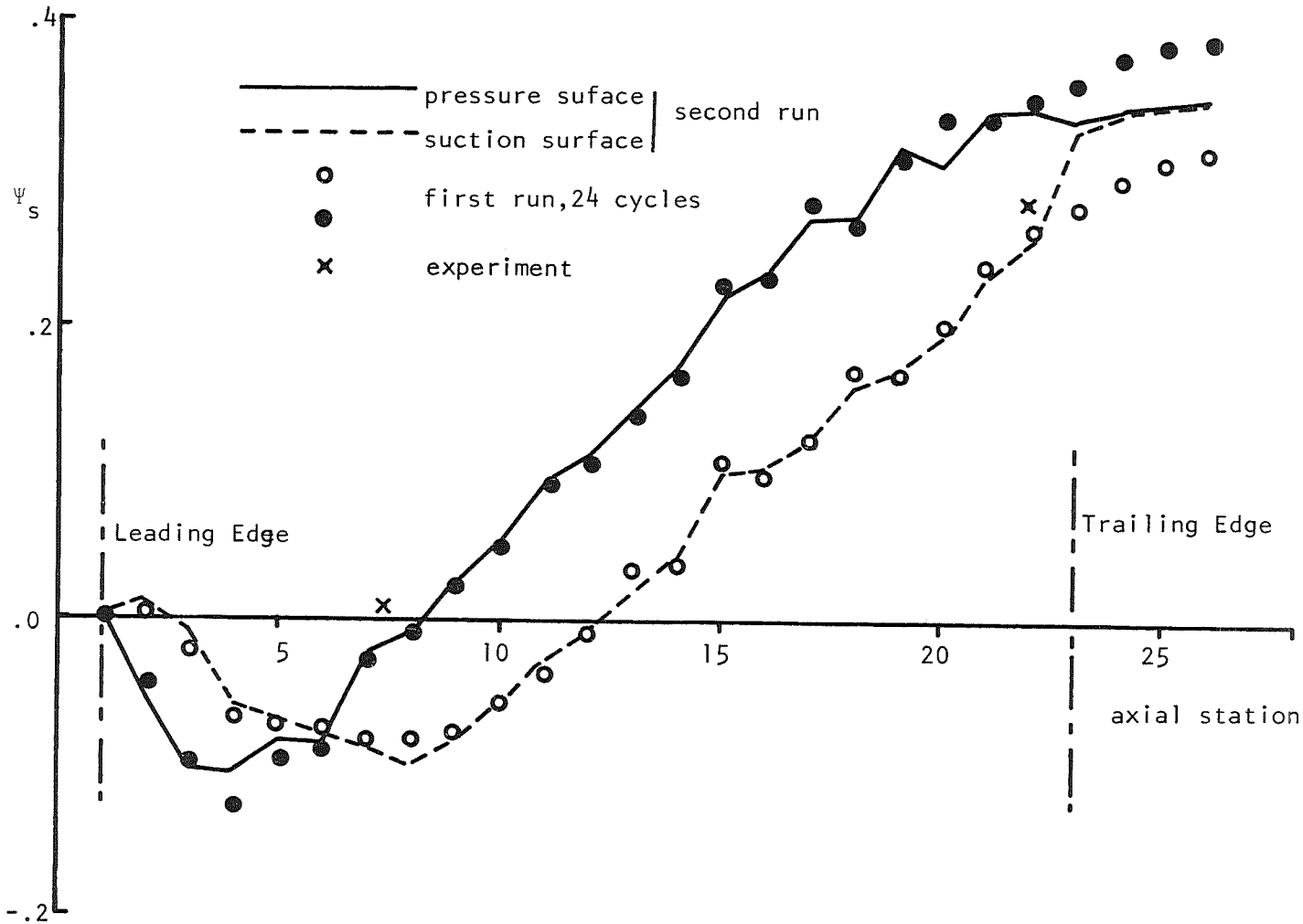

Figure 5b: Blade Pressure Distribution at Mid-Radius

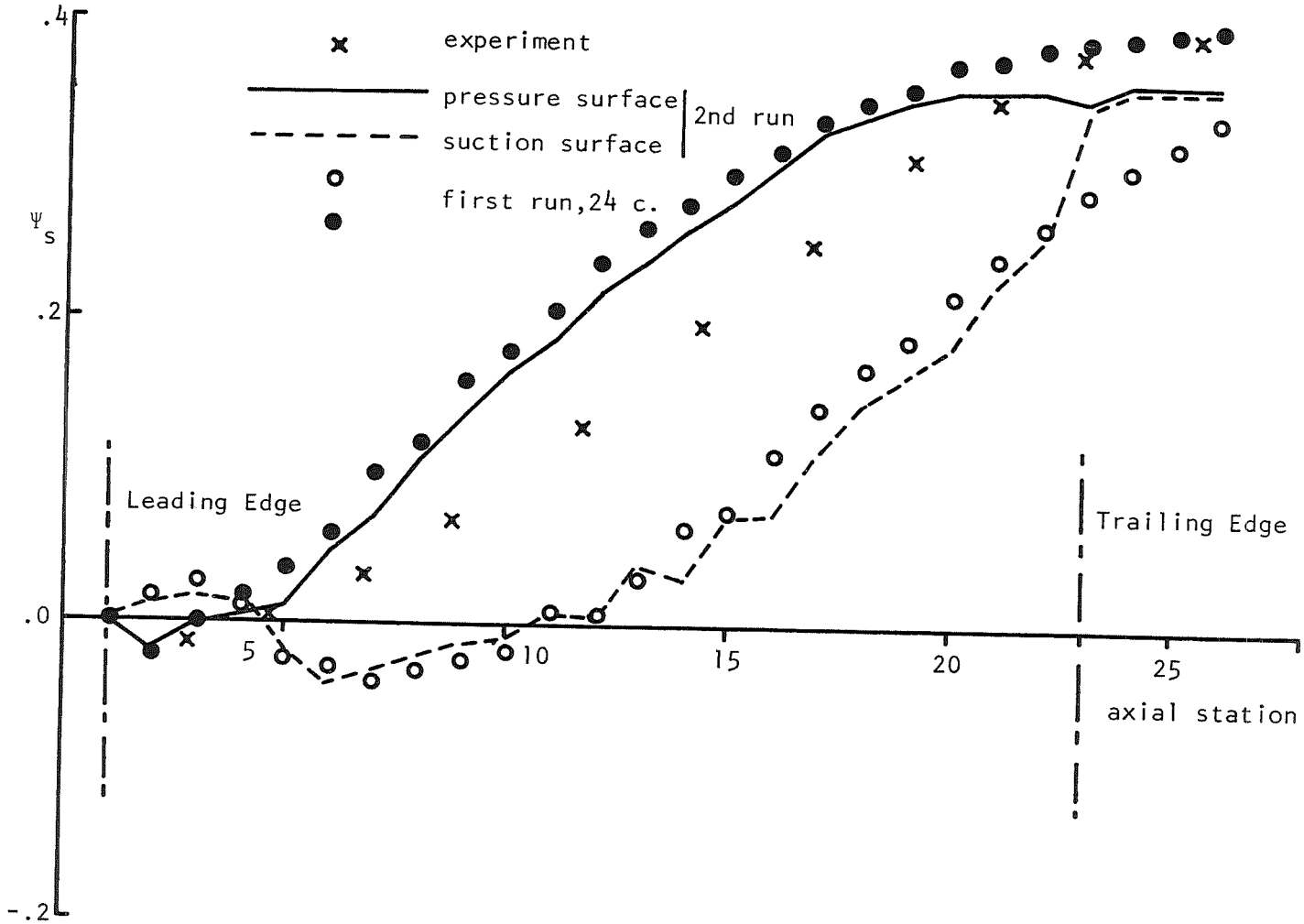

Figure 5c: Blade Pressure Distribution at TIP

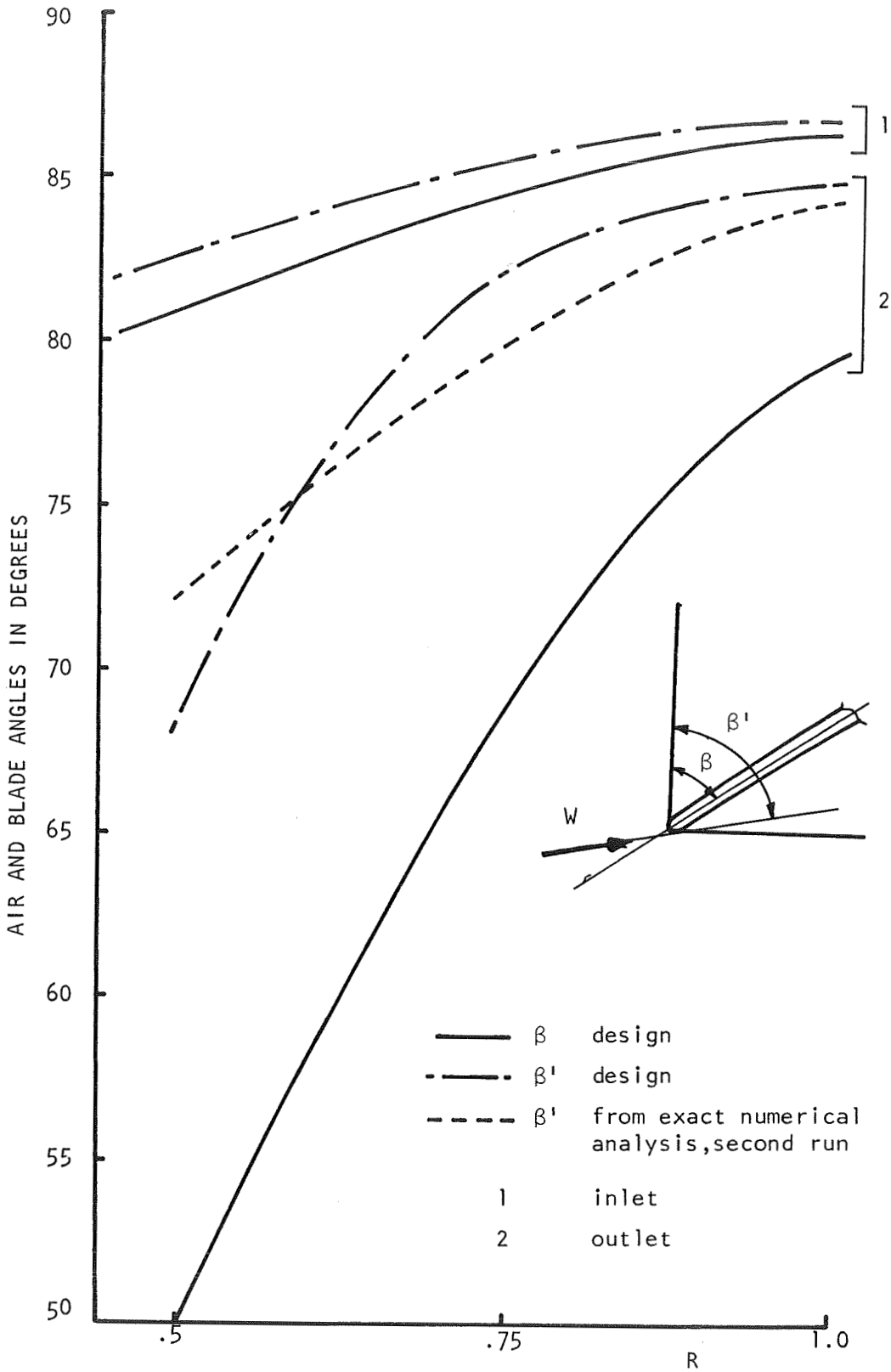

Figure 6: Inducer Inlet and Outlet Angles

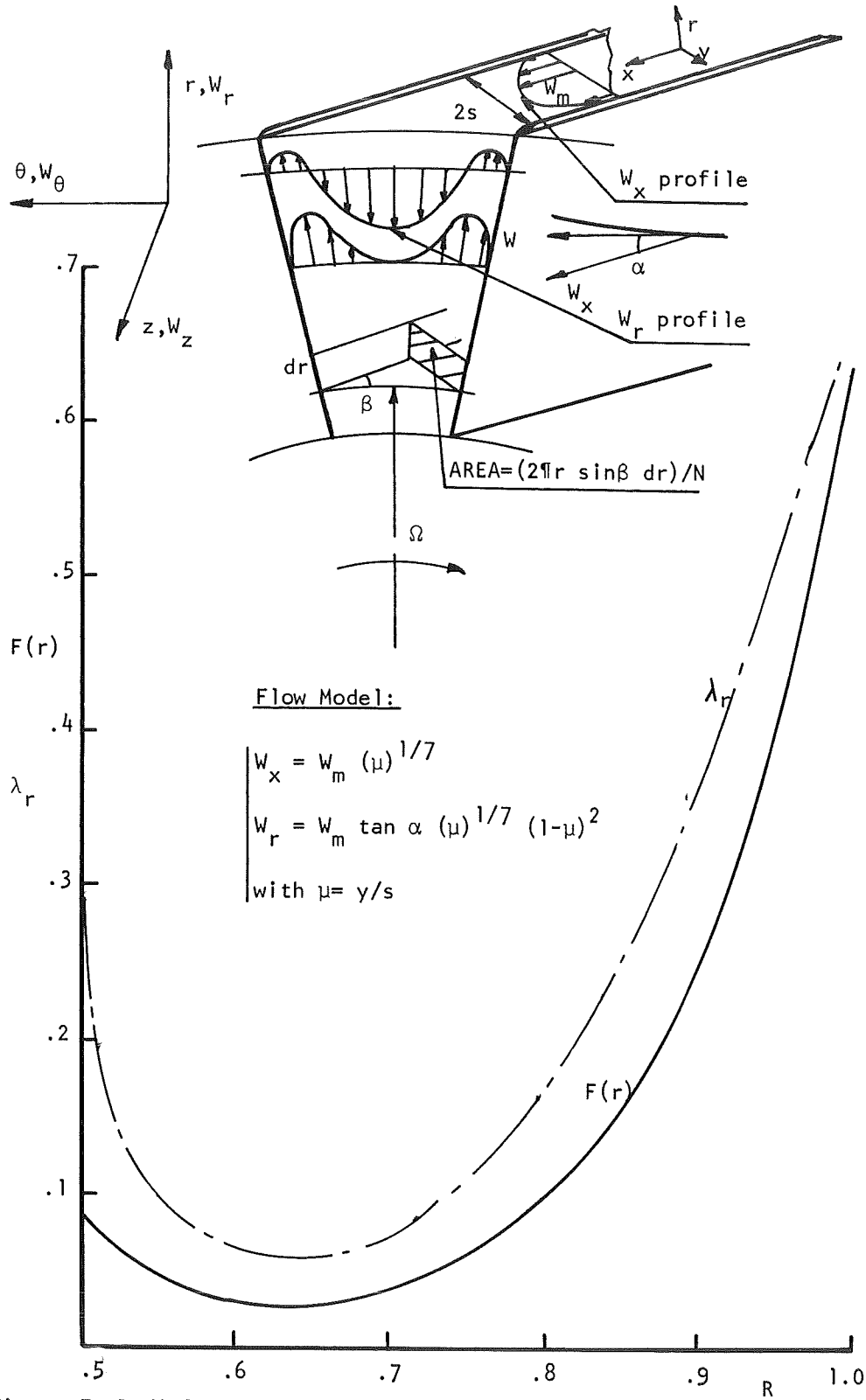

Figure 7: Radial Variation of the Loss Coefficient and Function F(r) (equation 17) for the Three Bladed Inducer

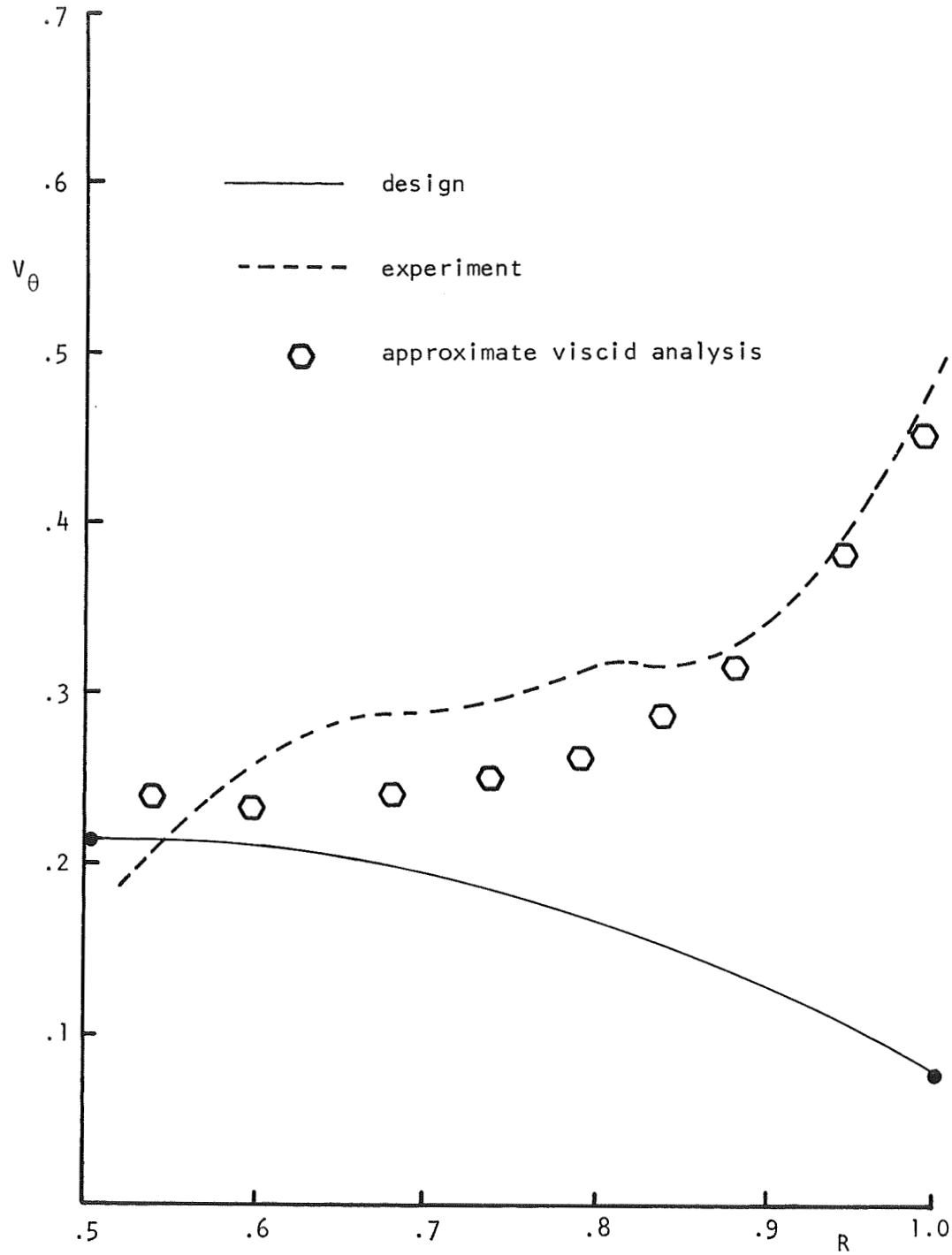

Figure 8: Radial Variation of Absolute Tangential Velocity at Station 4 from Approximate Viscid Analysis

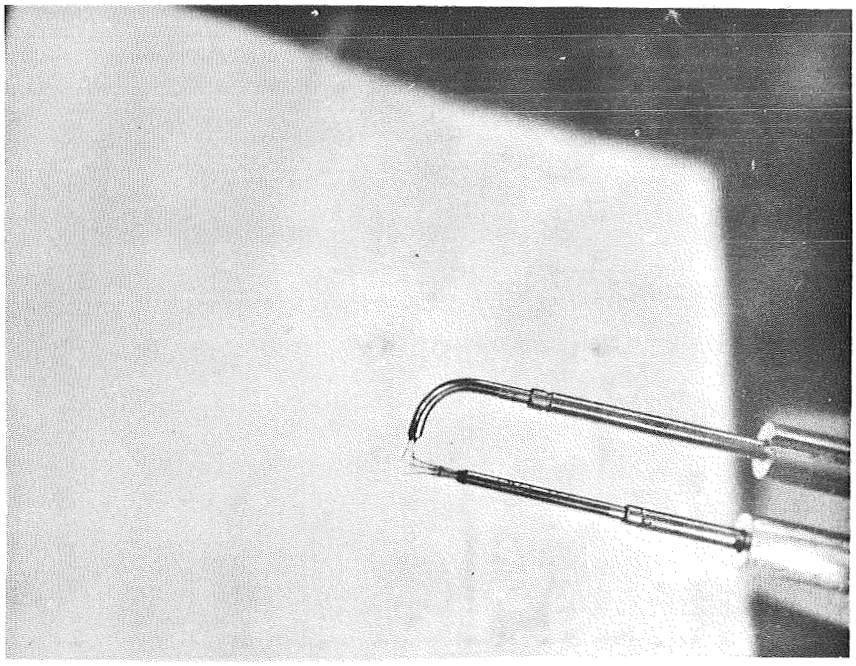

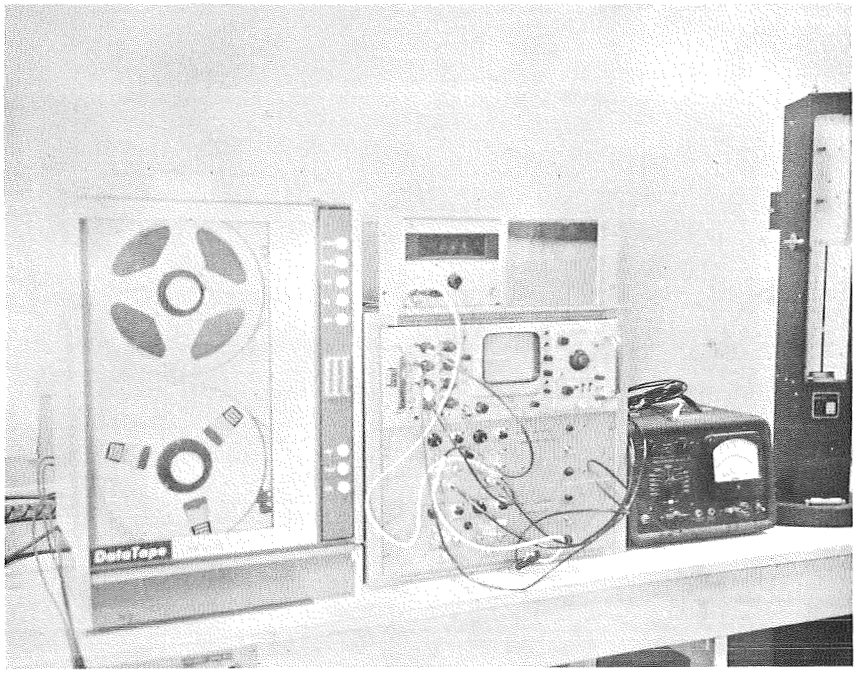

Figure 9: Hot Wire Probe and Associated Equipment

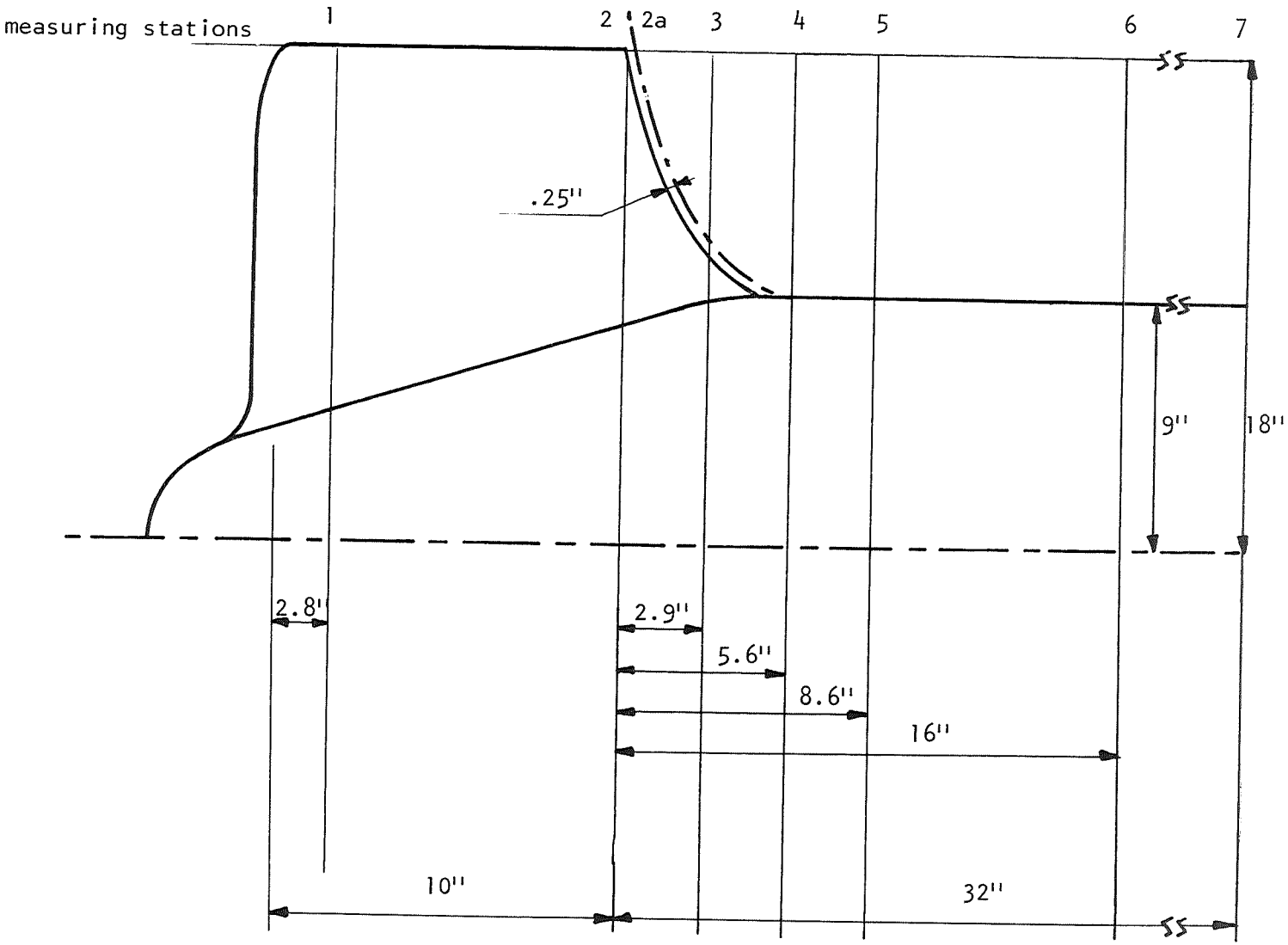

Figure 10: Location of the Flow Measuring Stations

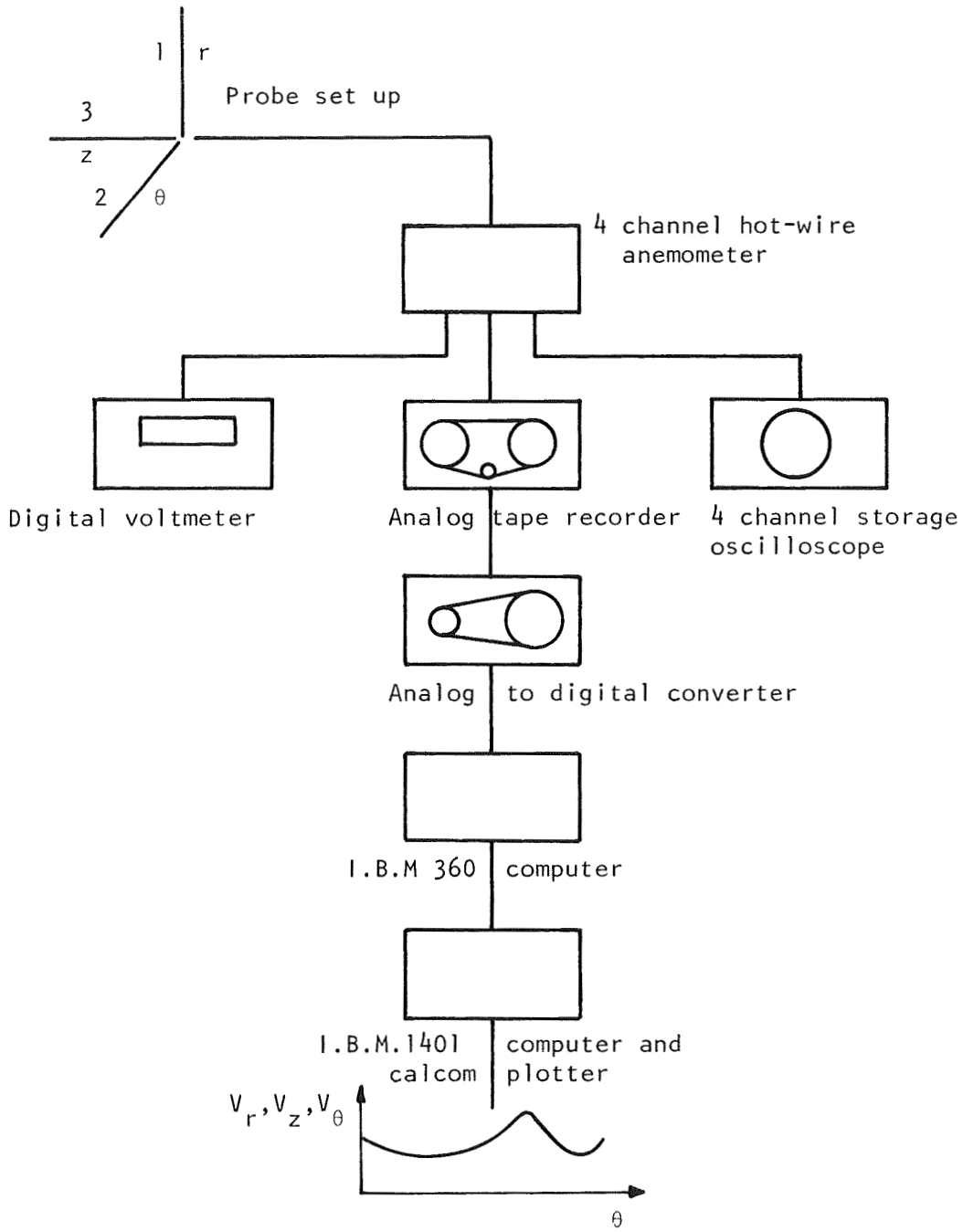

Figure 11a: Block Diagram for Instantaneous Velocity Measurements

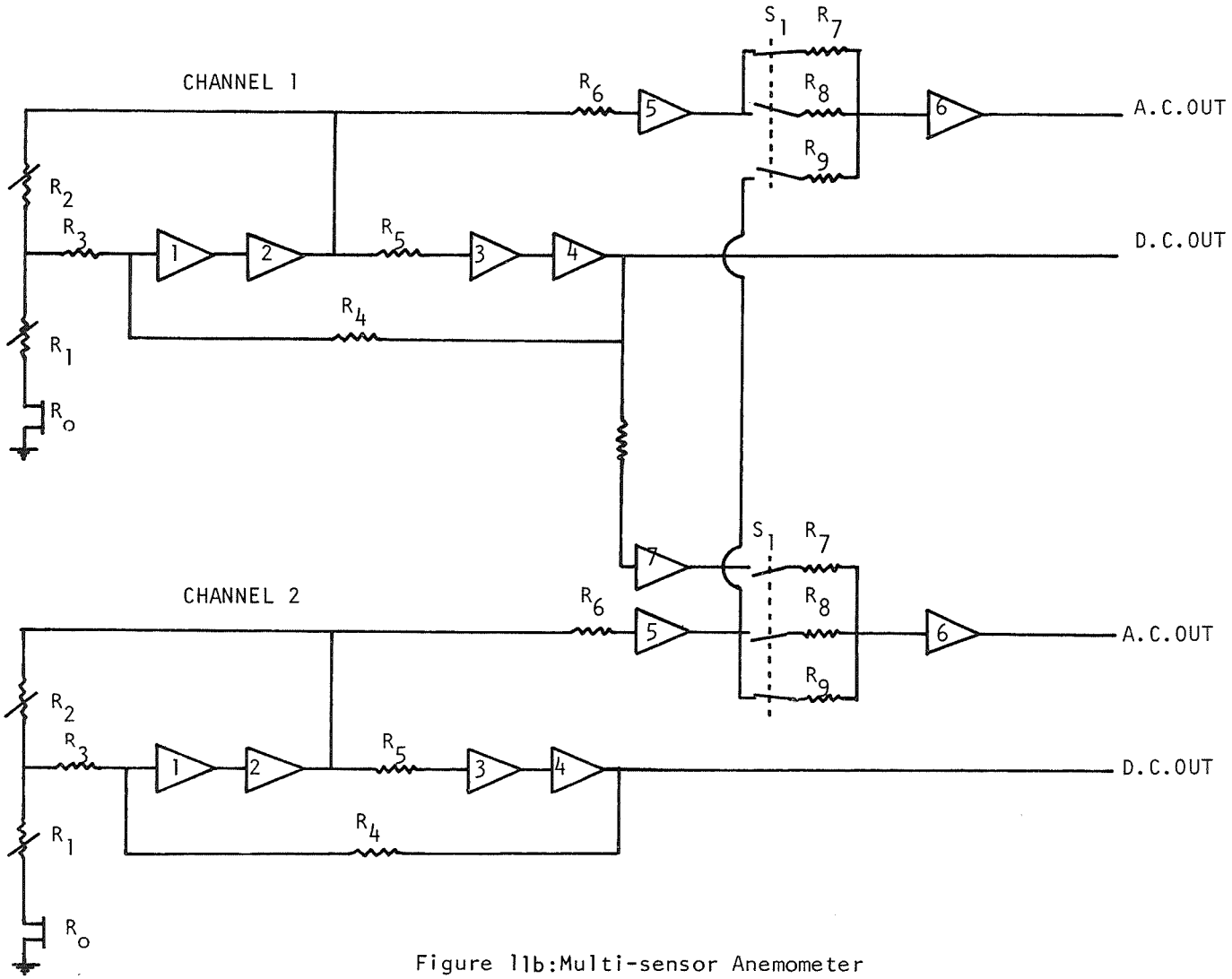

Figure 11b:Multi-sensor Anemometer

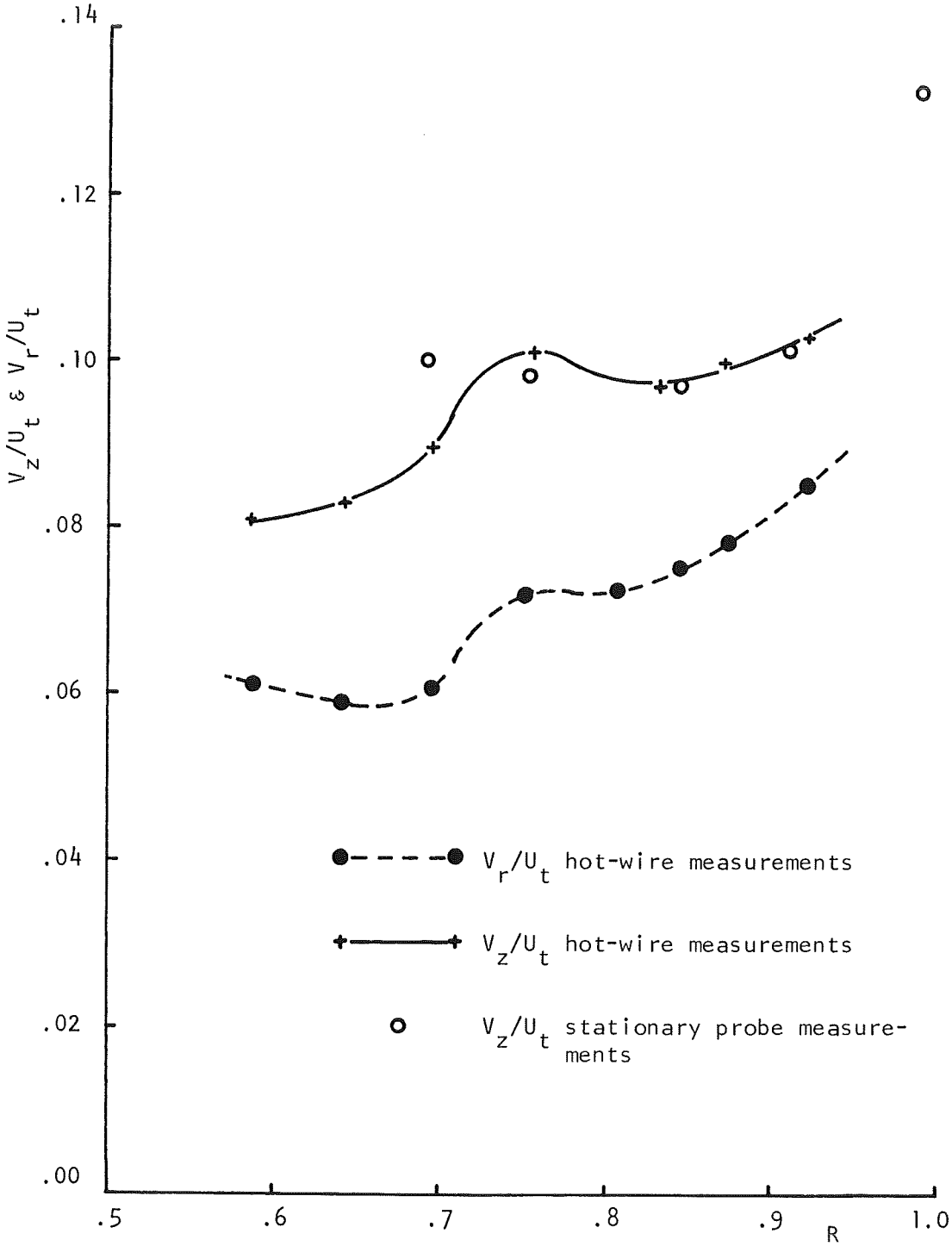

Figure 12a: Axial and Radial Velocity at Station 2a

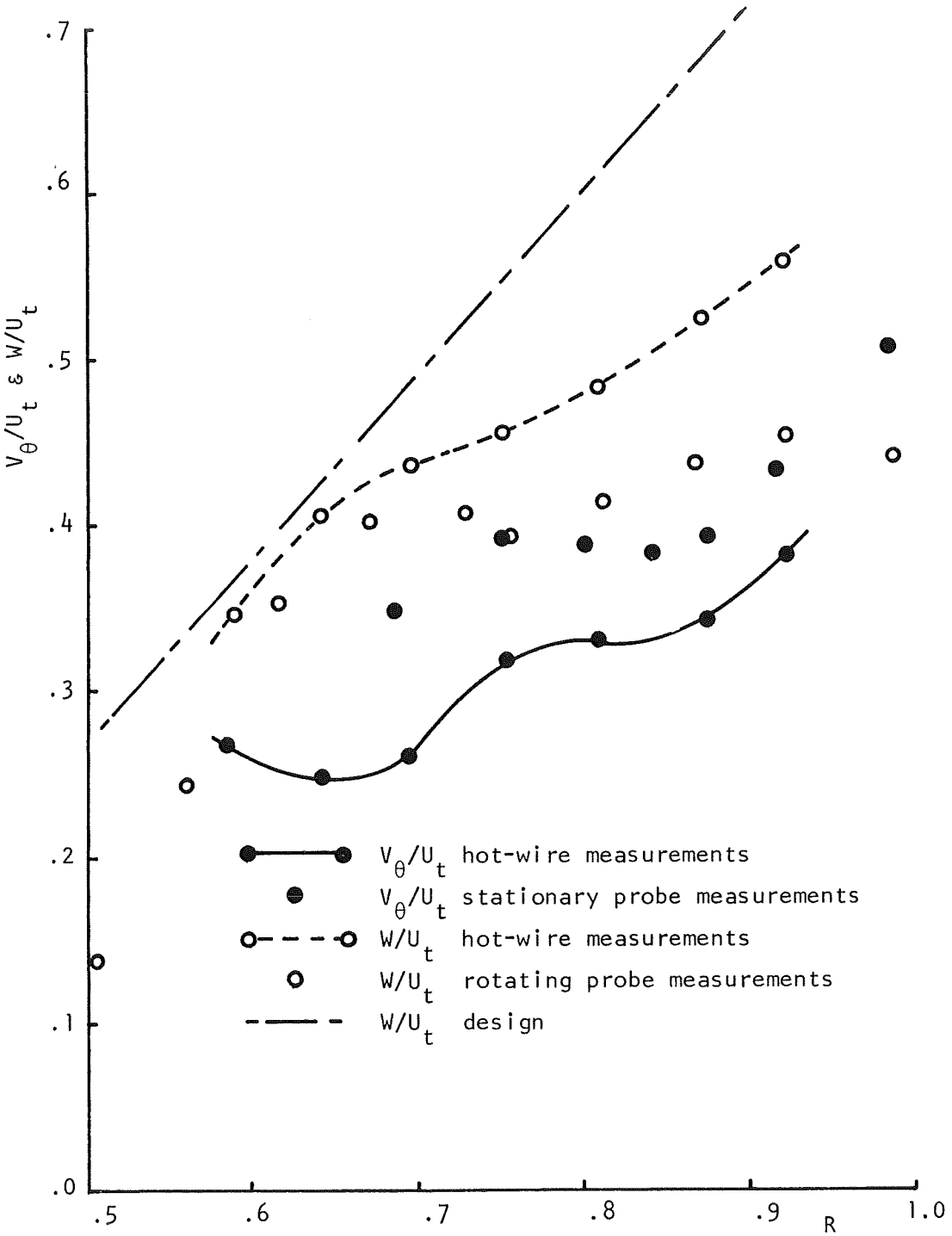

Figure 12b: Absolute Tangential andRelative Velocity at Station 2a

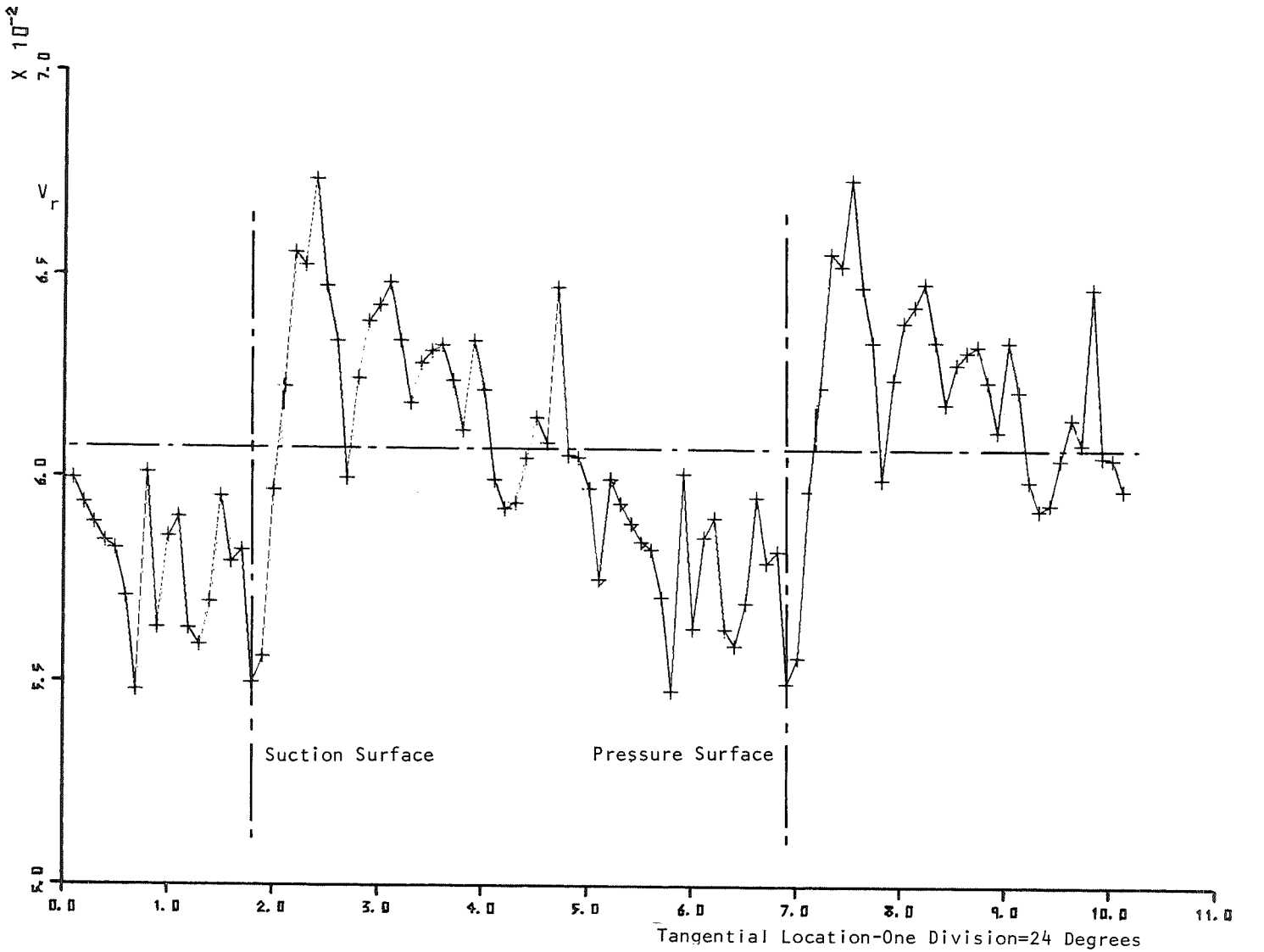

Figure 13a:Blade to Blade Distribution of Radial Velocity,R=0.582, Station 2a

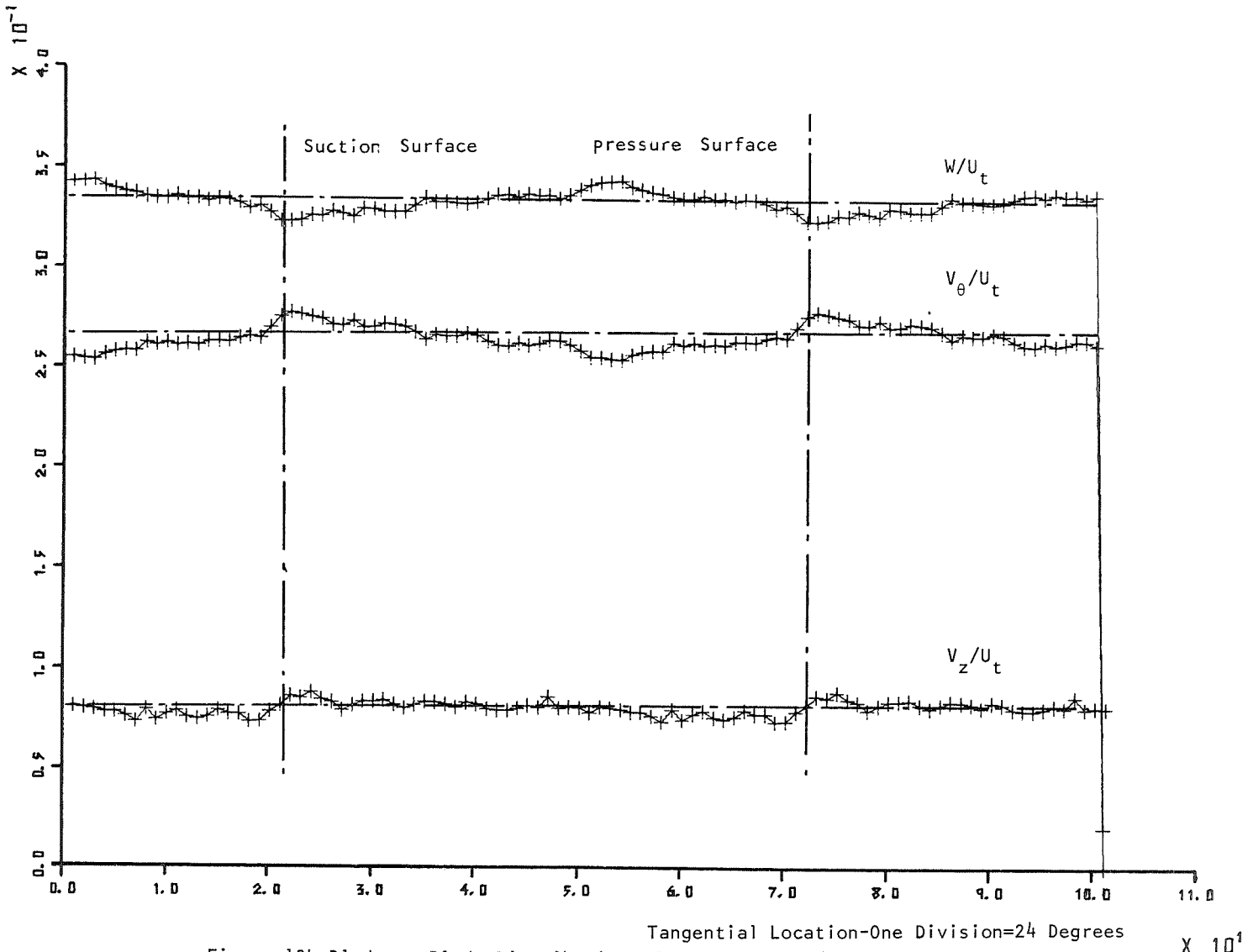

Figure 13b:Blade to Blade Distribution of Relative,Absolute Tangential and Axial Velocities,R=0.582 ,Station 2a

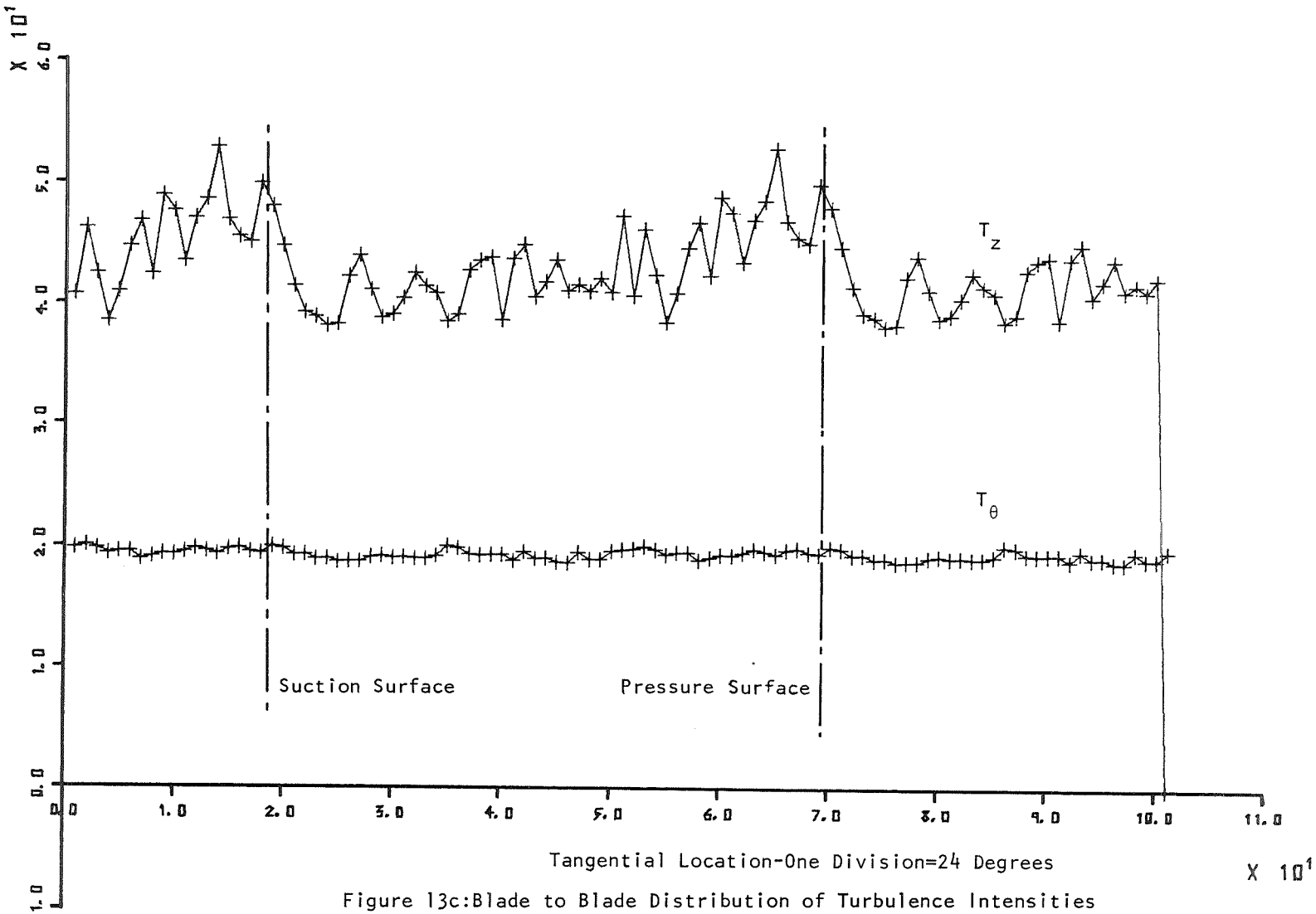

Figure 13c:Blade to Blade Distribution of Turbulence Intensities T_z, T_θ, R=0.582 ,Station 2a

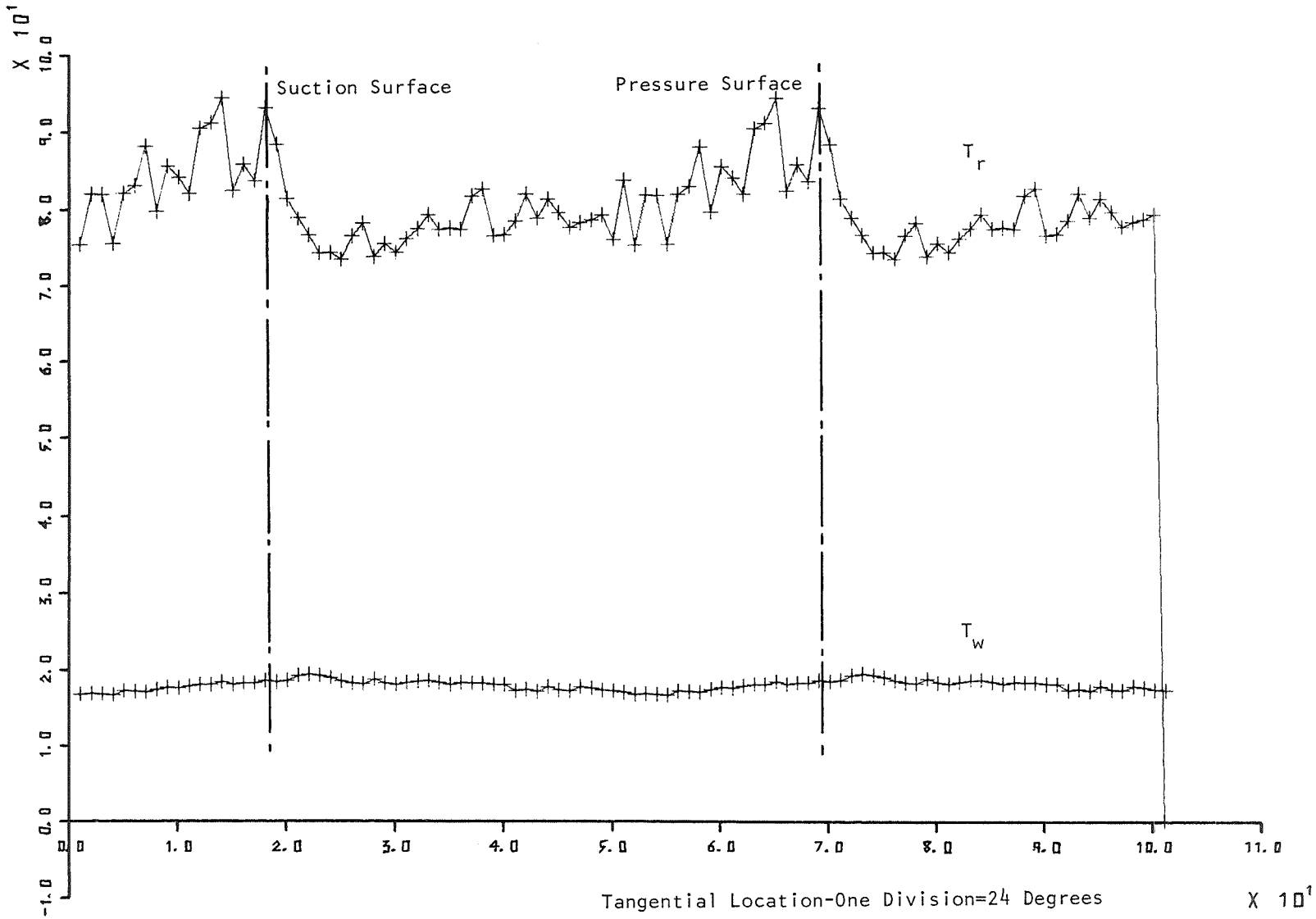

Figure 13d:Blade to blade Distribution of Turbulence Intensities
T_r,T_w,R=0.582,Station 2a

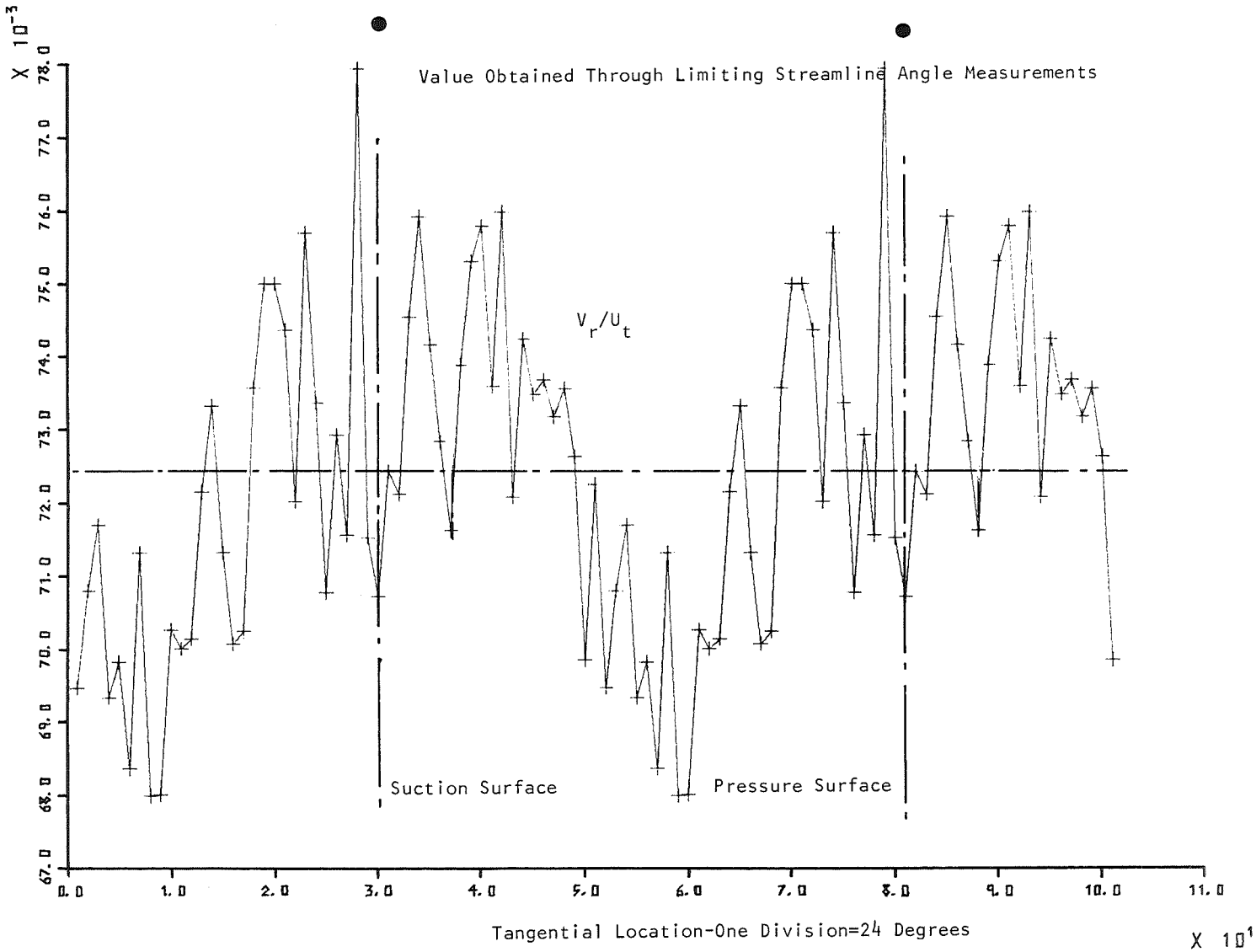

Figure 14a:Blade to Blade Distribution of Radial Velocity,R=0.752, Station 2a

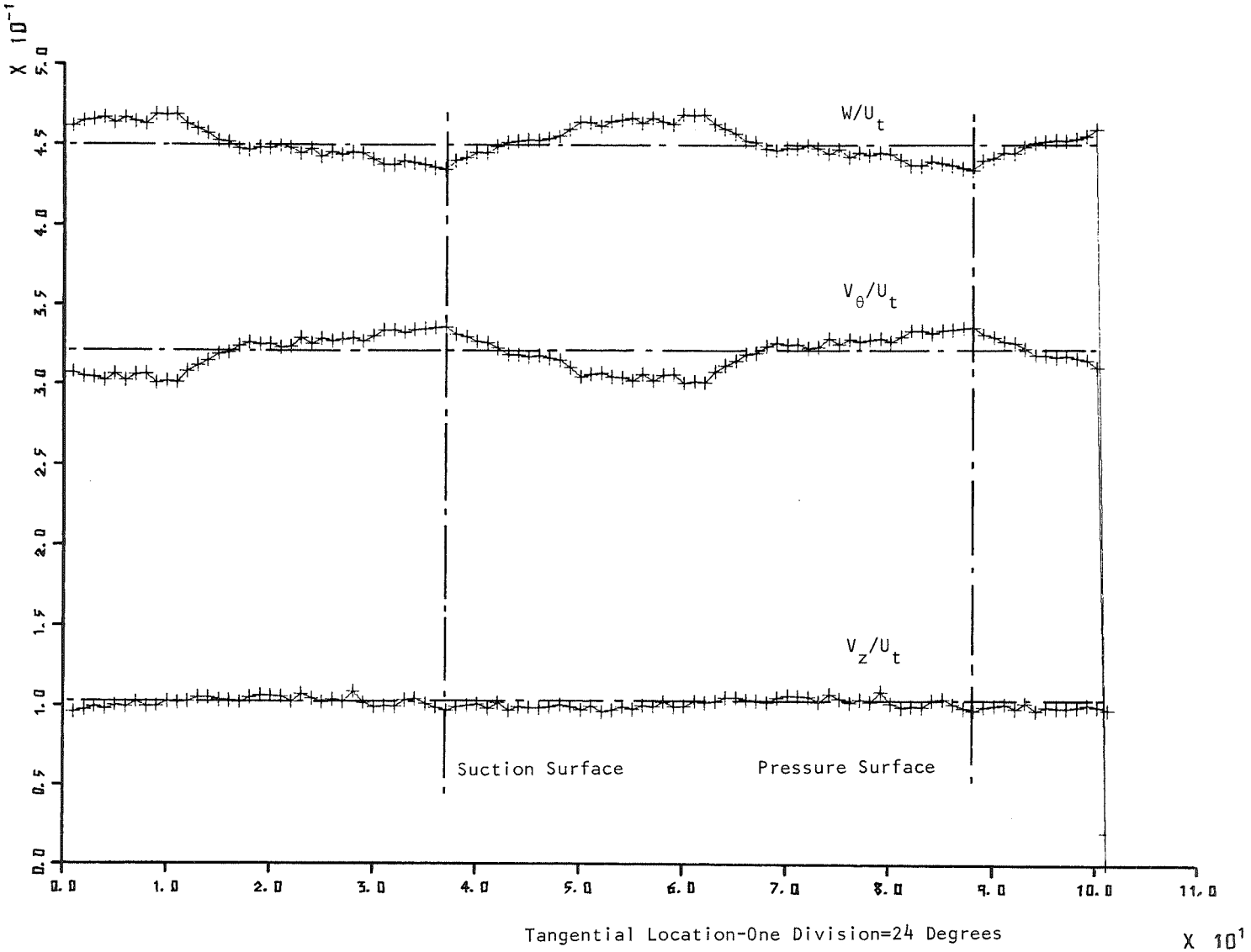

Figure 14b:Blade to Blade Variation of Relative,Absolute Tangential, and Axial Velocities,R=0.752,Station 2a

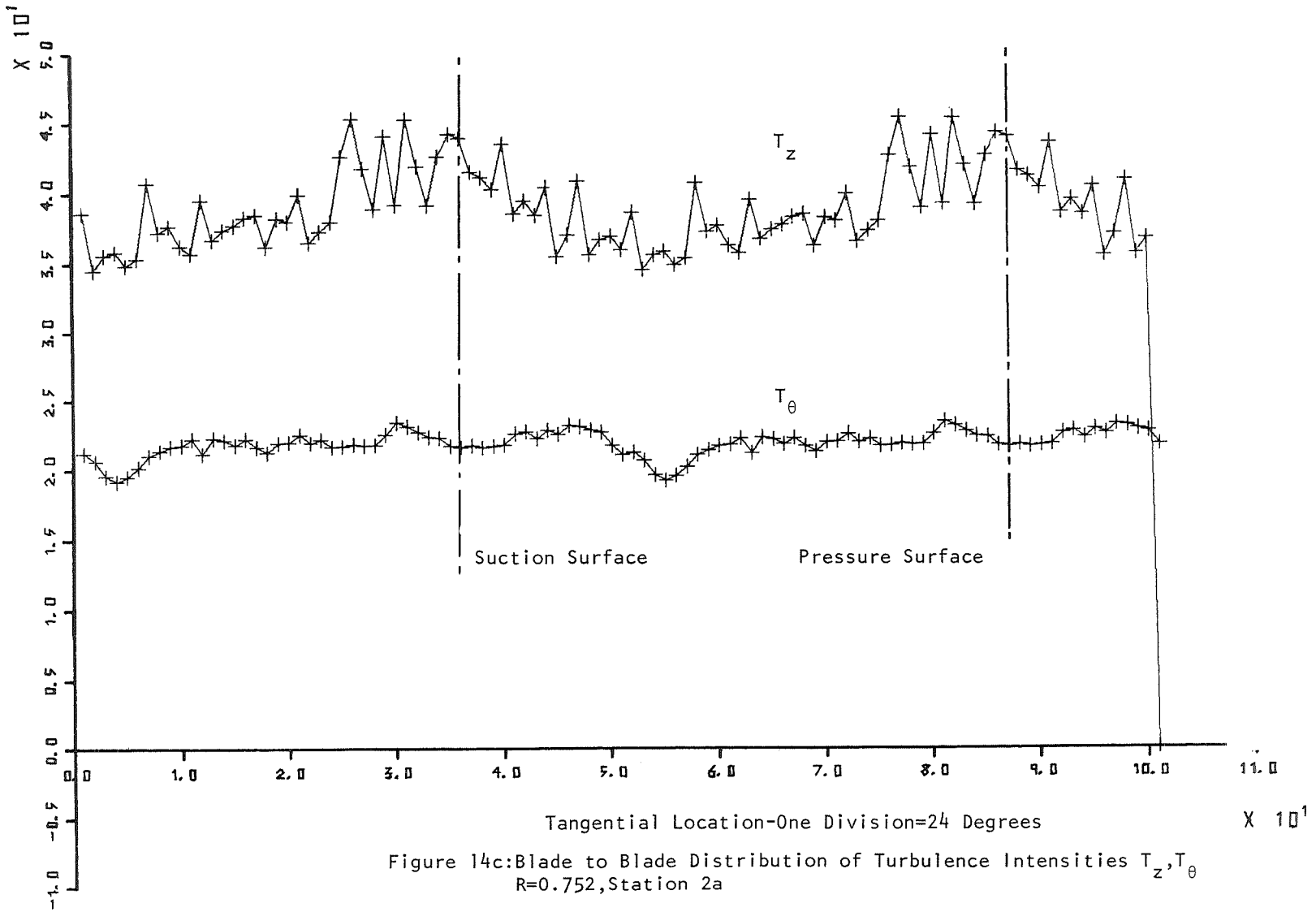

Figure 14c:Blade to Blade Distribution of Turbulence Intensities T_z,T_θ
R=0.752,Station 2a

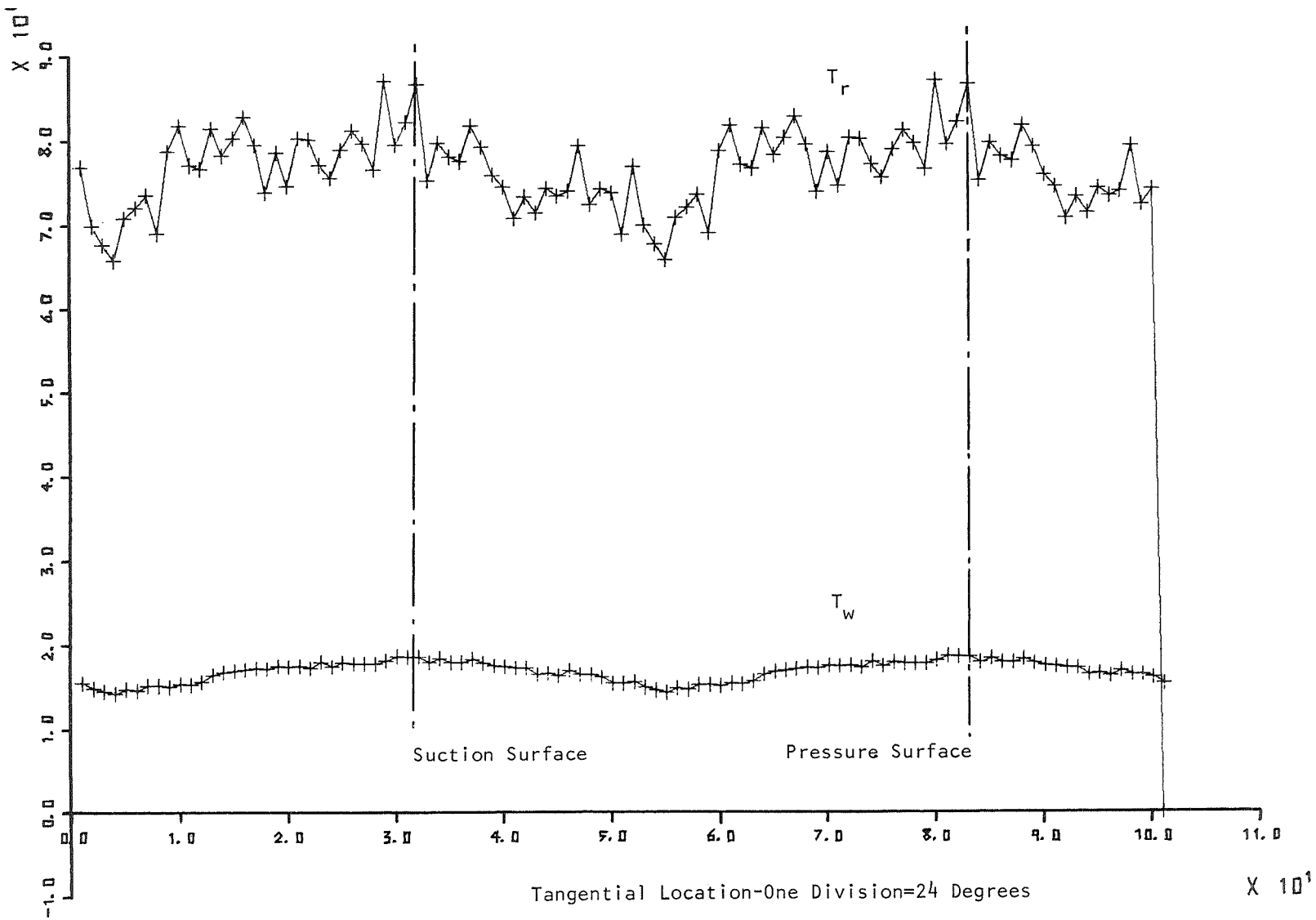

Figure 14d:Blade to Blade Distribution of Turbulence Intensities
T_r,T_w,R=0.752,Station 2a

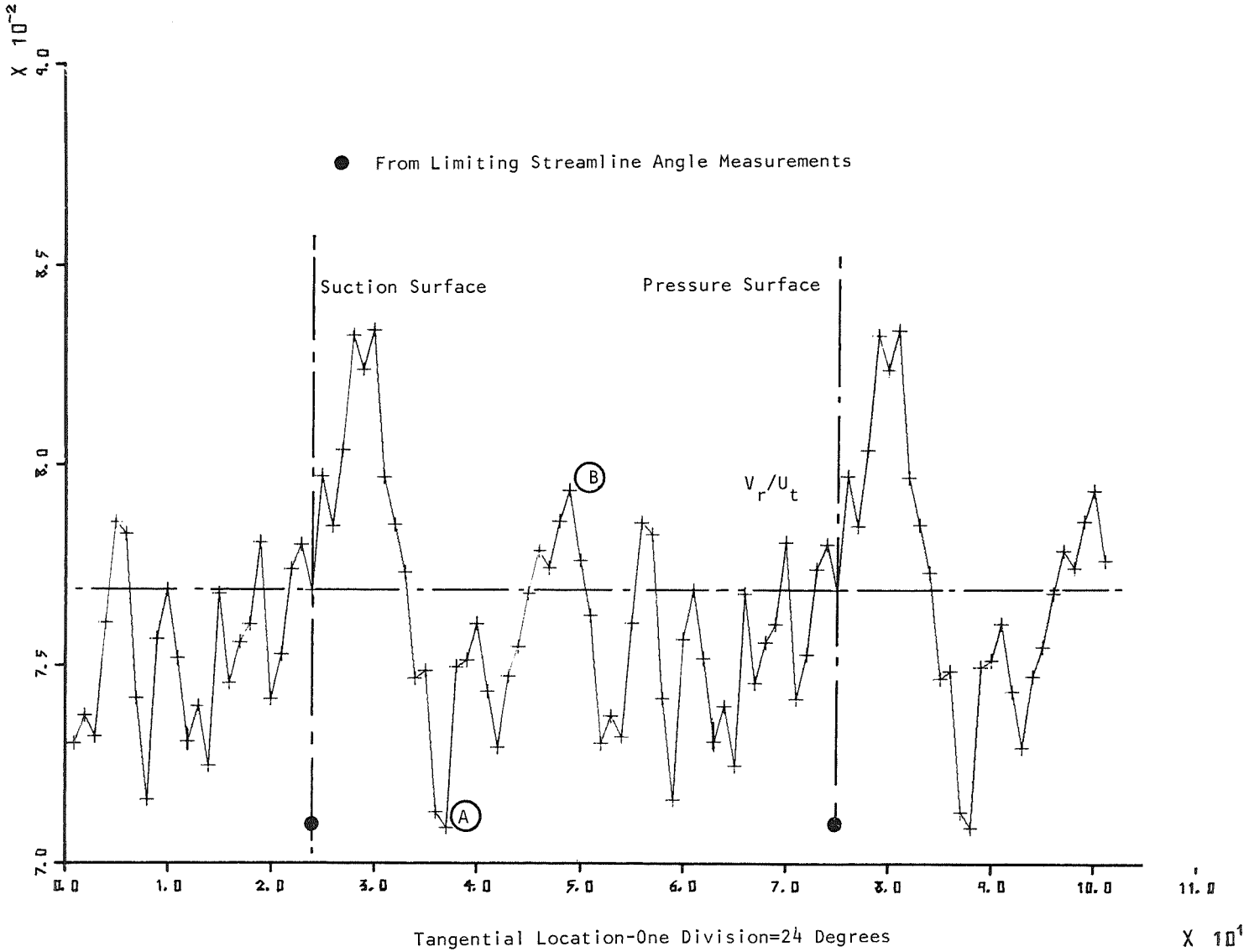

Figure 15a:Blade to Blade Distribution of Radial Velocity R=0.860
Station 2a

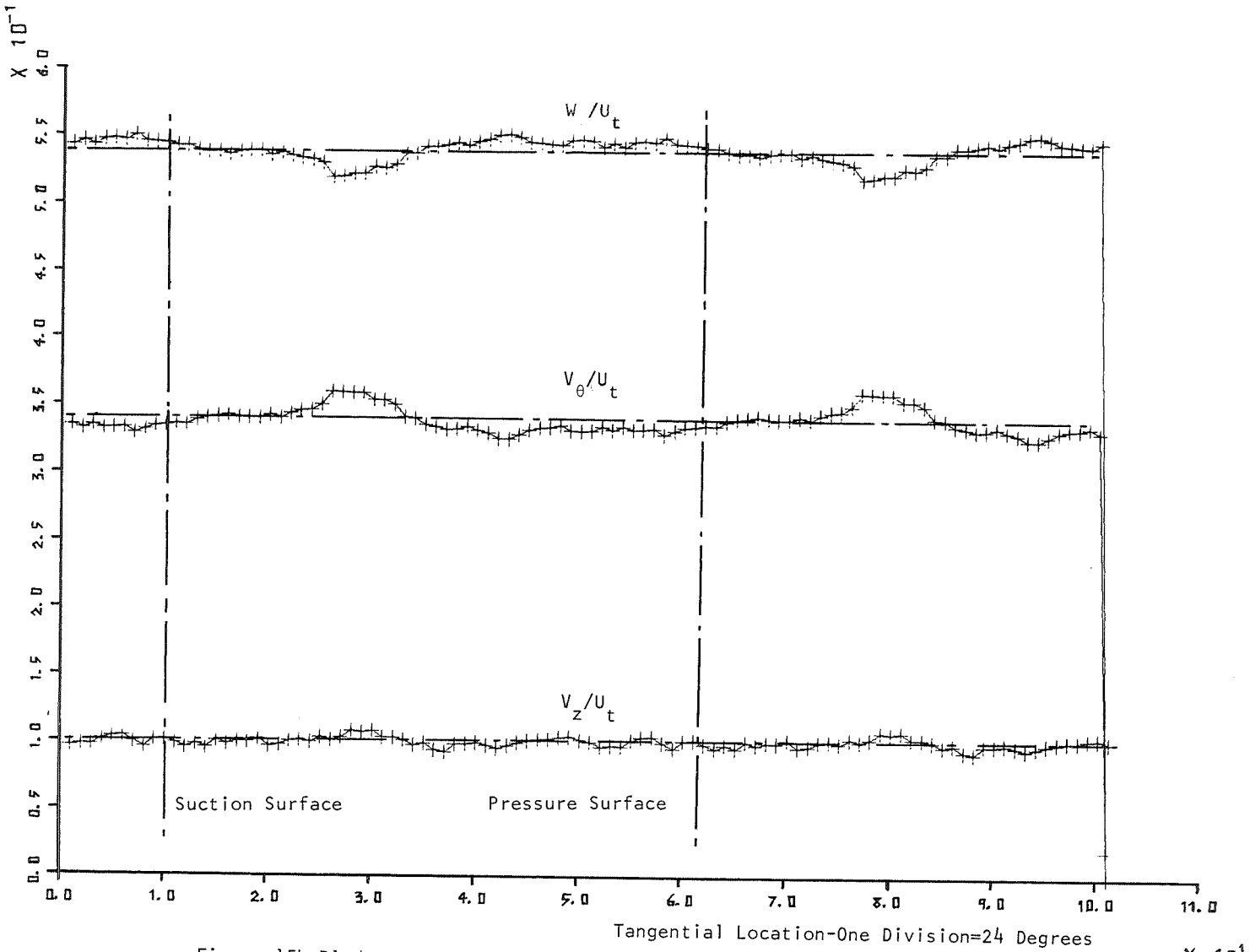

Figure 15b:Blade to Blade Distribution of Relative,Absolute Tangential, and Axial Velocities,R=0.860,Station 2a

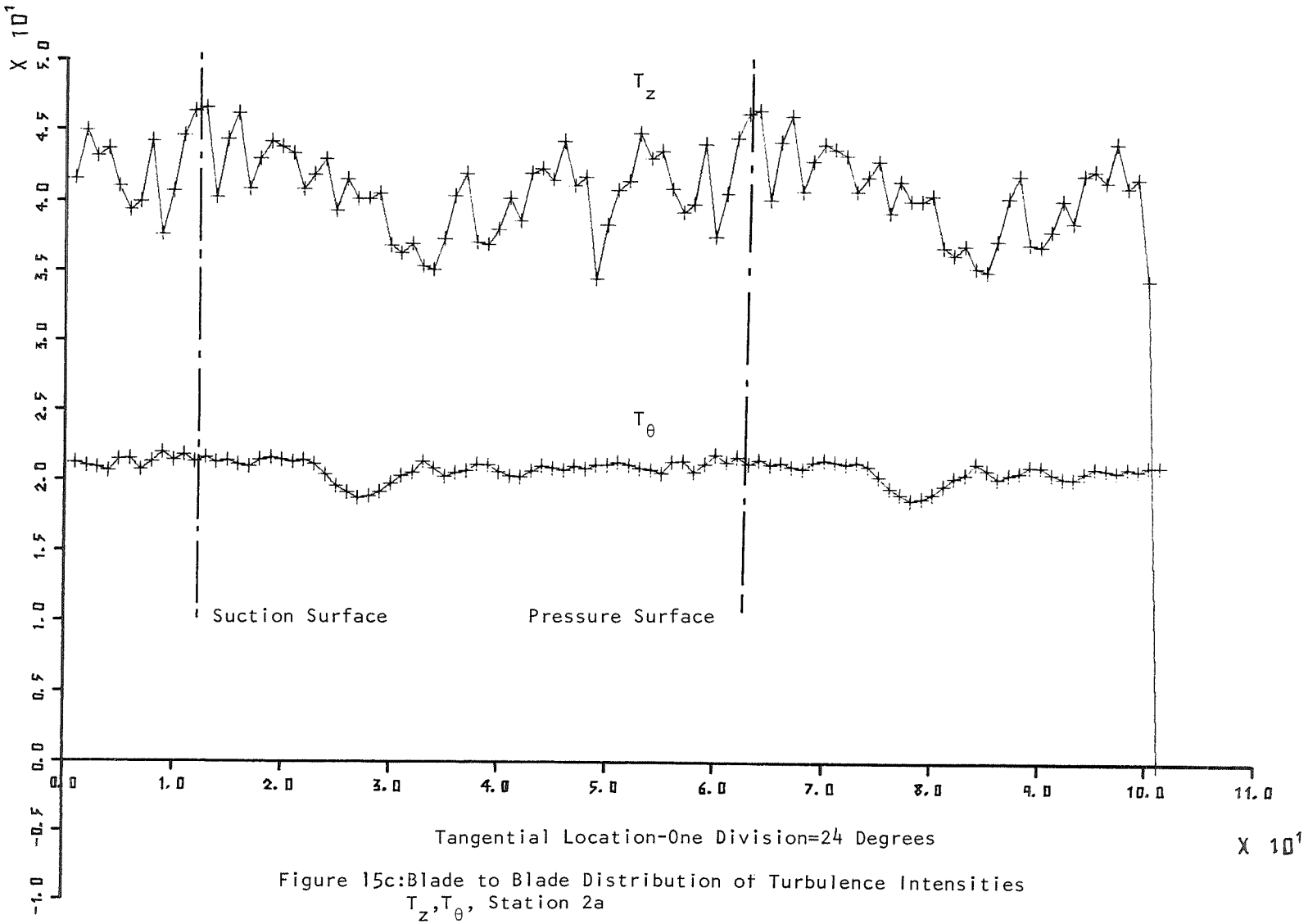

Figure 15c:Blade to Blade Distribution of Turbulence Intensities T_z,T_θ, Station 2a

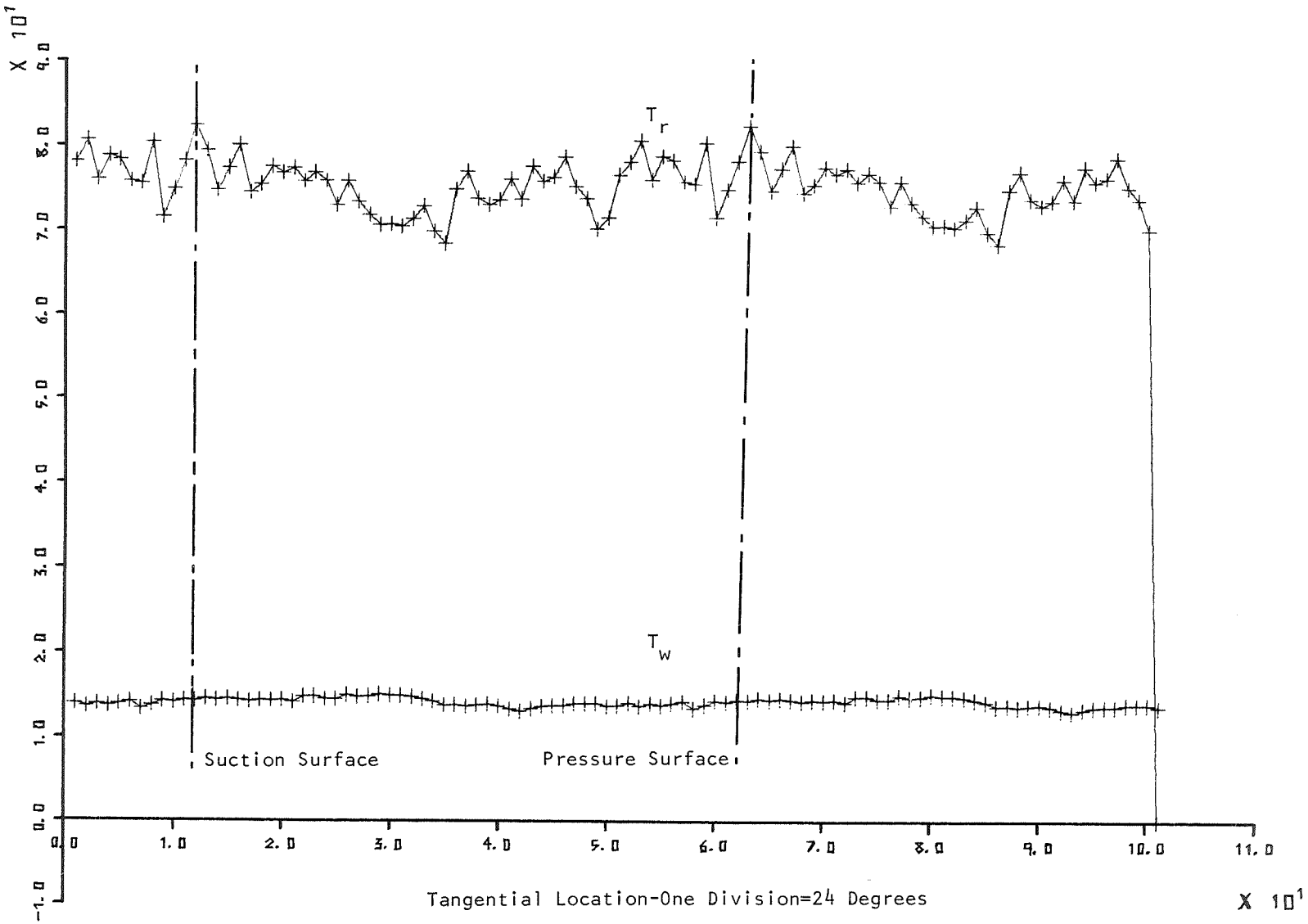

Figure 15d :Blade to Blade Distribution Of Turbulence Intensities T_r,T_w,Station 2a

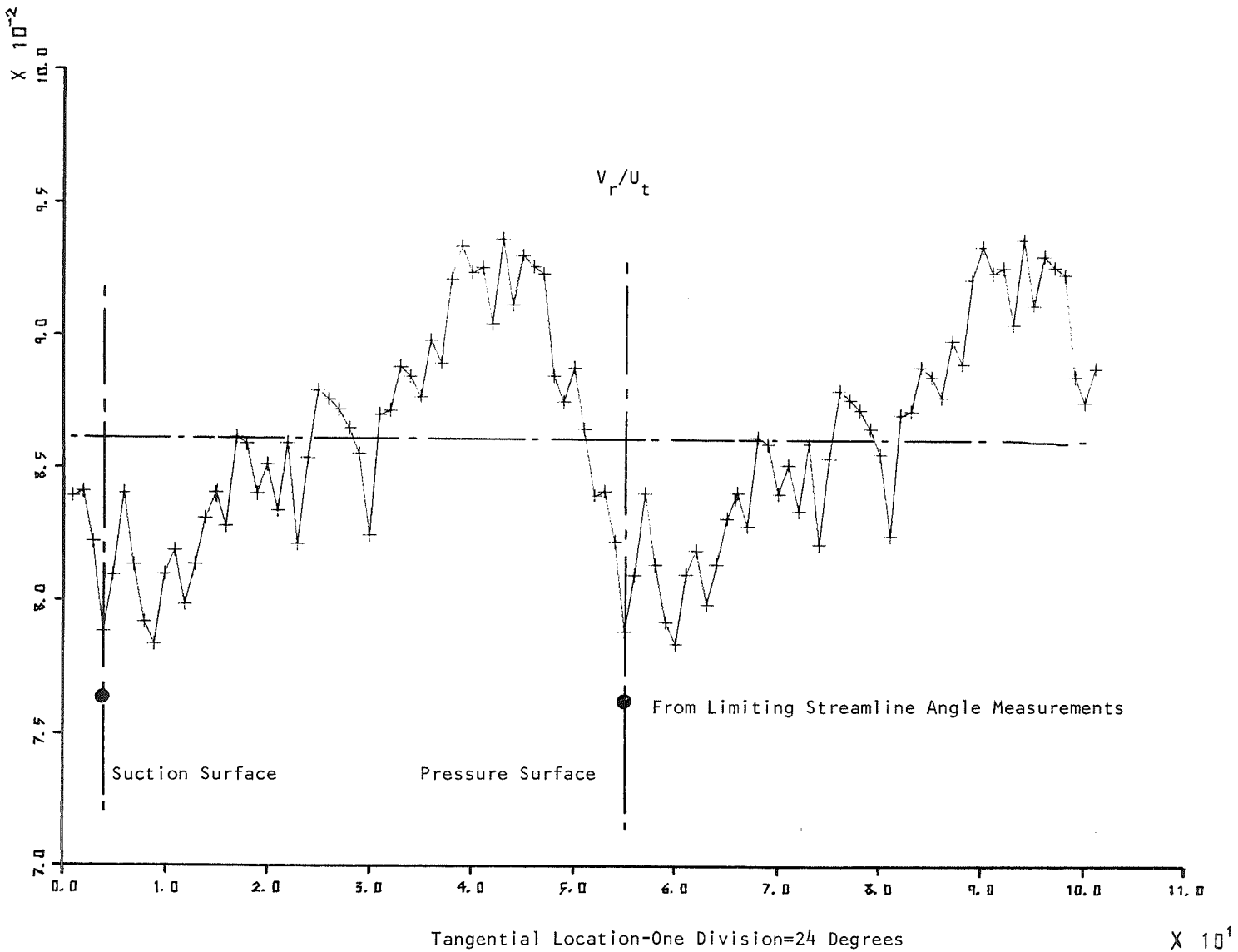

Figure 16a:Blade to Blade Distribution of Radial Velocity,R=0.920, Station 2a

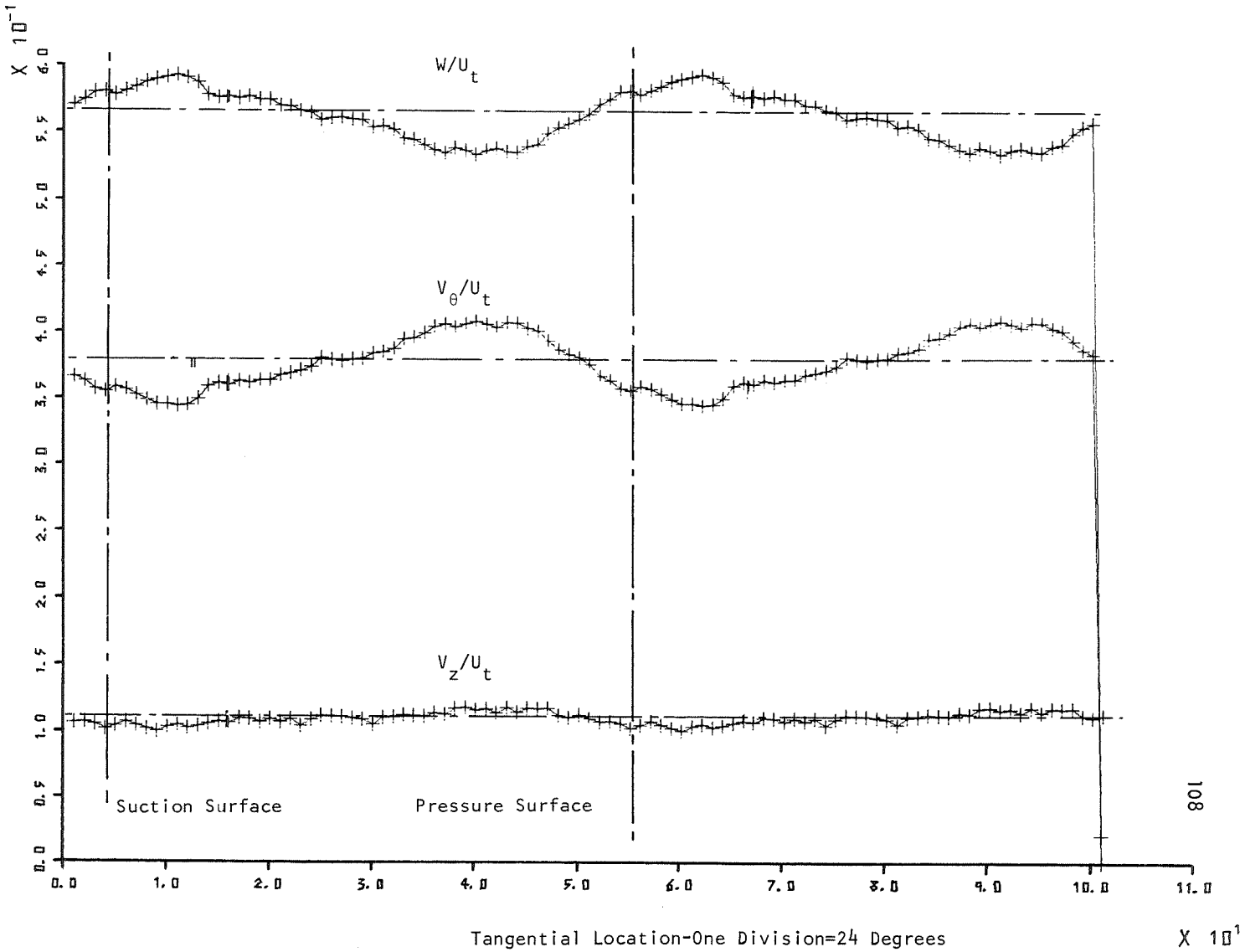

Figure 16b:Blade to Blade Distribution of Relative,Absolute Tangential, and Axial Velocities,R=0.920,Station 2a

108

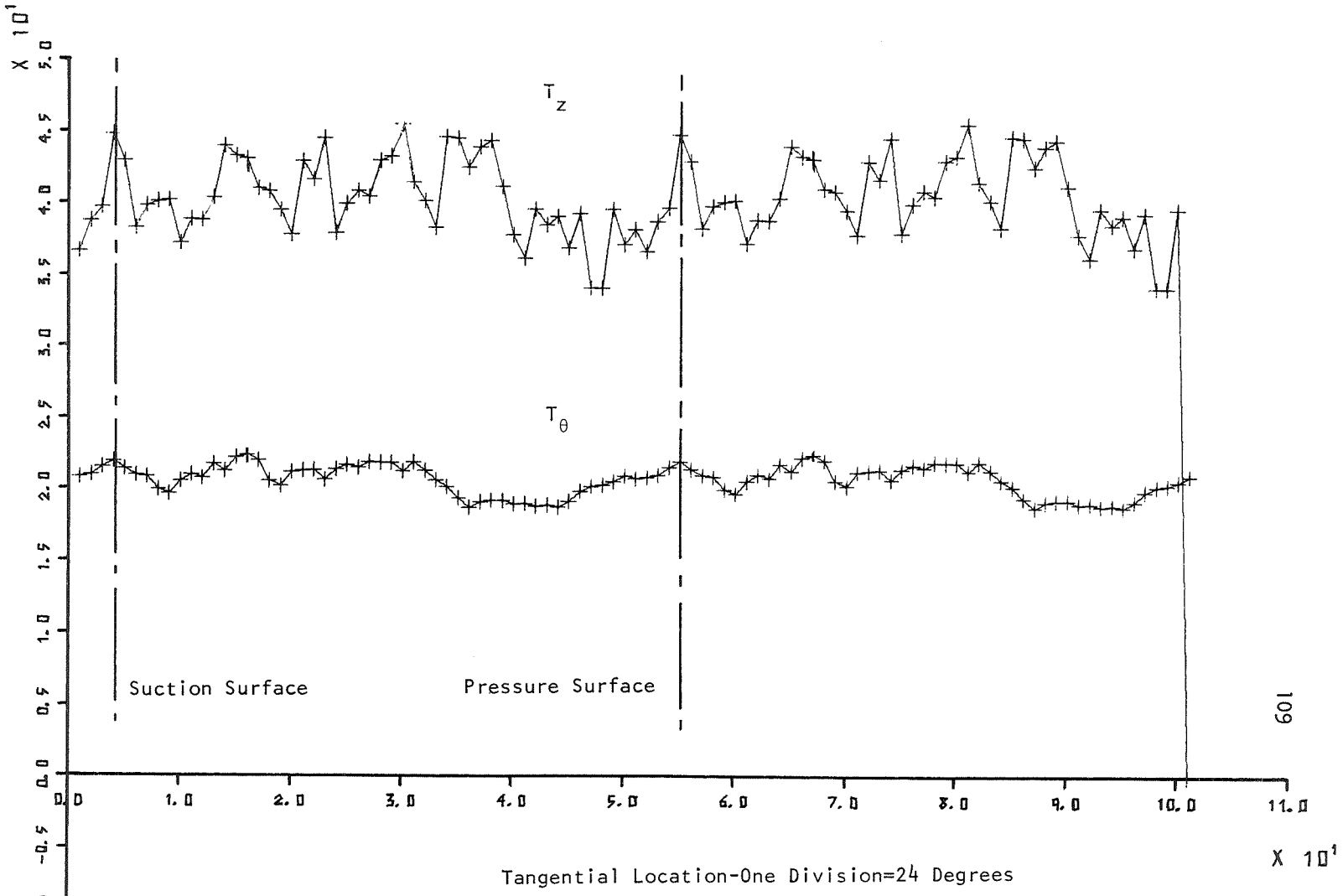

Figure 16c:Blade to Blade Distribution of Turbulence Intencities
T_z,T_θ,Station 2a,R=0.920

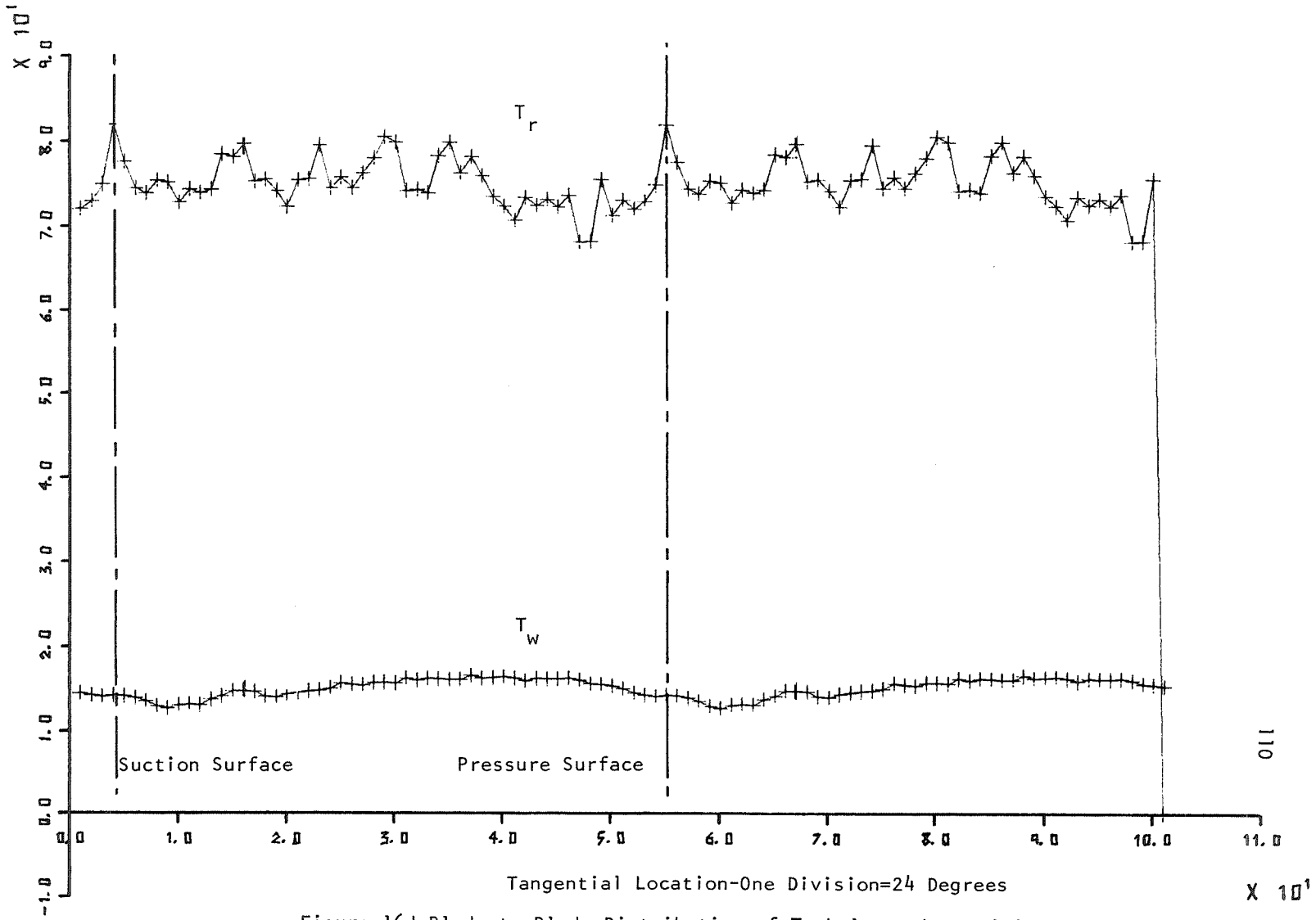

Figure 16d:Blade to Blade Distribution of Turbulence Intensities
T_r,T_w,R=0.920,Station 2a

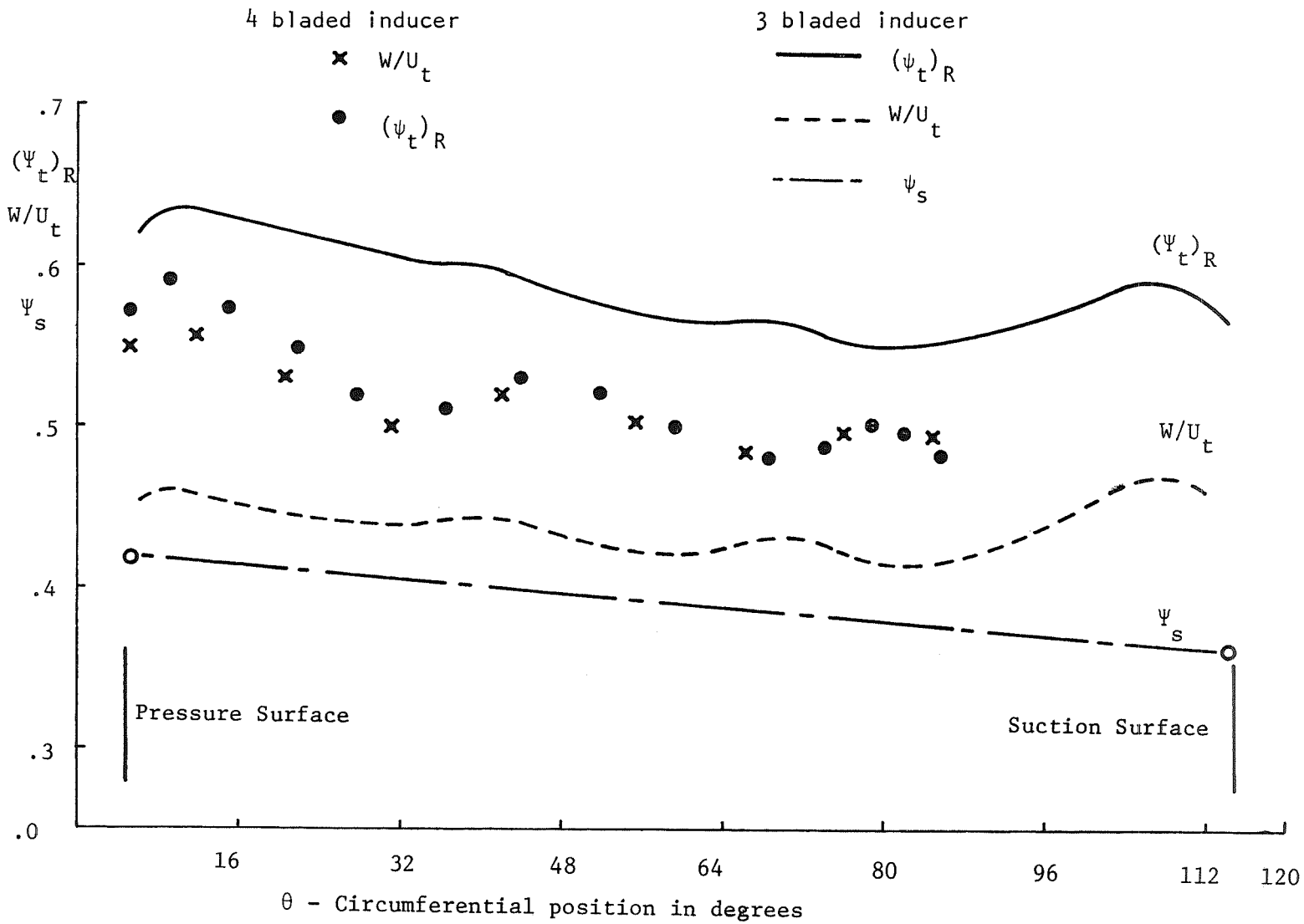

Figure 17a: Blade toBlade Variation of Stagnation and Static Heads, Resultant Velocity,of the Relative Flow at Station 2,R=.974

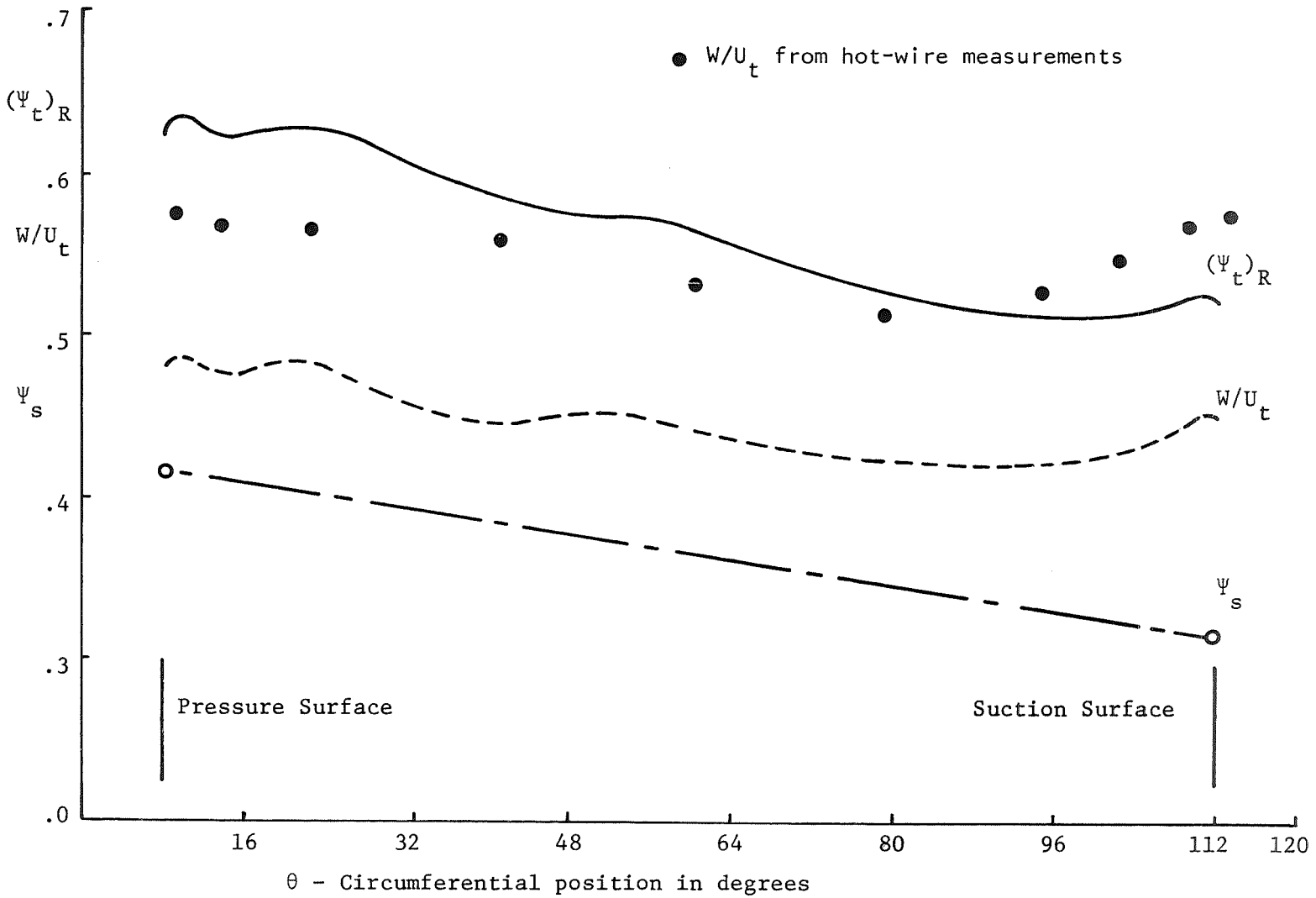

Figure 17b: Blade to Blade Variation of Stagnation and Static Heads, Resultant Velocity, of the Relative Flow at Station 2, R=.920

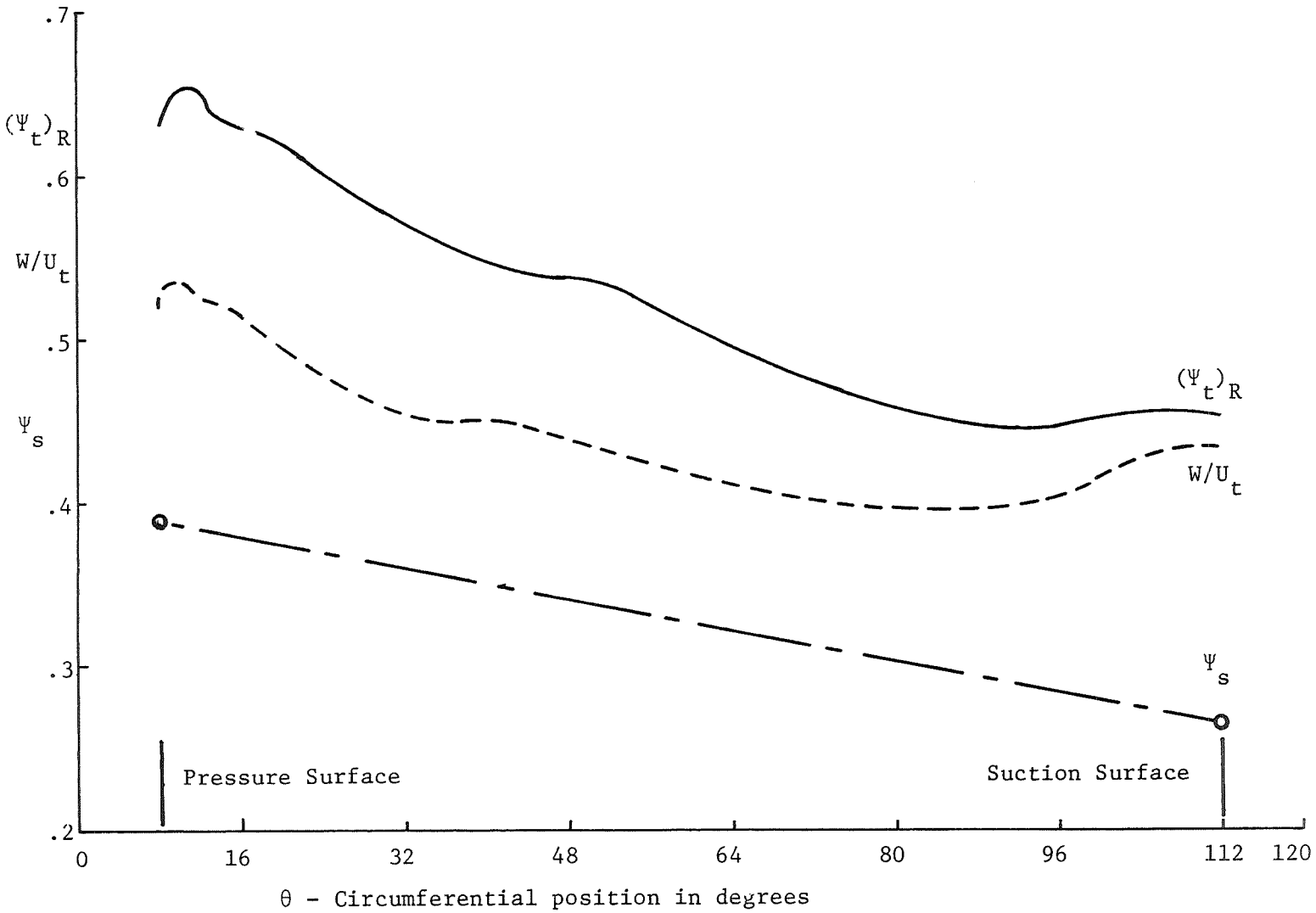

Figure 17c: Blade to Blade Variation of Stagnation and Statuc Heads, Resultant Velocity,of the Relative Flow at Station 2,R=.863

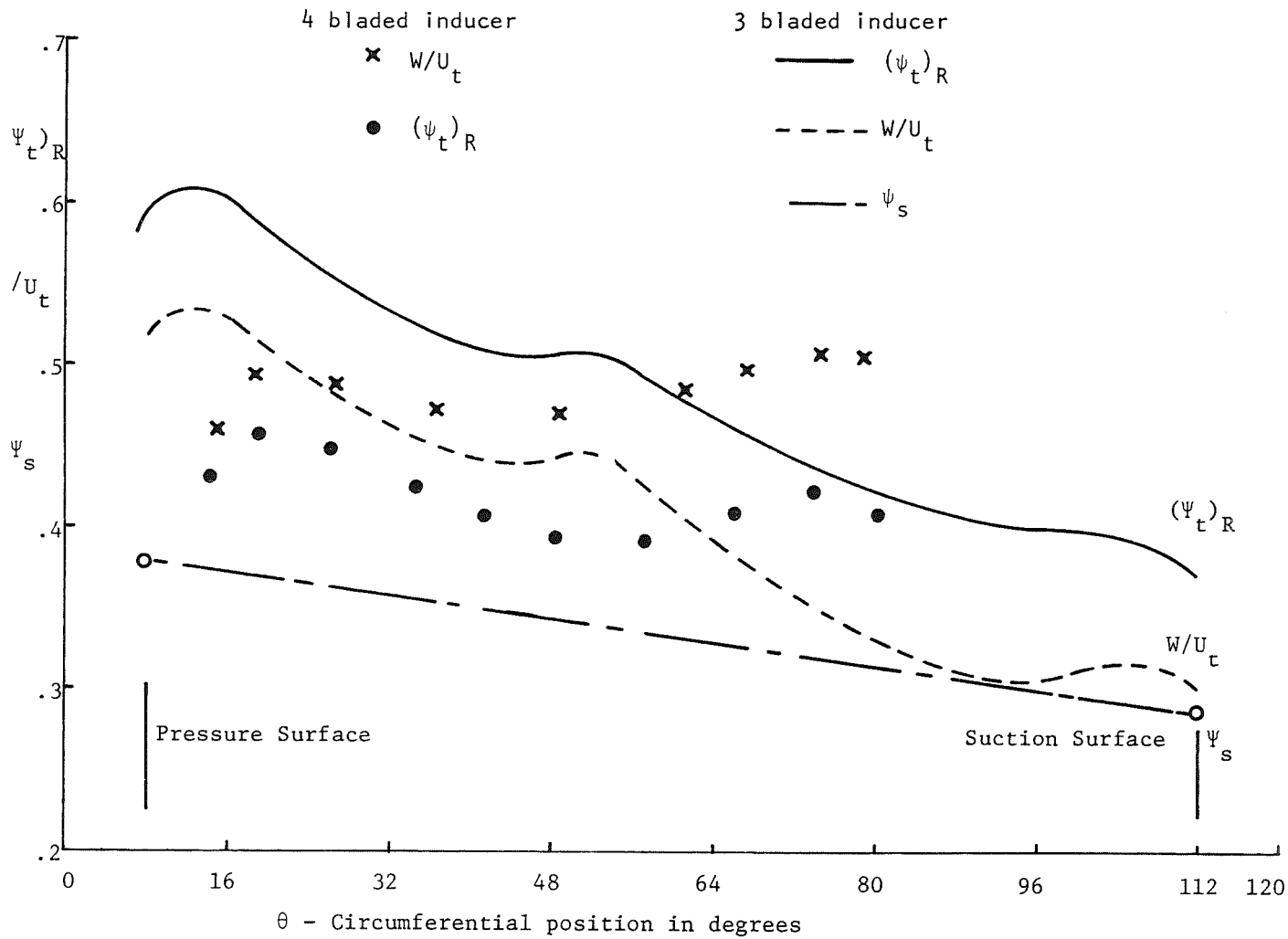

Figure 17d: Blade to Blade Variation of Stagnation and Static Heads, Resultant Velocity, of the Relative Flow at Station 2, R=.808

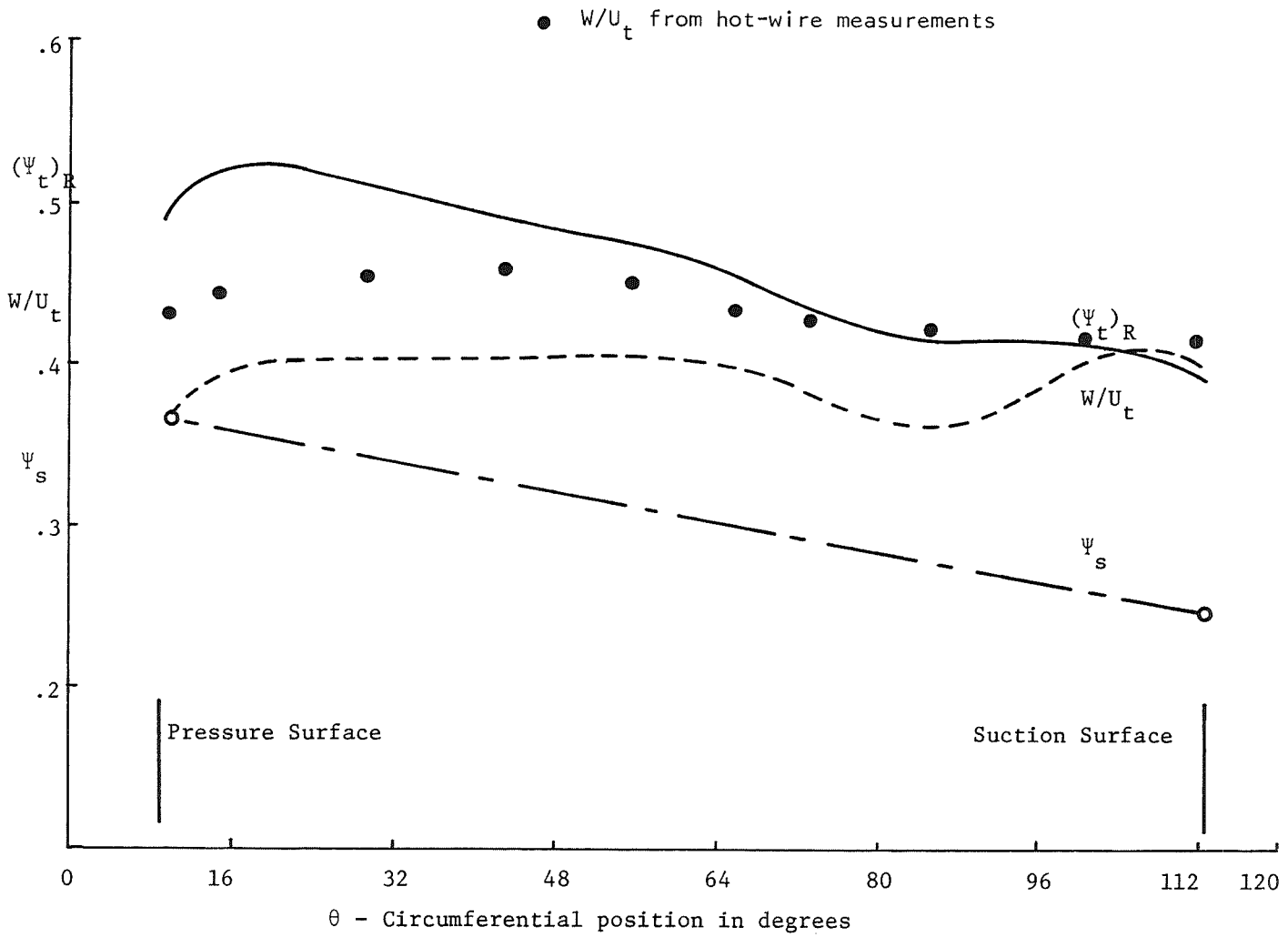

Figure 17e: Blade to Blade Variation of Stagnation and Static Heads, Resultant Velocity, of the Relative Flow at Station 2, R=.754

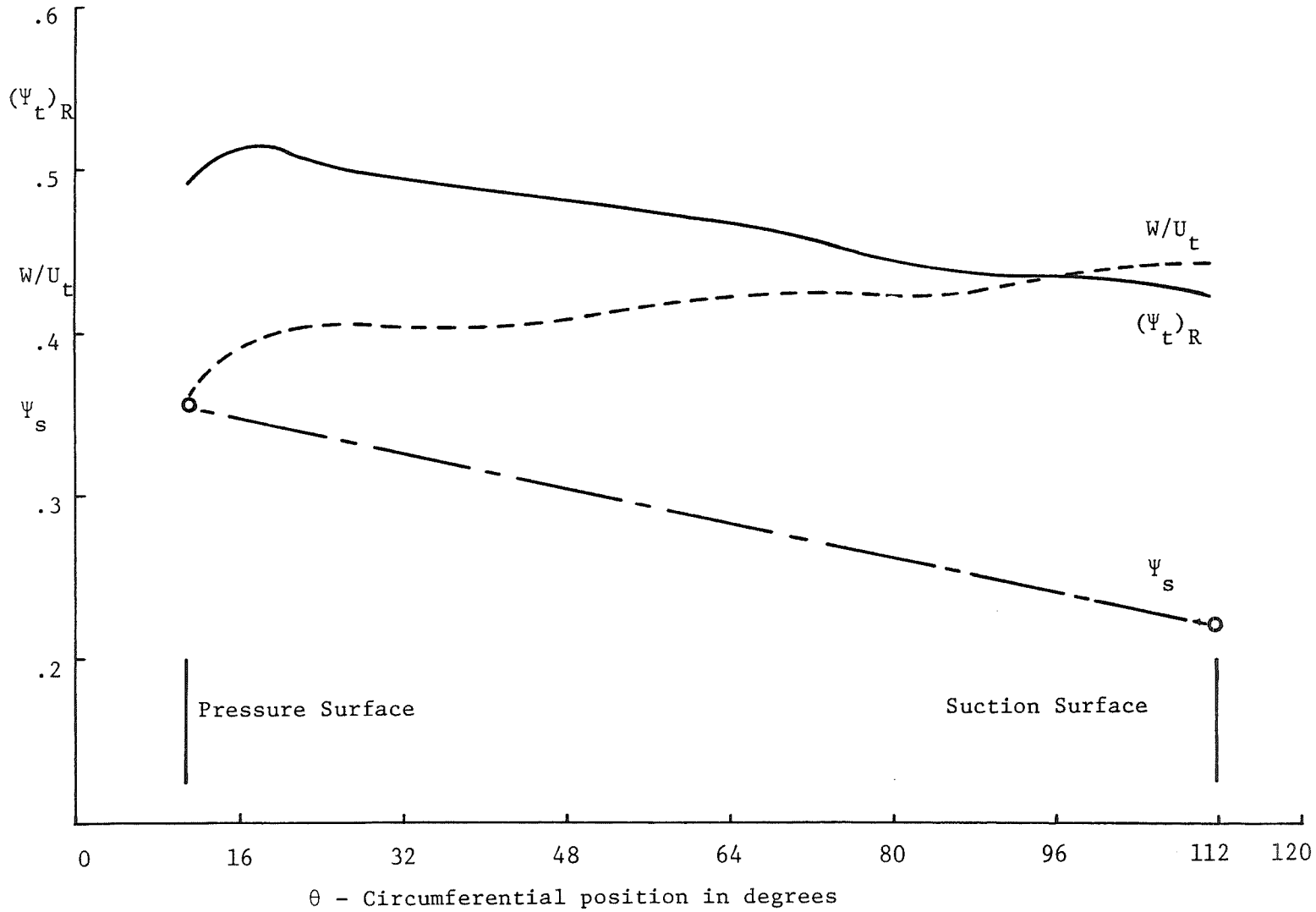

Figure 17f: Blade to Blade Variation of Stagnation and Static Heads, Resultant Velocity, of the Relative Flow at Station 2, R=.720

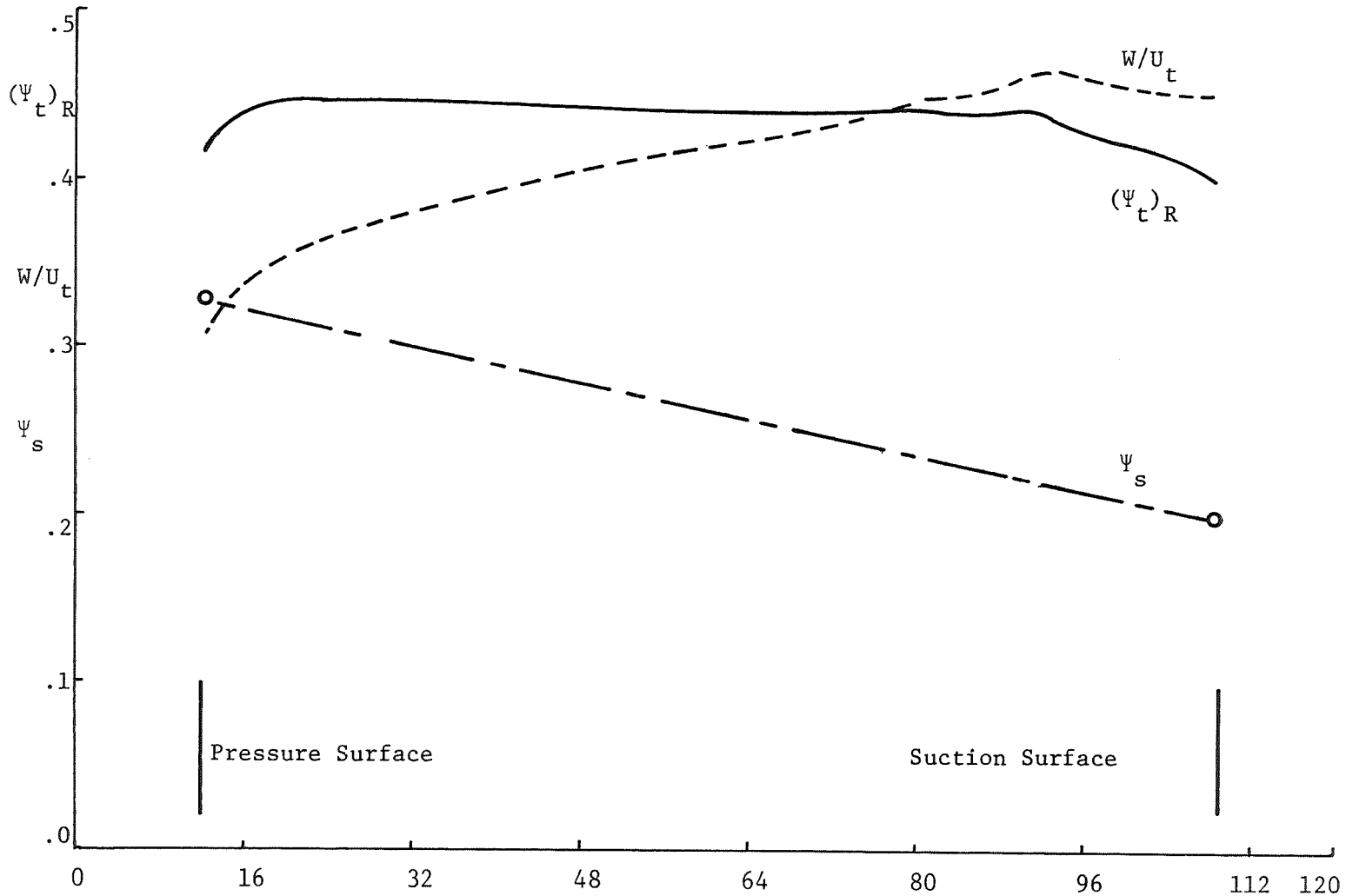

θ - Circumferential position in degrees

Figure 17 g: Blade to Blade Variation of Stagnation and Static Heads, Resultant Velocity, of the Relative Flow at Station 2, R=.672

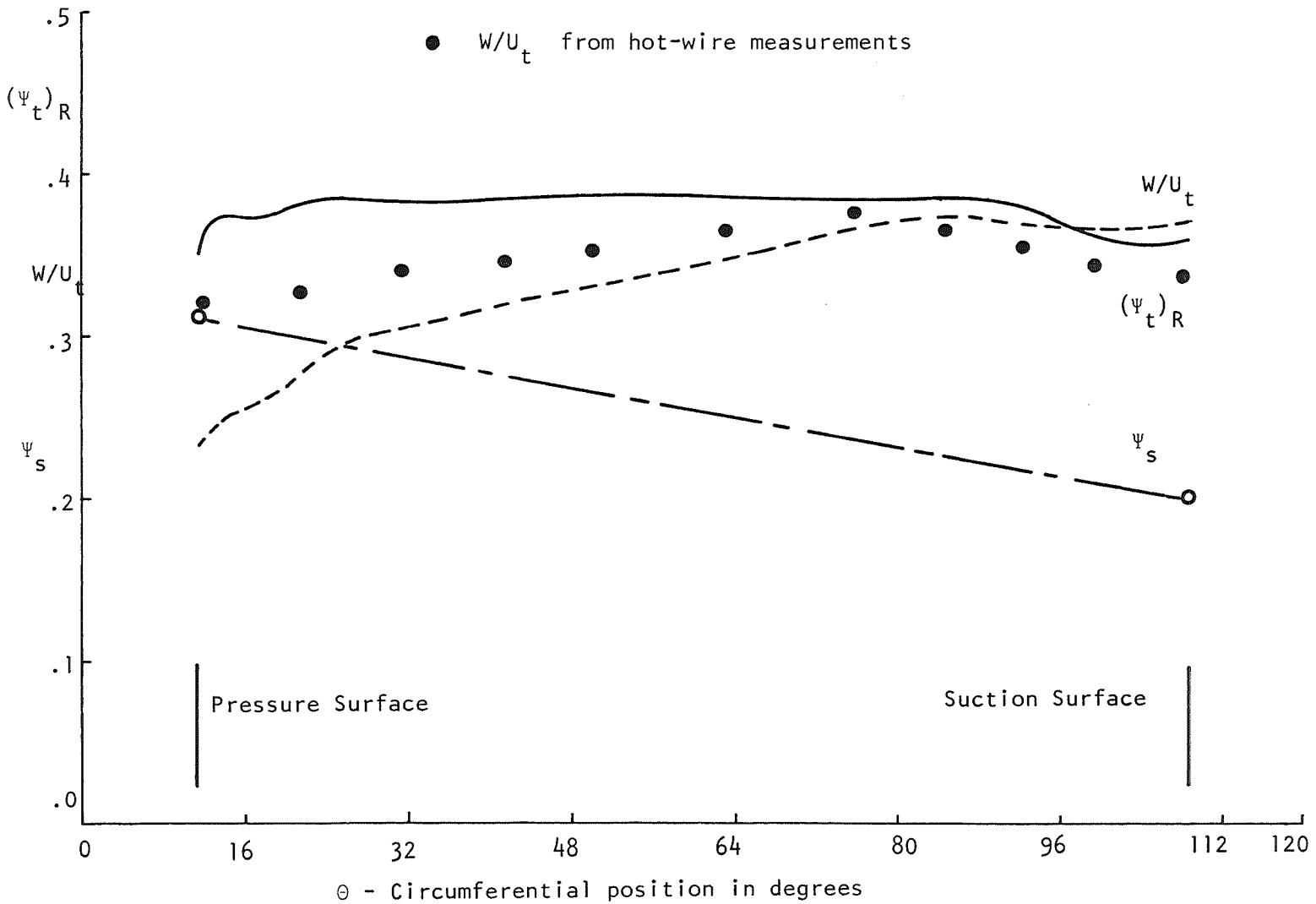

Figure 17h : Blade to Blade Variation of Stagnation and Static Heads, Resultant Velocity, of the Relative Flow at Station 2, R=.617

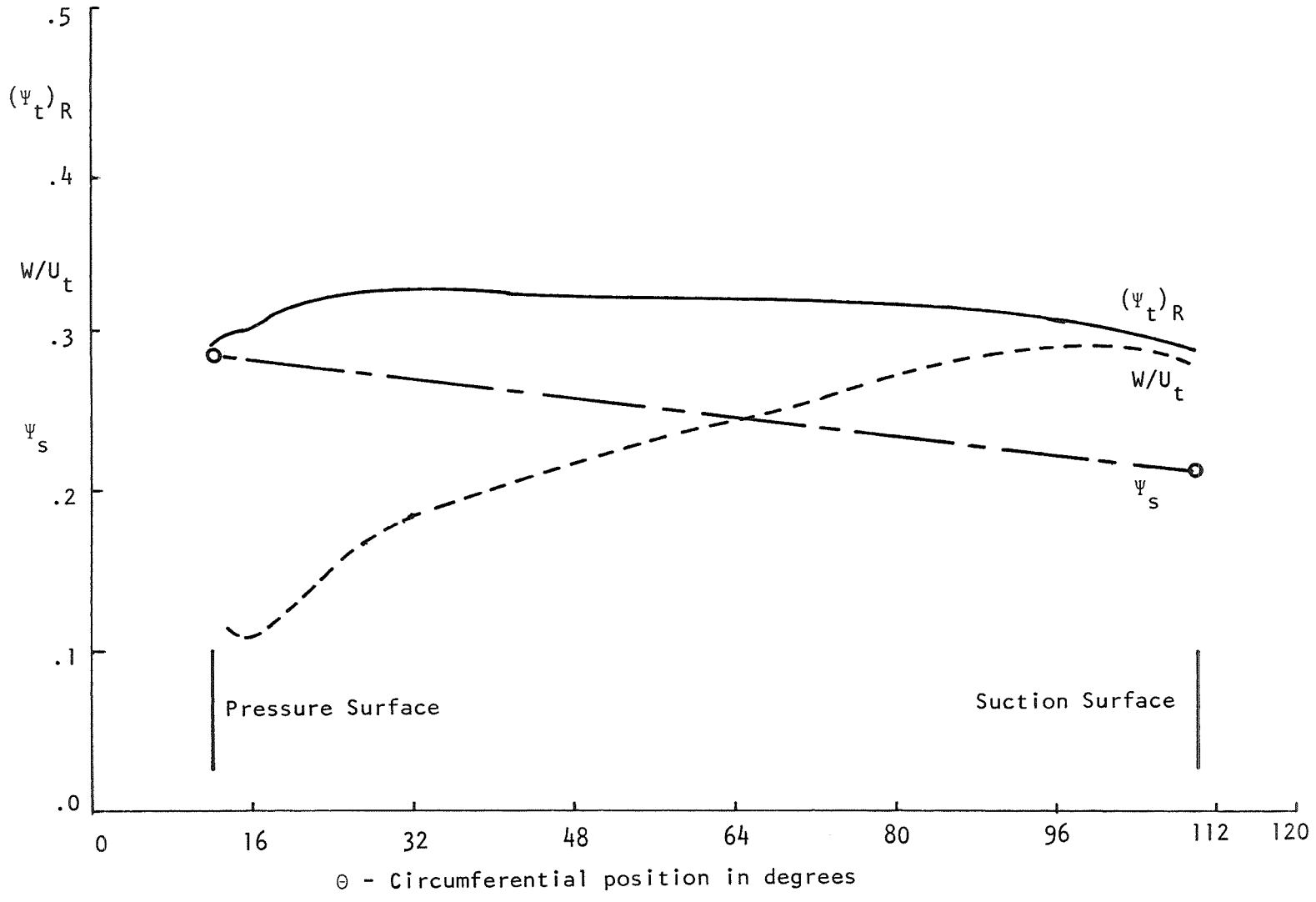

Figure 17i: Blade to Blade Variation of Stagnation and Static Heads, Resultant Velocity, of the Relative Flow at Station 2, R=.562

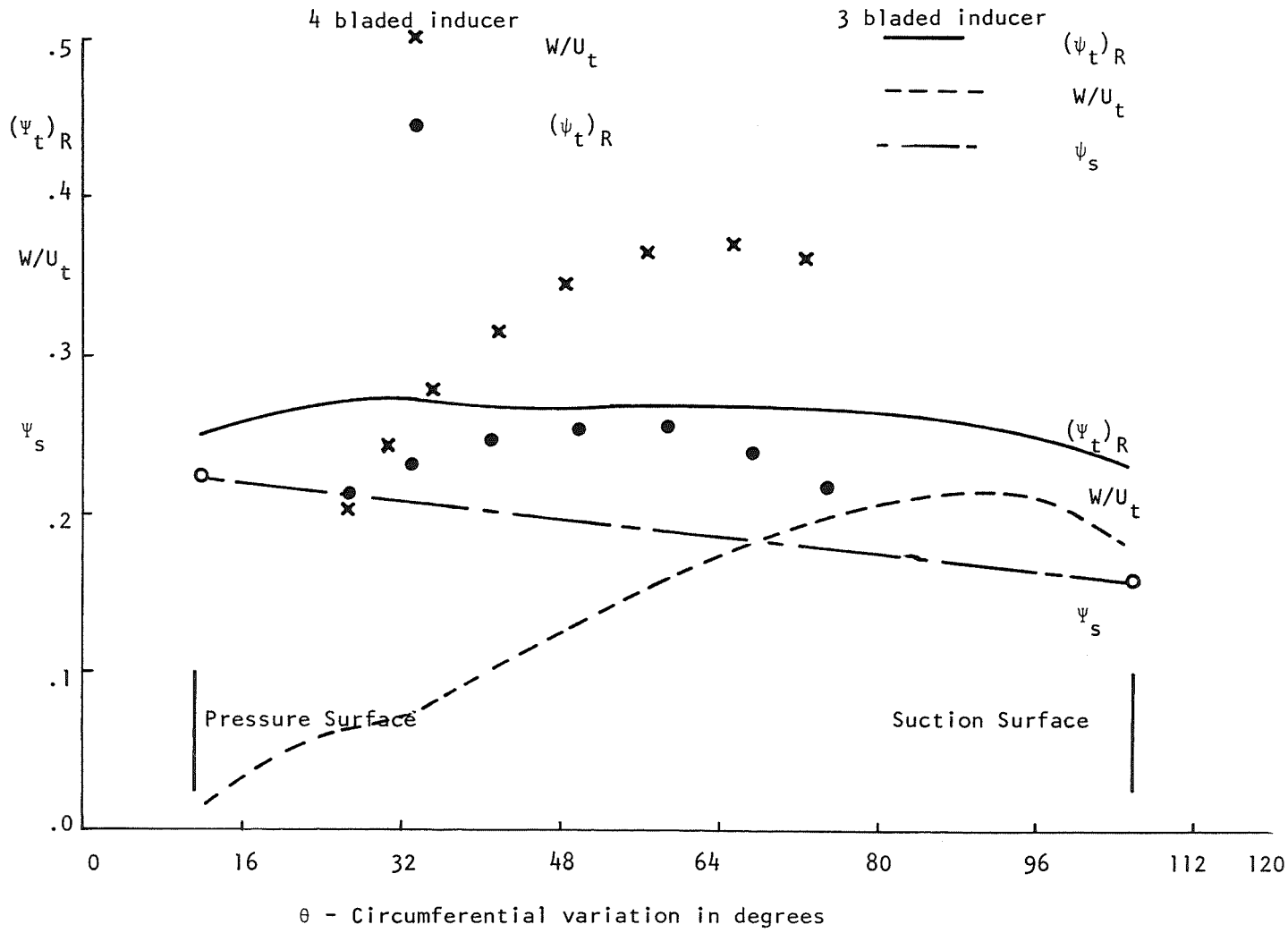

Figure 17 j: Blade to Blade Variation of Stagnation and Static Heads, Resultant Velocity, of the Relative Flow at Station 2, R=.506

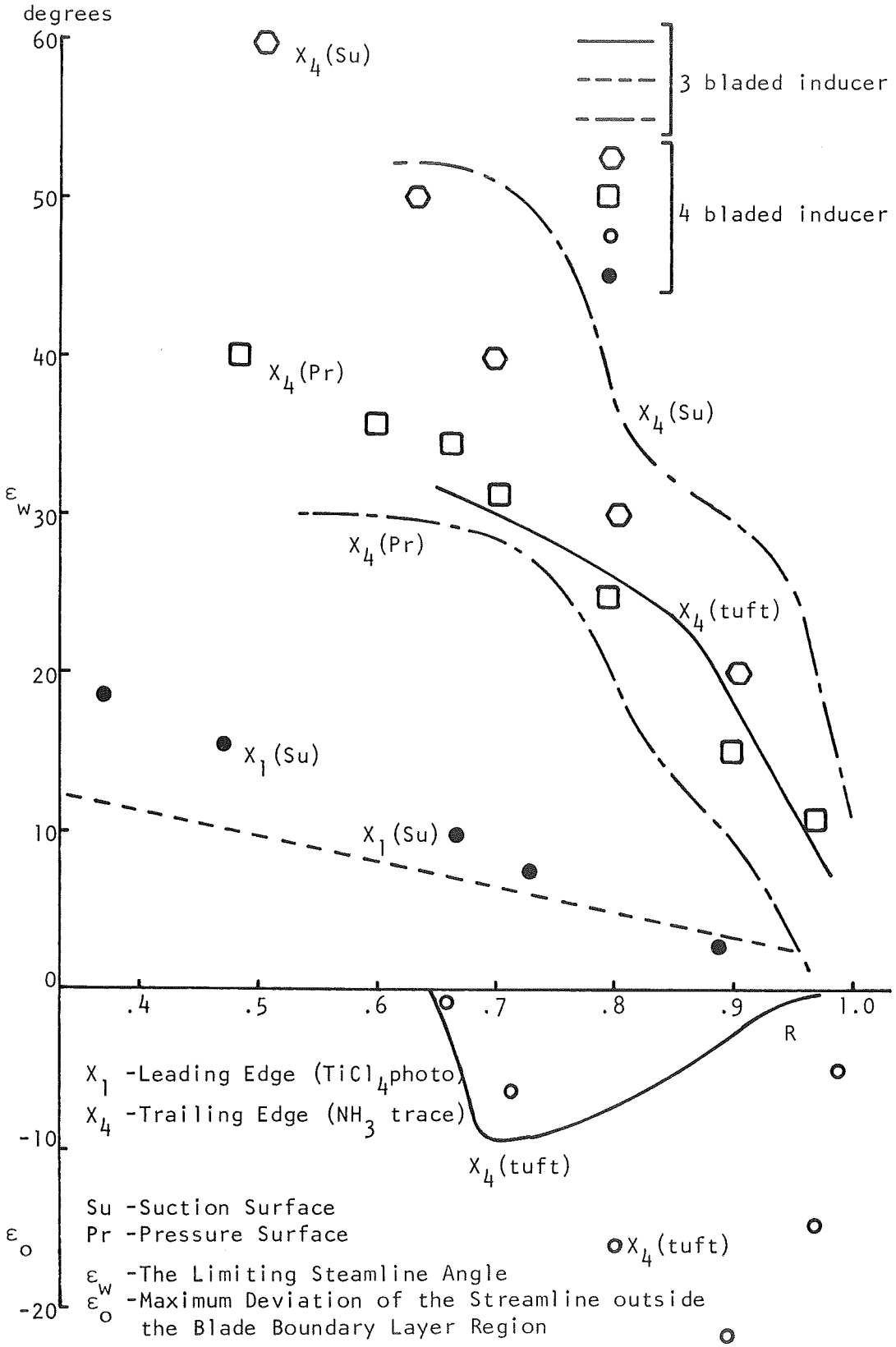

Figure 18: Radial Variation of ε_o and ε_w at Various Chordwise Location

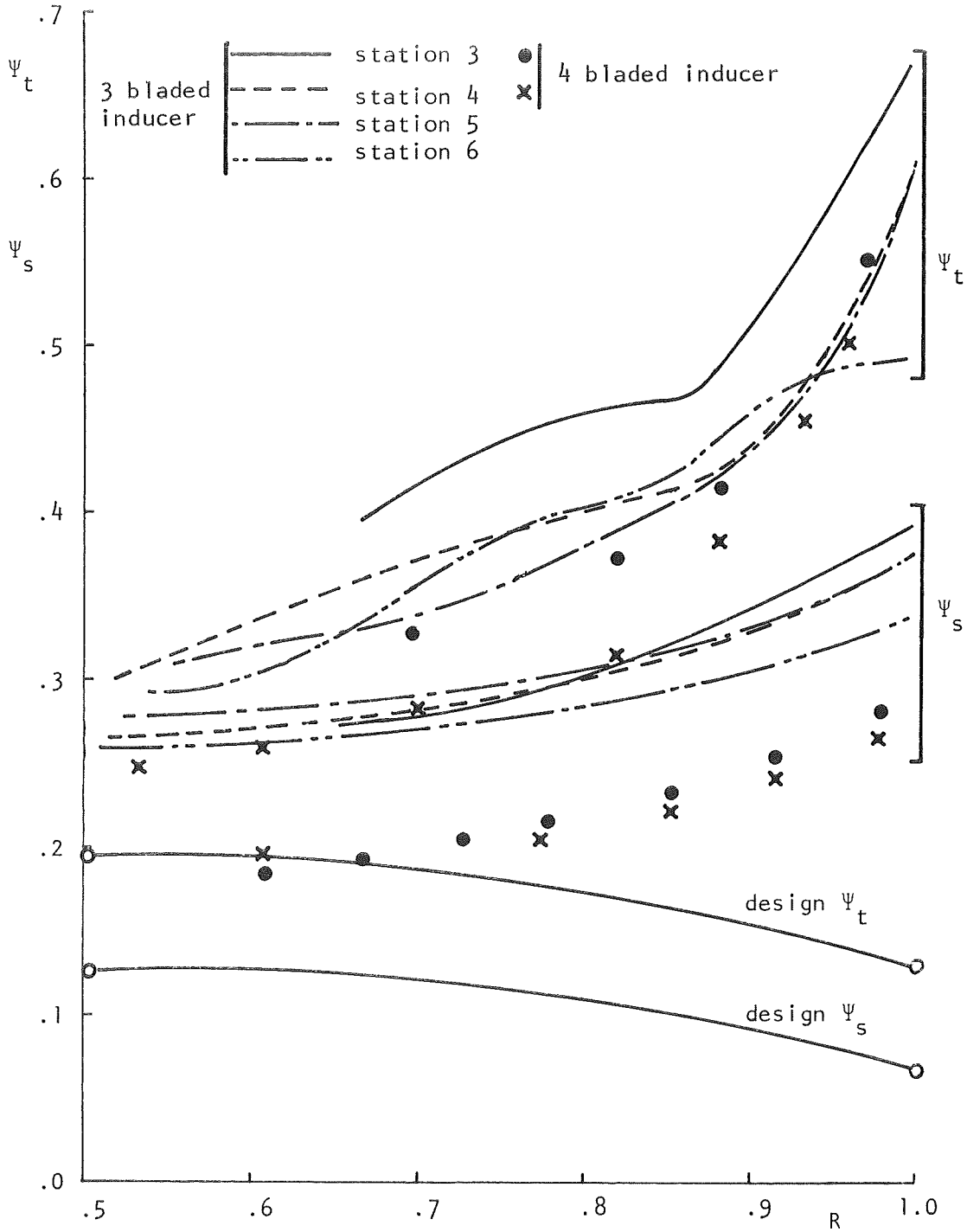

Figure 19a: Radial Variation of Stagnation and Static Coefficients at Various Axial Locations

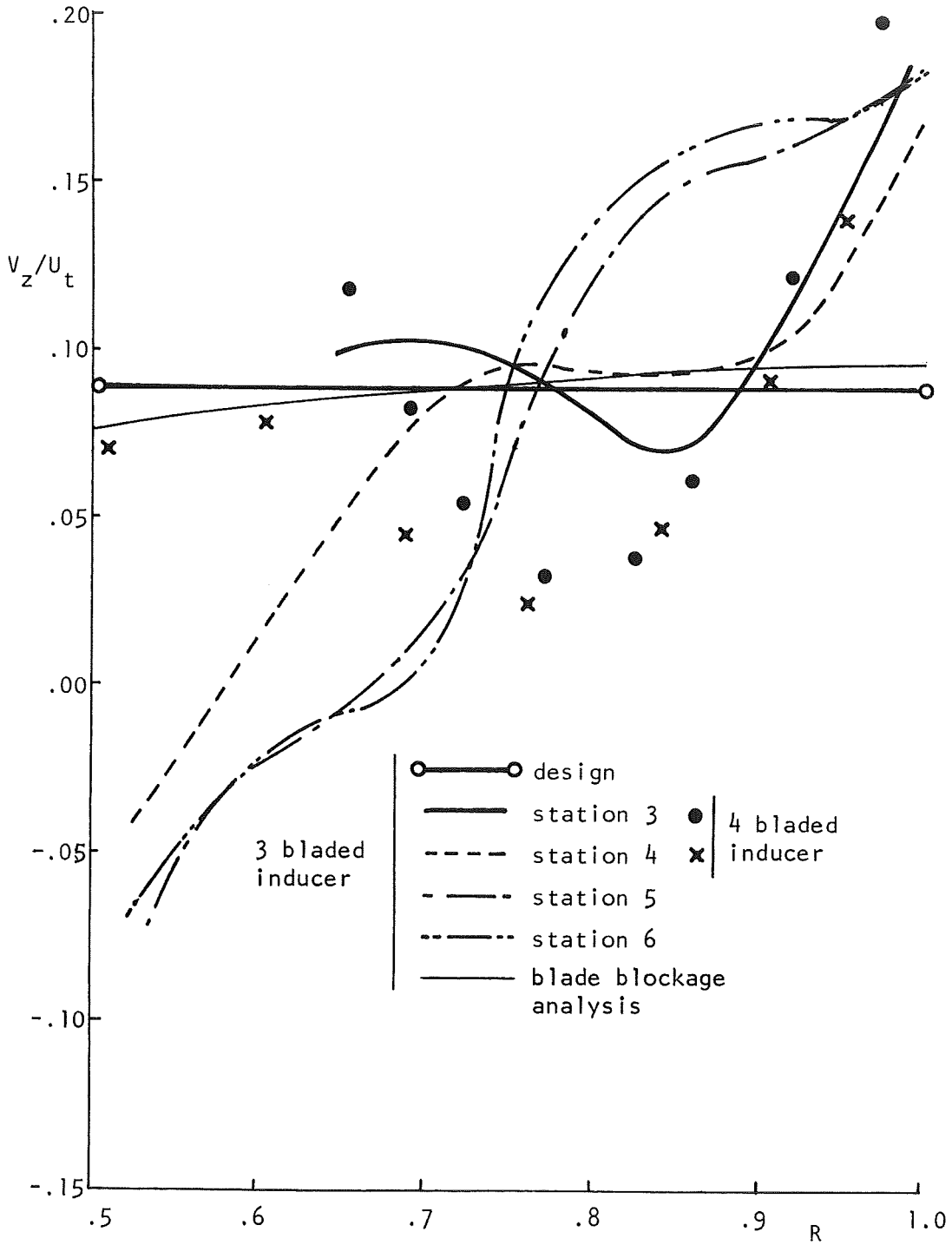

Figure 19b: Radial Variation of Axial Velocity at Various Axial Location

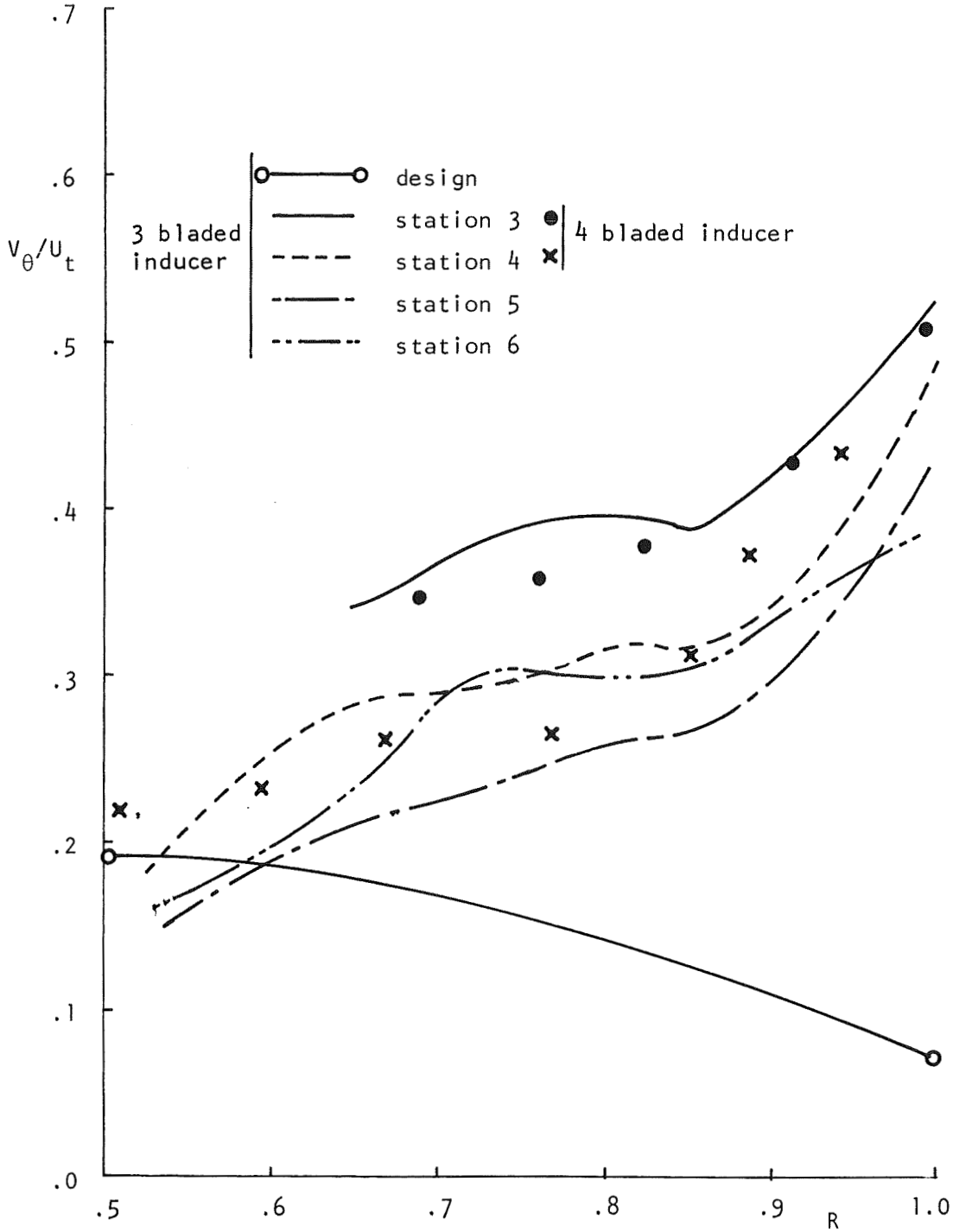

Figure 19c: Radial Variation of Absolute Tangential Velocity at Various Axial Location

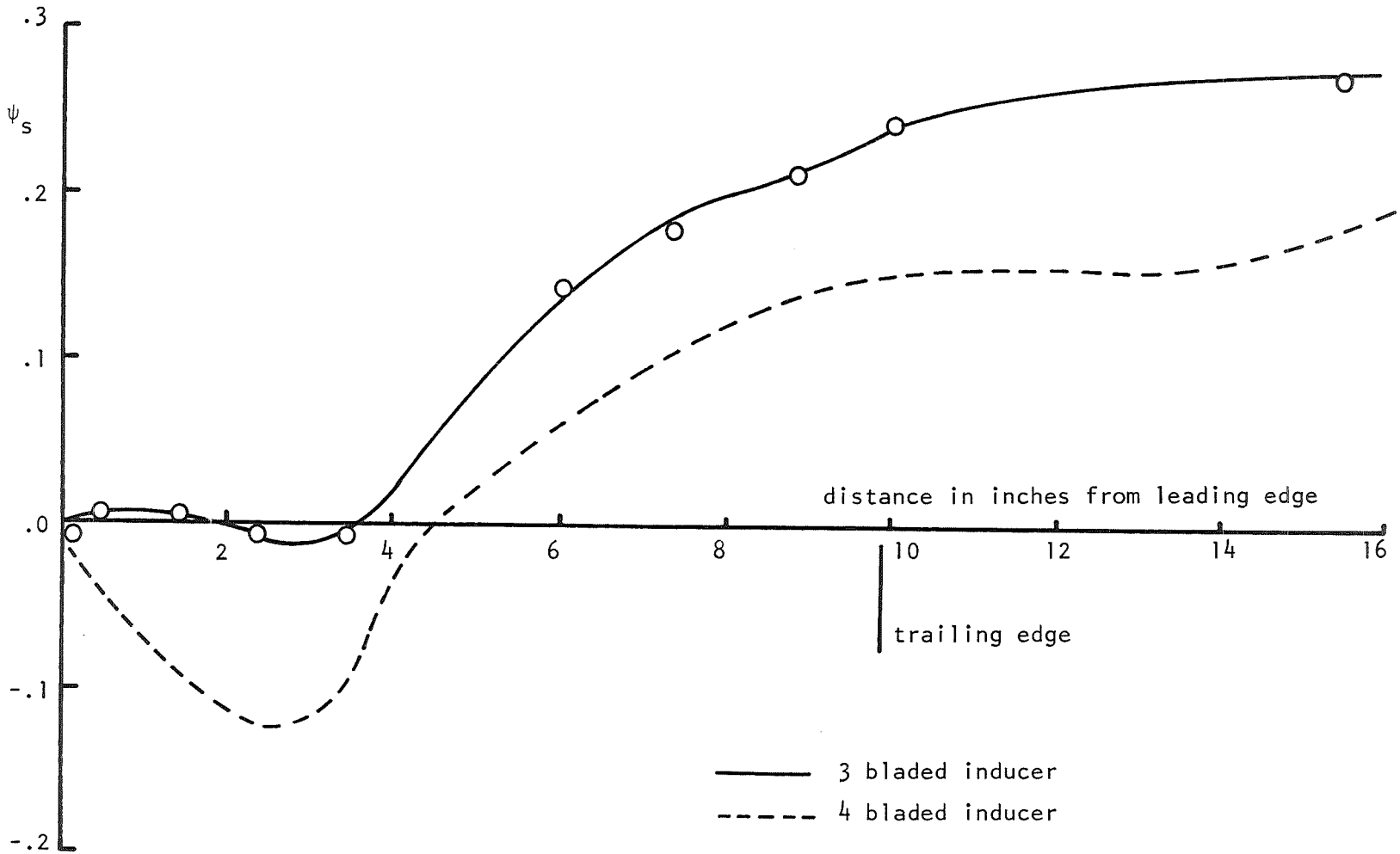

Figure 20 : Hub Static Pressure Distribution

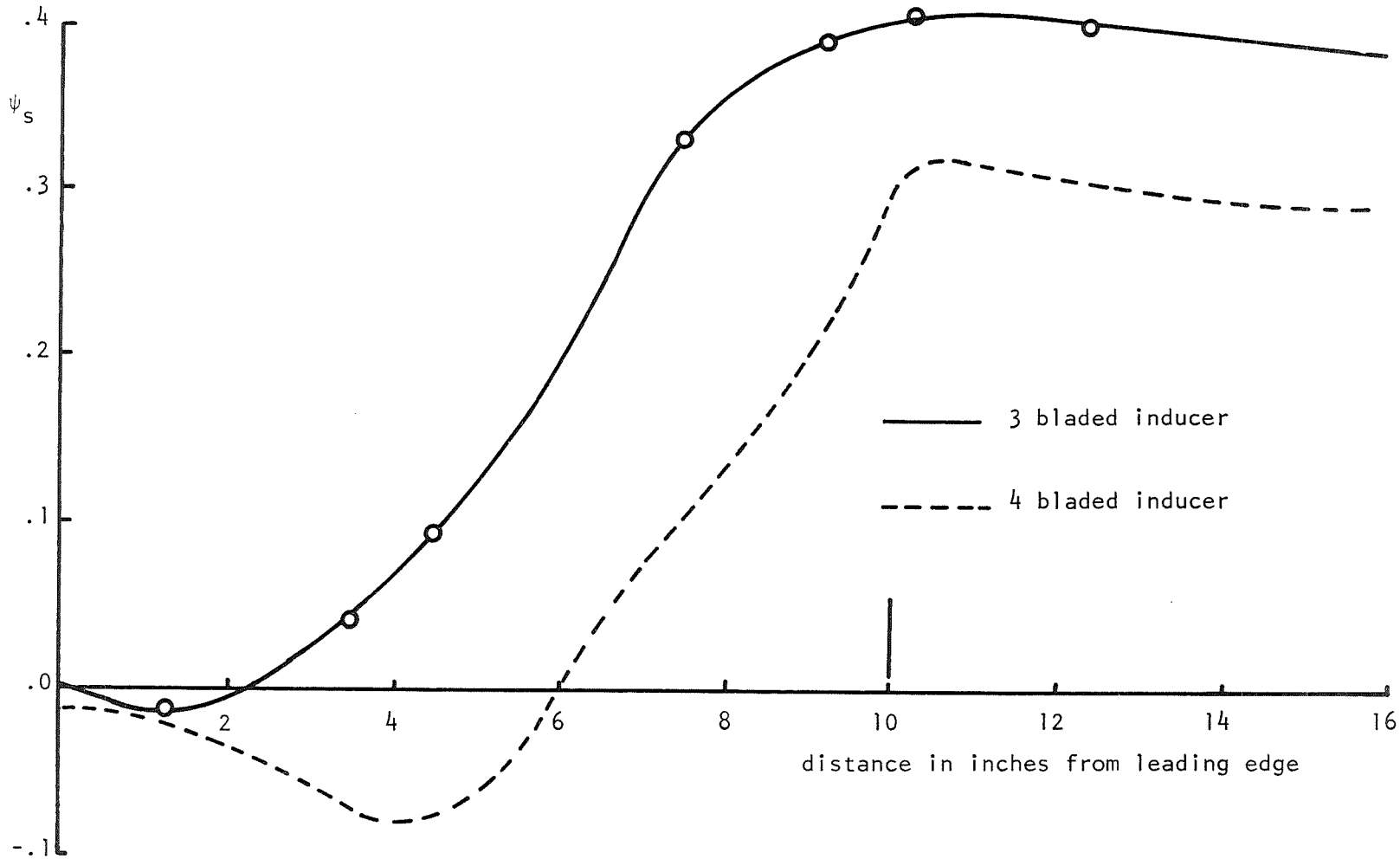

Figure 21 : Annulus Wall Static Pressure Distribution